Stony Brook University

The Climatology of Rossby Wave Packets Using Object-based Tracking Techniques

A Thesis Presented

by

Matthew B Souders

to

The Graduate School

in Partial Fulfillment of the

Requirements

for the Degree of

Master of Science

in

Marine and Atmospheric Sciences

(Concentration: Atmospheric Science)

Stony Brook University

May, 2013

Stony Brook University

The Graduate School

Matthew Souders

We the thesis committee for the above candidate for the

Master of Science degree, hereby recommend

acceptance of this thesis.

Brian A. Colle – Thesis Adviser

Professor, School of Marine and Atmospheric Science

Edmund K. M. Change – Second Reader

Professor, School of Marine and Atmospheric Science

Sultan Hameed – Third Reader

Professor, School of Marine and Atomspheric Science

The thesis is accepted by the Graduate School

Charles Taber

Interim Dead of the Graduate School

Abstract of the Thesis:

The Climatology of Rossby Wave Packets Using Object-based Tracking Techniques

by

Matthew Souders

Master of Science

in

Marine and Atomspheric Sciences

(Concentration – Atomspheric Science)

Stony Brook University

2013

This research produces an objective, track-based climatology of Rossby wave packets (RWPs) and tests the sensitivity of the results to changes in the methods used in filtering the raw data and in tracking. NCEP/NCAR Reanalysis wind and geopotential height data at 300 hPa every 6 hours were spectrally filtered using a Hilbert transform technique under the assumption that RWPs propagate along a waveguide defined by the 14-day running average of the 300 hPa wind. After some spatial smoothing, the local maxima in RWP envelope amplitude (WPA) were tracked using two objective techniques: a point-based cost optimization routine and a hybrid of point identification and object-based tracking following rules similar to those used in the tracking of tropical convective clusters. The total energy flux term of the eddy kinetic energy equation was used as a cross-check for the purpose of hand-verifying RWP tracks in order to compare the performance of each tracking method. Track data and object-based descriptive statistics (including area, average intensity, intensity volume, intensity-weighted centroid

position and velocity) were gathered to describe the inter-annual, annual, seasonal, and regime-based climatology of RWPs.

When tracking methods are verified over two winter seasons and compared, the hybrid technique statistically outperforms point-based tracking, particularly when estimating track duration and propagation. When long lived RWPs are verified, there is strong evidence that some RWPs can last over 30 days and circumnavigate the Northern (Southern) Hemisphere up to two (three) times. RWPs are found to exhibit a much more pronounced seasonal cycle in the Northern Hemisphere, where they are nearly non-existent in the summer months (JJA), as compared to nearly continuous RWP activity downwind of South Africa during Austral Summer (DJF). Interannual variability in packet frequency and intensity in the Northern Hemisphere is found to be strongly connected with the large scale flow regime, with oscillatory patterns like ENSO and the AO playing significant roles. Enhanced WPA is also found to coherently propagate in composites of regime change events (e.g. a reversal of the AO). No significant long-term changes in RWP frequency or intensity are found; however, the North Pacific storm track appears to have shifted northward in the last thirty years.

Table of Contents

Figure List

Table List

CHAPTER 1: Introduction

1.1. Background

Many previous studies have shown a linkage between extreme weather events in different parts of the hemisphere. For example, United States (U.S.) east coast snow storms (Brennan and Lackmann, 2005) and western Atlantic cyclones (Archambault et al., 2010; Cordeira and Bozart, 2011) have been linked to the downstream impacts of cyclones over the western Pacific (Harr and Dea, 2009; Ko and Hsu, 2010) through the generation and propagation of a Rossby wave packet (RWP). In January 2000, for example, an intense snow storm developed along the U.S. East coast in response to upstream forcing from an intense Pacific cyclone that developed six days earlier near Japan (Brennan and Lackmann 2005).

An RWP is defined as a region of high amplitude meridional flow in the upper atmosphere associated with the phenomenon of downstream development at scales larger than a single synoptic eddy (Hakim, 2003; Lee and Held, 1993). The structure and evolution of one such RWP occurring in late February and early March of 2009 can be found in Figure 1.1. Fig 1.1a is a Hovmoller diagram (longitude-time plot) of 300 hPa meridional wind latitude-averaged between 10 and 80 degrees north. The movement of higher amplitude meridional flow is tracked in Fig 1.1a, revealing a downstream propagation of higher amplitudes that is much faster than the movement of any individual trough. Figs. 1.1b-d show the same RWP through a series of spatial maps of 300 hPa geopotential height and meridional winds. The individual troughs are marked in both the Hovmoller diagram and the corresponding spatial maps to show the relationship between the RWP and the life cycles of individual eddies.

This phenomenon requires a waveguide to avoid meridional dispersion – usually a tight meridional gradient in potential vorticity and/or tropopause height (Martius et al., 2010). This downstream propagation of energy from one Rossby wave to the next is called downstream development (Chang and Orlanski, 1993). It occurs because the interaction of Rossby waves of different wavelength produces an interference pattern that must propagate with a group velocity that is eastward (Holton, 2004).

There has been a fair amount of research on the structure and evolution of RWPs (Chang, 2001; Chang, 2005; Hakim, 2003). For example, RWPs in the North Pacific commonly form over or just east of Japan and Siberia and they are slightly less intense and form further east in the midwinter months, particularly January, than during transition seasons (Hakim, 2003). Upstream short wave troughs and their baroclinic amplification are usually the trigger for RWP formation (Hakim, 2003). RWP movement is largely explained by the divergence of the fluxes of local eddy kinetic energy and ageostrophic geopotential (Chang, 2001), and they are important to the maintenance and even the formation of strong jets (Chang, 2005). Since RWPs need a strong waveguide to propagate a significant distance downstream of an initial disturbance, they are stronger and more prevalent during winter than other seasons (Chang, 1999). Also, since an RWP begins with an initial meridional perturbation (usually a baroclinic eddy), RWPs are tied to the storm tracks e.g. (Blackmon et al., 1984). Chang and Yu (1999) have confirmed this through the use of wave activity index.

There has been a recent attempt to quantify the climatology of RWPs using Hovmoller diagrams to distinguish and track them (Glatt and Wirth, 2013). However, the authors acknowledge that the use of Hovmoller diagrams to track RWPs may be problematic where there exists more than one active waveguide along a single longitude, as occurs during split flow

regimes (Glatt and Wirth, 2013). A major goal of this research is to produce a climatology of RWPs based on spatial tracking as has been done with surface cyclones and compare the results to this Hovmoller based approach. It is important to produce a fully robust climatology given the connection between RWPs and uncertainty in medium range (3-10 day) model forecasts (Anwender et al., 2008; Majumdar et al., 2010).

The subsequent sections in this chapter discuss the existing literature on RWPs and on attempts to track atmospheric features beginning with a discussion of RWP dynamics and life cycles, followed by the various attempts to identify them spatially, and concluding with tracking methods.

1.2. *Wave Packet Dynamics*

Chang (2001) investigated the horizontal and vertical structures of RWPs using a number of dynamical proxies drawn from energetics equations popularized by Lorenz (1950) and later re-expressed as a combination of a time mean flow and the perturbations in that flow (Chang and Orlanski, 1993; Orlanski and Katzfey, 1991). Equation 1.1, from Chang (2001), expresses changes in eddy kinetic energy as a combination of five terms:

Term A Term B Term C Term D Term E

$$\frac{\partial K}{\partial t} = -\nabla \bullet (vK + v_a\phi') - \omega'\alpha' - \left[v \bullet (v_3 \bullet \nabla_3)\bar{v} - v' \bullet \overline{(v_3' \bullet \nabla_3)v'}\right] - \left[\frac{\partial}{\partial p}\omega K + \frac{\partial}{\partial p}\omega'\phi'\right] - \mathrm{Re}\,s\text{: Eq. 1.1}$$

In (1.1), *K* is the eddy kinetic energy, in which eddy is defined as deviation from the time mean flow. From left to right, term A consists of the local advection of eddy kinetic energy (EKE) and the divergence of the flux in eddy geopotential by the ageostrophic component of the wind, or ageostrophic geopotential flux divergence (AGFD) and represents the horizontal movements of existing eddy kinetic energy. Term B represents EKE generated by the

conversion of eddy available potential energy to eddy kinetic energy through baroclinic growth (cyclogenesis) and is hereafter referred to as the baroclinic conversion term. Term C expresses the conversion between mean kinetic energy and eddy kinetic energy through eddy momentum flux (hereafter referred to as barotropic conversion). Barotropic conversion is explained by Holton (2004) as the result of the conservation of angular momentum caused by the combination of the normal shapes of upper atmospheric eddies and the planet's rotation. Since there are many more troughs that have a positive tilt than negative, which tends to disproportionately advect high momentum air poleward, this term helps to explain the maintenance of the polar front jets. Term D is similar to term A, except it now refers to the transfer of kinetic energy vertically. Finally we have a residual term, which is largely friction.

Chang's (2001) analysis of the internal structure of RWPs using the above dynamical framework helps to establish a conceptual model for the life cycle of a typical RWP. His results reveal that baroclinic conversion is frequently the catalyst for a RWP, since RWPs are generally formed after the development of a sufficiently intense baroclinic eddy. Chang's (2005b) subsequent study of the barotropic conversion term suggested that barotropic conversion may be important in some cases as well. After barotropic or baroclinic conversion, Chang demonstrated that in the presence of a well-defined waveguide, the local fluxes of EKE and AGFD found in term A of Eq. 1.1 become the dominant signal, driving the propagation of RWPs at their group velocity. In the absence of baroclinic growth, friction acts to gradually weaken RWPs until such time as the waveguide becomes weak or the baroclinic growth term becomes negative, acting to accelerate the weakening process and dissipate the packet. Vertical energy fluxes were found to be of small enough magnitude to be discounted (Chang, 2001).

Eq. 1.1 helps to explain the sources and sinks of RWP energy. The baroclinic term is most likely to become negative and the waveguide is most likely to weaken at the end of a storm track, where warm air advection and subsidence erase any baroclinicity by lifting heights (Kaspi and Schneider, 2011). Baroclinic generation is most likely in regions that favor cyclogenesis (Blackmon et al., 1984). We can therefore expect RWPs to develop most commonly near the western boundaries of storm tracks and dissipate near their eastern boundaries. Not all flow perturbations produce RWPs, however, and not all RWPs are limited to one storm track (Hakim, 2003; Majumdar et al., 2010). Some set of conditions, for example a stronger than normal waveguide, must be required to allow for downstream development and to maintain it even in regions not favoring baroclinic growth.

The genesis of RWPs has also been connected to tropical cyclones (TCs) undergoing extratropical transition (ET) and downstream development. Case studies have suggested that the presence of a strong waveguide is necessary in order to develop a Rossby RWP downstream of a recurving tropical cyclone (Harr and Dea, 2009). In fact, the manner in which each observed TC transitioned, their initial intensity and size, and the speed of their ET varied so much that Harr and Dea (2009) were led to conclude that the baroclinic environment was the most important factor in determining whether a RWP would develop. Anwender et al. (2008) also demonstrated that TCs that made ET in the presence of a strong waveguide were associated with the development of RWPs and that those were the TCs most likely to cause relatively large model forecast uncertainty over the entire hemisphere.

Aside from TCs, a number of attempts to understand changes in the large scale flow regime have been made in which RWPs appear to play a key role. Martius et al. (2007) classified Rossby wave breaking (RWB) events, found by looking for regions where the gradient

in total vorticity became negative, which suggested the presence of eddy instability. Their observations strongly suggest that both poleward breaking and equatorward breaking waves are frequently associated with strong wave trains (Martius et al., 2007). An attempt was also made to group a large number of blocking events and look for commonalities during their formation and the results of this analysis suggested that Rossby waves and wave trains were of critical importance (Altenhoff et al., 2008). Chang (2005) suggests that large scale changes in the strength of the meridional temperature gradient (and hence the jet) are dominated by RWP activity. It has been suggested that the North Atlantic Oscillation (NAO) may be the result of variability in the frequency of wave breaking events in the North Atlantic and likewise in the Pacific for the West Pacific pattern (Woollings et al., 2008). It is even suggested that cyclonic wave breaks are responsible for negative NAO (NAO-) conditions and vice versa (Reviere and Orlanski, 2007). Since the NAO and the Northern Annular Mode (NAM) are frequently linked to each other (Feldstein and Franzke, 2006), and wave breaking may be linked to RWPs, RWPs may play a role in changes in the NAM. It was found that the frequency of wave breaking of sufficient size has a statistically significant correlation with the magnitude of the NAM (Strong and Magnusdottir, 2008). The specific role of RWPs in these interactions between individual eddies and the mean flow, however, has not been clarified.

1.3. Identifying Rossby Wave Packets

The most common method for tracking a Rossby wave train is to construct a Hovmoller diagram (Hovmoller, 1949) of 300 hPa height or meridional wind and follow the highest amplitude signals as they propagate (Figure 1.1). This approach was recently used by a tracking study of RWPs (Glatt and Wirth, 2013), but it may fail when the flow becomes split. As a result,

two alternatives for identifying RWPs have been published (Lee and Held, 1993; Zimin et al., 2006).

Any wave-like signal will consist of oscillations, and in the atmosphere these oscillations on the large scale are expressed as troughs and ridges (either through poleward and equatorward meridional winds or positive and negative height anomalies). Lee and Held (1993) recognized that in order to view a RWP spatially, it was necessary to filter out the oscillations and focus only on the amplitude of the envelope enclosing the troughs and ridges of the wave. They proposed a method known as complex demodulation in order to extract this envelope amplitude. Equation 1.2 expresses any wave like signal as a combination of variable carrier wave period and amplitude functions,

$$f(x) = A(X) \cdot \cos(kx + c(x)) \ : \qquad \text{Eq. 1.2}$$

in which A(X) is a slowly varying amplitude modulation, k is the carrier wave number estimated based on single-point correlation analyses for each latitude and during each season, and c(x) is a slowly varying phase function all along a single latitude circle. There are problems with this approach as well. First, the carrier wave number must be estimated, and as noted by Zimin et al (2003), there exist flow regimes that may carry packets with completely different carrier wave numbers. Zimin et al (2003) proposed to select representative carrier wave numbers by using a Hilbert transform technique to filter out high wave number signals and extract the envelope amplitude from meridional wind data. A Hilbert transform involves conducting a fast-Fourier transform (FFT) of the data, selecting only wave numbers associated with the phenomenon of interest (in this case, wavenumbers 3-11) and then conducting an inverse FFT and taking double the real component of the IFFT as the envelop amplitude. However, RWPs don't always propagate zonally (e.g. during a positive Pacific-North American teleconnection pattern), and the

prominence of large quasi-stationary ridges distort most amplified flow regimes, leading to a disjointed appearance in WPA fields produced by either complex demodulation or the Hilbert transform technique when those methods are applied zonally (Glatt and Wirth, 2013). As a result, Zimin et al (2006) modified the approach by using a 28-day running mean of the 300 hPa zonal and meridional wind data to calculate the local stream flow at every point around the globe and conducting the Hilbert transform along a streamline.

Zimin et al. (2006) demonstrate the impact of using a streamline, rather than a latitude line, on a non-zonal flow regime – the shape of the WPA envelope is smoother and more contiguous. Figure 1.2 shows a comparison of the complex demodulation method and the Hilbert transform along stream flow techniques using NCEP-NCAR Reanalysis data, again revealing smoother, more coherent RWPs – likely the result of non-zonal flows near Alaska, and over Eurasia in particular. One other change is apparent: the Hilbert technique produces lower amplitudes within blocking signals (e.g. near Alaska in Fig. 1.2b) and to a lesser extent throughout the storm tracks. This is likely the result of removing the time-mean flow from the meridional winds used to calculate WPA. Blocks and long wave flow regimes carry meridional winds that can be filtered out when looking for the amplitude of eddies, and the use of such a filter aids in wave packet tracking. Given the non-zonal nature of blocks and long wave teleconnections, and noting that the Hilbert transform technique makes fewer assumptions than complex demodulation, the method of Zimin et al (2006) is likely the stronger alternative.

1.4. *Existing Feature-based Tracking Methods*

Previous RWP studies have had a limited sample size, and thus could not quantify the longer-term climatology of these packets. Chang (2000; 2001; 2005b) studied composites, hand-

tracked RWPs taken from one winter season, or, in the case of the 2005 study, a few cool seasons, while Hakim (2003) hand tracked RWP data for three years and only in the western North Pacific. Harr and Dea (2009) studied the extratropical transition of only four tropical cyclones over the western Pacific. Archambault et al. (2010) studied only the RWPs that impacted several Northeast U.S. high precipitation events during the cool season. A larger sample size over a few decades can be used to better understand the climatology and interannual variability of RWPs; however, to get a sample this large without using a Hovmoller diagram, a feature-based tracking technique must be chosen.

There are two common subcategories of feature-based tracking techniques in the literature to date (grouped by the type of feature chosen for tracking purposes). Those two families are point-based and object-based tracking schemes. Point based methods rely on the identification of significant (and distinct) relative minima or maxima in atmospheric data as the objects to be tracked, and during the stage of tracking where a decision must be made as to whether an existing track should continue into the next time step, only the identified local extrema are considered (Fig. 1.3). Tropical cyclones (Cassity and Colgan, 1973; Haraguchi, 1967; Hodges, 1994) and extratropical cyclones (Anderson and Graykum, 1989; Charles and Colle, 2009a; Charles and Colle, 2009b; Froude, 2009; Wang et al., 2006) have been tracked in this manner. Object-based tracking methods rely on the entire enclosed shape of an atmospheric phenomenon for tracking, and decisions regarding the continuation of existing tracks are made based on statistical similarity, overlap or object proximity from one time step to another. This approach has been used to track tropical convection (Arnaud et al., 1992; Endlich and Wolf, 1981), mesoscale convective systems (Machado et al., 1998), and quantitative precipitation forecasts (Davis et al., 2006).

However, when applied to RWPs, existing tracking techniques may be inadequate because RWPs are often large in scale, amorphous, split into multiple packets, and can be relatively short-lived. Hakim (2003) characterized the typical scale of a RWP (wavelengths of at least 2000 km and envelopes with north/south widths of thousands of km), which far exceeds the typical scale of a mesoscale convective system (MCS), hurricane, extratropical cyclone, or African easterly wave. Something as large as an RWP has the capacity to change shape and intensity relatively quickly compared to its speed of motion. The large size also presents the problem of interdependence. A packet that covers anywhere from 1-20% the total surface area of the globe in extreme cases is bound to collide with other packets and they may even dynamically merge or spilt more commonly than a cyclone or an MCS (rather like a tropical convective cluster). The shape of RWPs also constantly evolves, which distorts the distribution of intensity and the apparent motion of any local maximum, rendering point-based tracking problematic. Object based approaches are also troublesome – not only because RWPs tend to interact with each other commonly, but also because, unlike convective systems, there are no hard physical parameters that neatly govern the outer boundary of an RWP. In radar data, an MCS might be isolated using the 45 dBZ contour in smoothed radar composites (Lombardo and Colle, 2010). In satellite imagery, a convective cluster might be isolated using a brightness temperature of -40 C (Arnaud et al., 1992), and these quantities don't change over time. An RWP, on the other hand, is a perturbation on an existing flow and the strength of the existing flow may determine the strength of the perturbation necessary to stand out as significant. It is hypothesized that a RWP tracking method that considers both the local maxima in WPA and the overall structure of packet objects will outperform point-based and object-based approaches when compared to a manual verification.

1.5. Motivational Questions

RWPs are a critical piece of our understanding of atmospheric dynamics, since they serve as an intermediate step between individual Rossby waves and the storm tracks. In order to understand the general circulation of the atmosphere, we must not only understand baroclinic eddies and quasi-stationary waves, but also the mechanisms that disperse energy upscale (from eddies to storm tracks). RWPs may hold some of the keys to understanding storm track variability from the decadal to the intra-seasonal timescales. Also, understanding wave/mean flow interactions cannot be complete without a tracking-based climatology of RWPs. Therefore, this thesis will develop an objective climatology based on the automated tracking of RWPs for the common satellite era (1979-2010), which will help to address the following questions:

- Can a reliable method be found for identifying and tracking RWPs objectively?
- How does the RWP climatology relate to the spatial and temporal changes in the seasonal hemispheric storm tracks in the northern and southern hemisphere? Are these changes related to common teleconnection patterns such as ENSO, NAM and the MJO?
- What role do large terrain features such as the Tibetan High Plateau and the North American Rockies play in tracks, genesis and decay of RWPs and their associated storm track belts?
- Do RWPs play a role in sudden changes in the large scale flow regime?
- Have there been any significant changes in the intensity, frequency or position of RWPs during the common satellite era?

Chapter 2 of this thesis will describe the data and tracking methods used in the creation of the climatology of RWPs, verification of tracking skill and determining the sensitivity of the

climatology to the methods chosen. Chapter 3 verifies and compares the skill of three RWP tracking methods. Chapter 4 presents the climatology of RWPs and Chapter 5 is a discussion of the results in chapters 3 and 4, including additional sensitivity tests along with conclusions drawn from this research.

CHATPER 2: Data and Methods

2.1. Datasets and Preprocessing

In order to track the RWPs, wind and geopotential height data every 6-h at 300 hPa from 2.5 degree NCEP/NCAR reanalysis (Kalnay et al., 1996) from 1979-2010 was obtained. Although three different methods for identifying RWPs and calculating RWP envelope amplitude (WPA) have been used in previous literature – namely: Hovmoller-based tracking (Glatt and Wirth, 2013), complex demodulation (Lee and Held, 1993), and Hilbert transformation (Zimin et al., 2006; Zimin et al., 2003) – the method of Zimin et al (2006), which makes allowances for non-zonal flow regimes, produced more realistic results, as discussed in the previous section and was thus the method of choice.

Some smoothing of the data is required to track signals at the RWP scale defined by Hakim (2003). A T21 Cholesky filter (Hodges, 1999) was applied to the data in order to filter out wavelengths too small to be associated with RWPs. Other resolutions were also tested and the results of those experiments will be discussed in Chapter 5. A temporal smoothing (running mean), similar to the method of Hodges et al. (2005) or Froude (2009), with a 24-hour width was also applied to the data in order to aid the tracking methods and smooth the progression of local maxima in WPA.

2.2. Wave Packet Tracking Approach

Multiple tracking techniques were tested for this research, and for each tracking method, a standard minimum WPA threshold (14 m s^{-1}), a minimum object size (40 grid points from 2.5 degree resolution data) and a search range for track continuity (20 degrees N/S, 30 degrees W

and 90 degrees E as shown in Fig. 2.1) was chosen. The sensitivity of each of these parameters will be tested in Chapter 5. In addition, a definition for "significant" RWPs was needed for the climatology to separate robust features from noise. Given that an RWP must include more than one synoptic eddy (as in Hakim, 2003) and propagate downstream long enough to move high amplitude meridional flow from one eddy to another, a packet centroid must travel eastward by at least 40^{o} longitude and be tracked for longer than two days to be considered significant. Froude (2009), Charles and Colle (2008) and Hodges et al (2005) have all used similar criteria to identify significant cyclones when conducting cyclone tracking studies. Other definitions of track significance, minimum tracking threshold, continuity search range, and minimum object size were tested and will be discussed in Chapter 5 of the thesis. A summary of the general rules for RWP tracking can be found in Table 2.1.

Three different RWP tracking techniques were tested and compared. Table 2.2 is a comparison of the tracking attributes and rules for each of the three approaches. The first method uses an approach called TRACK (Hodges 1999), which is a feature-based tracking algorithm that has been employed in cyclone tracking climatologies (Hoskins and Hodges, 2005). The second and third methods are based on a combination of point-based object identification similar to the cyclone tracking scheme of (Charles and Colle, 2009a) and object-based tracking similar to methods used in the tracking of tropical convective clouds (Arnaud et al., 1992). These two schemes differ only in the assumptions made when resolving complex tracks and settling tracking conflicts. These methods will henceforth be referred to as hybrid 1 (or H1) and hybrid 2 (H2).

This first approach (TRACK) uses the existing points, selected from the local maxima in an atmospheric variable (in this case WPA), in an ongoing track to estimate the object's current

velocity, and from that estimate, guess the location of the next track point. It then searches the subsequent time step in the data set for points relatively close to that estimated location and selects either the most likely next track point or the end time of the track if no points are likely (Fig. 2.2). The method includes a number of user-specified parameters: maximum displacement (the largest distance in great circle degrees that can exist between any two points in a track), track smoothness (the maximum allowable difference between the expected track velocity and the actual track velocity if a point is adopted as the next track point), minimum tracking threshold, and minimum object size. Some trial and error was required to find parameters that worked the best for tracking RWPs. The maximum displacement was set to 30 great circle degrees after early trials indicated that larger values led to nonsensical tracks linking multiple objects, but smaller values led to highly fragmented tracks. The track smoothness is a value between zero and one, which defines how much the velocity vector for the 18-hr running mean track velocity is allowed to fluctuate. A setting of 0 would allow for no directional changes in motion (linear motion only) and a value of 1 allows any direction to be the next one selected as long as it is reasonably close to the last track point. The smoothness is also set differently for different propagation speeds. The faster an object is moving, the more we should expect the motion to be consistent, whereas slow-moving objects tend to wobble. The smoothness parameter settings used for this climatology can be found in Table 2.3. For fast-moving RWPs, nearly perfect smoothness is expected (s=0.1), whereas for slow moving RWPs, some changes in direction of motion are allowed (s=0.7).

Additional merging of related track segments is done based on geographical proximity and inclusion within the same significant object boundary to arrive at final tracks for use in the climatology. Two tracks were considered candidates for merging if during the period where both

tracks coexisted, they remained in the same WPA object and never passed further than 120 degrees in longitude apart. The features found by TRACK were also attributed to WPA objects bounded by the minimum tracking threshold using a k-nearest-neighbor technique to give a spatial context to each tracked feature.

The hybrid tracking algorithm identifies unique RWPs by selecting significant local maxima in WPA, attributing the object space inside the minimum tracking threshold to each local maximum, and then tracking the objects by searching for significant overlap across a single time interval. The first step for the hybrid tracking is feature selection. Choosing all local maxima would leave a number of "features" which were merely local noise. Even after the data is smoothed as described in section 2a, there are a number of local maxima in WPA above the minimum tracking threshold that are related to stronger peaks in WPA and are therefore not isolated packets (see Fig. 2.3). WPA maxima which can be encircled by drawing a WPA contour that encloses a particular feature at 95% of the feature's intensity without enclosing other, more intense features are retained (shown in Fig. 2.4).

Object attribution is the process of defining which grid points with WPA values greater than the minimum tracking threshold are most closely related to each significant WPA max and is now required. Objects are defined using the minimum tracking threshold. Each object may include one or more significant WPA maxima. If a closed contour at the tracking threshold can be drawn that includes just one local maximum, all grid points within that object are attributed to its' local max. If more than one max is found within the borders of a unique WPA object, a k-nearest-neighbor technique is used to attribute grid points to their nearest significant tracking feature (as shown in Fig. 2.5).

Once RWP objects are attributed to representative local maxima in WPA as described above, the next step is object tracking using the 50% overlap technique of Arnaud et al (1992). Two such tracking methods have been constructed around this basic theme. Each method is built using different rules to resolve tracking conflicts so that a direct comparison of these methods may test the impacts of those assumptions on the final results. Both methods relied on a simple scheme in which any two objects in consecutive time steps whose local maxima fell within the predefined search range and which overlapped such that the overlapping region filled 50% of the area in either object would be given the same track ID (see Fig. 2.6). The first method (Hybrid 1) used a future snapshot to search for continuity in tracks ongoing in the current snapshot, whereas the second method (Hybrid 2) used the current snapshot to search for candidates to merge with ongoing tracks in a previous time. Hybrid 1 resolved instances where multiple ongoing tracks could claim a future object by awarding that object to the family that was longest lived, with ties going to the family that would propagate the furthest east to continue to the track. Hybrid 2 awarded conflicted objects to the largest existing object with a potential claim, with ties going to the most intense object. Hybrid 1 prevented the occurrence of multiple distinct objects with the same track ID after merging by requiring that no two objects may have the same track ID and be separated by more than 120 longitude degrees and renaming the furthest west object in such cases. Hybrid 2 solves this problem by taking the most intense local WPA maximum in a multi-member track family and enclosing it in a WPA contour at half the distance between the minimum tracking threshold and the peak WPA. If objects with the same track ID were found to be separable by this contour, the weakest object was renamed. These differences are shown schematically in figure 2.7. These rules were developed by hand-verifying tracks produced by each method between January and March of 2009 and in January of 2010.

2.3. Verification of Tracking Techniques

Before general conclusions were drawn from either the TRACK or hybrid tracking datasets, the results were verified manually. This was done both to confirm that these tracking techniques are constructing reasonable tracks from the WPA data and to prove that WPA is a reasonable tracking variable when compared with the dynamics that drive RWP propagation and intensity. It was therefore necessary to produce an independent tracking variable from terms in the eddy energetics equation (eq.1.1 above) against which WPA could be compared. Term A in the eddy energetics equation, the divergence of the sum of the local flux of eddy kinetic energy by the total wind and the local flux of geopotential by the ageostrophic wind, is associated with the propagation of RWPs. This term oscillates along the waveguide much like 300 hPa meridional wind and the same technique that was used to produce WPA can be used to convert it to a wave-packet-like positive definite tracking variable. However, term A of the eddy energetics equations is proportional to EKE (order v^2) and WPA is proportional to the meridional wind (order v), meaning that the distribution of term A will be steeply peaked and right skewed compared with the distribution of WPA. The square root of term A is more comparable, and is given the name Wave Packet Index (WPI). A contiguous region having high WPI values indicates the presence of significant energy fluxes between energy centers and thus is indicative of RWP propagation.

Two three-month cool seasons – January to March, 1996 and January to March, 2007 – were chosen for a seasonal verification of the tracking approaches, and every RWP track found by either hybrid tracking technique to have lasted at least 25 days was manually verified to test the validity of long-duration RWPs produced by the automated tracking techniques. All hand

verification was done by tracking the WPI manually, while considering the movement of 300 hPa height perturbations and the existence of WPA exceeding the minimum tracking threshold in order to resolve tracking ambiguities. Based on composites of all RWPs possessing WPA maxima between 14 and 16 m s^{-1} (Fig. 2.8a) and the first eight time steps for all significant RWPs (Fig. 2.8b), a WPI value of 18 was required for the dynamics to be considered significant enough for visual tracking and a WPI value of 25 was required to fall within the 14 m s^{-1} WPA contour enclosing any RWP for at least 24 hours.

CHAPTER 3: Verification of Tracking Methods

3.1. Summary Verification

It is hypothesized that RWPs can be tracked reliably with an automated approach, but this needs to be quantified. Hand tracking the seasonal verification period (JAN-MAR, 1996, JAN-MAR 2007) revealed 96 significant RWPs, 39 in the Southern Hemisphere, 57 in the Northern Hemisphere. For each RWP tracked, basic information about its formation, propagation and dissipation, as well as the performance of each of three tracking methods, was recorded. This chapter will describe the life cycles of hand tracked RWPs, and compare observed tracks with automated tracking methods.

Table 3.1 reveals the overall performance of each tracker at identifying significant RWP tracks that matched those found in the seasonal hand tracking study. Hybrid 1 and 2 are not statistically different from each other (see discussions of statistical tests below) in terms of the false alarm rate (a detected track that is unsupported by the dynamic index data) or the detection rate (the rate of success of the algorithm to detect a good track when a clear propagating dynamic signal is found), but TRACK performs noticeably worse. Both hybrid approaches carry approximately a 20% probability of false detection, while TRACK produces false packets 32% of the time. Both hybrid approaches carry a greater than 90% detection rate, but TRACK detects only 78% of the hand tracks correctly. For all methods, false detection was most likely to be caused by the erroneous merging of two or more unrelated and non-significant RWP objects or the false splitting of one RWP track into two or more related tracks. For all methods, a track was most likely to be missed if it was incorrectly merged in with another significant track. Missed tracks and false detections were most common at the ends of storm track belts where RWPs

move more erratically (Eastern Pacific and Western North America, near the Prime Meridian, in the vicinity of the Tibetan High Plateau, and near and South of Australia and South America).

Figure 3.1 compares the duration of RWPs for the various tracking approaches with the manual tracking for packets that are short lived (less than 4 days), average duration (between 4 and 12 days) and long lived (> 12 days), as well as the frequencies for tracks that did not travel eastward more than 120 degrees, traveled a moderate distance (120-480 degrees), and farther than 480 degrees. TRACK identifies too many distinct, short-lived features persisting for greater than eight six-hourly time steps (2 days). Thus, TRACK creates too many false alarms and erroneous merges and splits, which shorten track life expectancy and boost the total number of track points. In fact, a simple comparison of both the number of unique track points and the number of unique packets found by TRACK and the two hybrid methods is illuminating. From 1979-2010, Hybrid 1 detects 16,107 tracks, Hybrid 2 detects 13,898 tracks and TRACK finds 21,210 tracks. Both hybrid methods use an identical feature detection formula and thus they both find roughly 250,000 unique features, whereas TRACK finds in excess of 320,000 features. Next, some of the patterns that lead to the errors produced by each tracking method during wave packet formation, movement and dissipation are presented.

3.2. Wave Packet Formation

The formation of an RWP is defined when a distinct local maximum in WPA above the minimum tracking threshold is first observed. Figures 3.2-3.5 shows the four types of initiation observed during the hand verification using a representative example. Although some RWPs develop locally, forced by cyclogenesis in the presence of a strong waveguide as shown in Figure 3.2 (this occurred 47 times in 96 cases), roughly 50% of hand-verified events required the prior existence of other packets to develop. This occurred by either: a dissipating or non-significant

RWP perturbing the flow downstream, hereafter called an upstream seeder (34 cases, an example of which is shown in Fig. 3.3), the forward flank of a wave packet splitting away and becoming independent (8 cases of the leading split, Fig. 3.4) or the rear flank of an RWP stalling and becoming independent (7 cases of the trailing split, Fig. 3.5).

The RWP development shown in figure 3.2 is representative of new cyclogenesis and downstream development in the absence of pre-existing significant RWP activity. A rapidly deepening cyclone near Japan intensifies a 300 hPa long wave trough and results in downstream ridge amplification in the entrance region of a strong zonal jet in the North Pacific. This leads to the development of a robust, 26 m s^{-1} RWP (labeled "35" in Fig. 3.2) within two days and this packet spreads east toward the Western US coastline shortly thereafter. Due to the development of a new WPA object, all methods identified this type of formation quite well – no method produced a formation error more than four times (out of 47 events) in the entire seasonal verification period. In fact, when formation errors occurred with in situ development, the cause was generally a subsequent merging or splitting of packets that changed the location and timing of the first recognized point along the track.

Another common occurrence within the hand verification period involved a dying wave packet or a region of slightly amplified flow that failed to qualify as a significant wave packet. The upstream "seed" disturbance can result in the necessary meridional perturbation to excite a new significant wave packet (an upstream seeded development). An example of this is shown in figure 3.3. Here, dying RWP 486 (2006) has entered a region where the lack of WPI favors its dissipation. Indeed, #486 dissipates entirely based on the WPA field for a full day. However, while the packet was more intense, it produced a wave break (and a cut-off low) near Tibet. That cut off low subsequently excites the development of a new RWP near Japan (RWP #11 in Fig.

3.3). The most common type of tracking error associated with upstream seeded wave packet development is the false merging of the upstream (non-significant) seed with the new RWP, though this error was rare (occurring only once in both Hybrid methods combined and three times using TRACK, out of a total of 34 cases).

When a packet splits into two or more distinct objects, one part of the split system is the existing RWP and the other is a new packet. The decision as to which object continues the existing track depends on the eastward propagations speeds of each of the two now-distinct objects. Figure 3.6 shows the typical eastward movement rates of RWPs (degrees longitude per six hours), revealing that most RWPs move eastward roughly 3-10 degrees every six hours. In hand tracking, trailing and leading splits were distinguished from one another by observing the propagation of each piece of the splitting packet. The piece that continues to move at the speeds typical of most RWPs is considered the continuing track, and a new identification is given to the remaining piece. Trailing splits occur when the leading edge of the packet propagates normally while the trailing edge slows or stalls, creating the split (shown for one example – see objects 35 and 41 – in figure 3.5). Leading splits occur when the leading edge of the packet moves very rapidly while the trailing edge continues propagating at normal speeds (shown in figure 3.4 – see objects 10 and 22). Distinguishing which process is occurring within an automated tracking algorithm can be difficult. As a result, this process produces much false detection and many missed tracks in both hybrid methods and TRACK, and it also increases the observed error in the starting time and longitude of RWPs. In fact, TRACK misattributes packet IDs during splitting events over half the time (9 of 15), while the Hybrid techniques failed 5 (H1) and 4 (H2) times respectively. One possibility for improving all of these tracking techniques would be to account

for the recent propagation speeds of tracked WPA maxima in order to improve conflict resolution during RWP merges and splits.

When the nearest-matching track starting points from each method are compared with hand tracking and 90% confidence intervals are generated from bootstrapping, real differences emerge between TRACK and the hybrid methods (Fig. 3.7). A positive location error means that the track started too far east when compared with hand tracking results. A positive error in timing means that the track began later than hand verification. At first glance, the fact that TRACK evinces significantly less bias in the starting longitude and time of hand verified packets would suggest meaningful skill, but there is a slight increase in mean absolute error and spread (albeit not a statistically significant increase). This suggests that TRACK is not less error prone with formation, but that its errors cancel out more evenly.

3.3. Duration and Propagation

Previous studies of RWPs using composites from Reanalysis (Chang, 1993, Lee and Held, 1993, Hakim, 2005 e.g.) showed packets that formed and moved at some nearly-constant group velocity. Analysis of the hand tracked packets from the seasonal verification suggests that their movement is better described as pulse-like. This fact was likely obscured in previous studies due to statistical smoothing which occurs in composites. RWPs tend to intensify in bursts with the rapid intensification of cyclones, streak eastward at their leading edge along the wave guide at 5-15 degrees east every six hours (as seen in Fig. 3.6) until they reach the end of a storm track belt (Eastern North Pacific, Eastern North Atlantic, India, southwest of Australia and the southern tip of South America). They then slow down or even stall or retrograde (speeds of -10 to +5 degrees per six hours), weaken and either dissipate or reach a new area of high

amplitude flow, and thus, begin a new pulse of intensification and downstream development. This pattern recurs regularly enough to give it a hard definition. A pulse, in this context, is defined as the addition of at least 5 m s^{-1} of WPA after any period of weakening of at least 5 m s^{-1} or at the time of packet formation. Figure 3.8 illustrates a typical pulse cycle by displaying the average eastward movement rate, peak WPI and peak WPA for the 96 hand tracked packets during the beginning, middle and end of a movement pulse along with example images from one such pulse. Note that WPI is strongest during a period of rapid intensification, but that WPA peaks later as the packet is moving eastward. Also note that RWPs, on average, move eastward very slowly during their weakening phase.

Table 3.2 illustrates the number of times this cyclic intensification, movement and weakening occurred for the 96 hand tracked RWPs in this study, as well as some summary statistics on the typical propagation and duration for packets with a given number of burst cycles. Table 3.3 shows the relative position of the dynamic intensification compared to the active packet centroid. About 81% (80 out of 96) of all RWPs burst downstream once or twice, but one Southern Hemisphere track lasted for over 36 days, made three complete revolutions around the hemisphere and repeated the downstream burst cycle seven times. Most dynamic pulses occur over the center of an RWP, but 52 out of 187 hand-counted pulses (about 28%) occurred more than 30 longitude degrees to the east or west of the packet centroid. The majority of pulses occurring west of a centroid that did not result in a trailing split or merge occurred during packet formation. However, most bursts occurring east of the packet centroid occurred after the packet had already formed.

All tracking methods are generally reliable at detecting the propagation of RWPs when that propagation does not result in a merge or split. Errors in track duration are tightly linked to

merging and splitting errors, and each method has different tendencies for splitting and merging errors. Figure 3.9 shows the two most common error sources with the TRACK feature based approach. Because TRACK assumes that individual local maxima can represent a larger spatial object (like an RWP), and a merging script is needed to link features when more than one such maximum is needed to describe an RWP, errors related to deciding where a merger should take place are common. In particular, TRACK produces 15 failed merge errors related to merges, trailing splits or upstream seeder formations, in situations where a pre-existing feature should be given the packet ID of another track approaching from the west (Fig. 3.9a, b). Also, TRACK sees every local maximum of sufficient size (at least 40 grid points) as significant for tracking, whereas the Hybrid techniques apply a prominence threshold to screen out local maxima that are related to more intense nearby peaks in WPA. This causes TRACK to see many more features and thus many more tracks, leading to challenges with mergers of multiple "features" which should probably not be tracked (Fig. 3.9c, d). Figure 3.10 shows the common merging and splitting errors found in the Hybrid tracking techniques. Figures 3.10a and 3.10b show a problem unique to Hybrid 1 involving the sometimes erroneous assumption that the furthest east feature should take possession of an object when a merger is taking place and more than one significant track can claim the merged object. Figures 3.10c and 3.10d show a situation where a trailing split is not properly detected and the tracking identification of the leading track is falsely applied to the trailing (new) packet.

3.4. Wave Packet Dissipation

An RWP is dissipated when no significant local maximum in WPA above the tracking threshold can be found that is in close enough proximity to an established track to continue that

track. Thus, the dissipation point is the last centroid found for each track. A track can end in two different ways (Figs. 3.11 and 3.12). Total dissipation (Fig. 3.11) is the most common end, occurring about 70% of the time (66 out of 96 cases), but an RWP can also merge (Fig 3.12).

Because TRACK treats every significant maximum in WPA as a distinct feature and proper tracking of RWPs requires a separate merging algorithm to account for the many times where one RWP may include multiple significant WPA maxima, this feature-based approach has difficulty handling merges, ending the track arriving from the west in favor of the easternmost (and dying) track – this error occurs 15 times in the seasonal verification period alone. All methods handle total dissipation very well, since no interactions with other RWPs are usually occurring when the dynamics are weakening. Merge errors within the Hybrid tracking schemes are relatively rare when compared with TRACK.

Figure 3.13 shows the performance of each tracking method that compares the best-fitting end point for each track to the hand tracks and uses a bootstrapping technique to give 90% confidence intervals. Here, the deficiencies of TRACK become much more apparent. While H1 and H2 are not statistically different in bias, mean absolute error or spread, TRACK produces twice as much spread in the error in end point location as H2, three times as much bias in the end timing, and twice as much mean absolute error in the end timing and location. In all cases, these differences are statistically significant with 90% confidence. Given these findings, TRACK has been excluded from any further analysis in this thesis.

3.5. Long Lived Wave Packets

The seasonal verification study, which is comprised of two winter seasons chosen at random reveals a few tracks that persisted for as many as 12-25 days and circled the hemisphere

2-3 times before dissipating (Fig. 3.1). Previous research has shown that an individual short wave trough may survive for up to two revolutions around the Northern Hemisphere (Everson et al., 2008); however, some confirmation that these longer tracks really do exist is necessary. Therefore, the 63 (H1 – 20 NH, 43 SH) and 48 (H2 – 11 NH, 37 SH) tracks found by each hybrid method that lasted at least 25 days – documented in Table 3.4 – were extracted from the track database from each method and individually verified using the same hand tracking technique as was performed for seasonal analysis. Note from Table 3.4 that H1 and H2, when combined, found 75 long tracked RWPs, implying significant overlap between the methods. Table 3.4 also reveals that H2 found only four tracks that did not verify as being of sufficient length to qualify for the study (25 days), and two of those four tracks were also found by H1. H1 found far too many tracks in the NH – a major source of tracking errors given the more complex flow regimes in the NH forced by quasi-stationary waves due to topographic barriers like the Rockies and the Tibetan High Plateau.

Table 3.5, a summary of the long-track verification study, demonstrates that the second hybrid scheme is more reliable and more conservative in its estimates of track duration for long lived RWPs than the first. First, when H2 identifies a long tracked event, it is usually correct (90% verification rate). Second, when H1 sees a long tracked event that H2 does not, there is only a 12/27 (44%) chance that this event really survived for at least 25 days. And third, the reason for the apparent problems with over-detection in H1 becomes clear when you look at the types of errors and the frequency of those errors found by each method. A failed split or false merge error would favor an erroneously long-lived RWP, whereas a bogus split or failed merge error would favor a shorter life span. In the 63 long tracks found by H1, the track-lengthening errors are found 59 times versus 21 track-lengthening mistakes found by H2 in 48 long tracks.

As well, 24 track-shortening errors were found by H1 versus 43 found by H2. Given the more conservative track lengths found by H2, we will use this method when discussing the climatology results that follow in chapter 4, but must conclude that RWPs do in fact sometimes travel great distances and survive for a month or more.

CHAPTER 4: Climatology of Rossby Wave Packets

4.1. Intensity and Spatial Distribution

This section describes RWP intensities and their spatial distribution in the northern and southern hemispheres. Figure 4.1 shows the global and hemispheric distributions of all significant RWPs (minimum WPA of 14 m s^{-1}) for all packet times (each packet counted more than once during lifetime) and the maximum WPA during the RWP lifetime (binned by one m s^{-1} intervals). RWPs are very common, with ~6000 packets observed globally from 1979 to 2010 (~200 per year). The weakest significant RWPs are bounded by the minimum tracking threshold, while the most intense RWPs have a WPA of 48-50 m s^{-1}. These strongest RWPs (exceeding 45 m s^{-1}) only occurred roughly once every other year globally, and were more likely in the Northern Hemisphere (19 RWPs with >45 m s^{-1} peak intensity were recorded and 13 of them were in the NH). The average RWP has a mean (median) peak intensity of 27.1 m s^{-1} (23.8 m s^{-1}); however, the average (median) intensity of RWPs at any observing time is only 22.3 m s^{-1} (20.6 m s^{-1}). RWP intensities using all times are skewed towards larger values, making the distributions non-Gaussian. The intensity distribution is less skewed for the most intense time of the RWPs, but there is still a tail towards the strongest events. The 95th percentile in all RWP intensities occurs at 29.7 m s^{-1} and WPA values above this threshold will be referred to throughout the chapter as the "extreme" RWP events.

Figure 4.2 shows the annual spatial climatology of significant and extreme RWPs for the probabilities of exceeding the 14 and 30 m s^{-1} thresholds per 2.5x2.5 degrees latitude-longitude. As expected, the RWP frequency maximum is closely tied to the mid latitude storm track belts of the North Pacific, western Atlantic and east of the southern tip of Africa. However, the

climatology suggests there is a RWP connection of the north Pacific and Atlantic storm tracks as suggested by (Hoskins and Hodges, 2002) and less horizontal variations in RWP frequency in the southern hemisphere than the northern hemisphere, which has been shown in (Trenberth, 1991). Although the Southern Indian Ocean storm track belt is the most active globally when considering all significant RWP activity, with probabilities of > 14 m s^{-1} WPA approaching 50%, the most intense packets occurred more commonly over the North Atlantic, where there is a ~2.5 to 3% chance to produce an extreme RWP, whereas the North Pacific and Southern Indian Ocean storm tracks produce extreme events 2% and 1.5% of the time, respectively. This is likely due to the North Atlantic being the only storm track that receives significant downstream inputs from another active storm track (the North Pacific) and serves as a secondary region of active cyclogenesis, allowing already strong RWPs to become extreme more often. Although the SH does not have topographic barriers and thus its storm track is interconnected and continuous, it also lacks distinct regions of climatologically favored cyclogenesis of the same focus and magnitude as the North Atlantic other than in the vicinity of South Africa.

Figure 4.3 shows the frequency of RWP formation (the first packet centroid listed in a packet track) and dissipation (the last centroid listed) points spatially, as well as the formation points for extreme packets. Glatt and Wirth (2013) found that RWPs most commonly formed at 115-145 E and 100-80 W in the NH. As shown in Fig. 4.3a, however, the most common formation points for RWPs in the NH are at 160 E and 70 W, and the primary reason for this difference is the manner in which starting points are chosen. Our study uses the first packet centroid as the point of formation, whereas Glatt (2013) used the first longitude showing WPA above the tracking threshold. The difference between a packet centroid and the western edge of a packet can be as much as 30-60 degrees in longitude, thus explaining the different results.

Similarly, Glatt and Wirth (2013) found that packets tended to dissipate near the prime meridian (10 W – 10 E) and at 110-130 W, whereas this study finds RWPs dissipating at 50-20 W and 120-150 W. Glatt and Wirth (2013) use the last longitude showing significant WPA after smoothing, whereas we use the last centroid. Figure 4.3c highlights the origin of the enhanced probabilities of extreme packets over the northern Atlantic. Such extreme packets rarely form in the North Atlantic. Rather, they form in the North Pacific more than 70% of the time based on a simple counting of all extreme packet cases in the Northern Hemisphere.

RWPs exhibit a significant seasonal cycle. Figure 4.4 shows the frequency of significant and extreme packet formation by month in the NH and SH, as well as in the North Atlantic (240-360 E, 10-80 N) and North Pacific (120-240 E, 10-80 N) basins separately. While both hemispheres have a notable maximum in RWP activity in their respective winter months, the reduction during the NH (JJA) summer (an 80% loss in total activity) is far more pronounced than Austral (DJF) summer (a ~40 drop in activity). Meanwhile, extreme packets do not occur in the NH summer, while there are extreme events in the SH all year, without much variation in their frequency. The continued presence of strong baroclinicity in the vicinity of the circumpolar jet near Antarctica favors a relatively active SH storm track and RWPs even in Austral summer (DJF). The North Pacific and North Atlantic regions are compared to the Northern Hemisphere as a whole in Fig. 4.4c, d. While the North Atlantic experiences a clear peak in RWP formation frequency in January and follows a smooth seasonal cycle, as does the NH as a whole, the North Pacific experiences a slight depression in formations during January and February, making its' formation frequency peak broader, extending from September to April. This midwinter suppression of RWP activity is even more apparent when RWP activity is viewed spatially, and has significant support in the literature (Nakamura, 1992).

Figure 4.5 shows mean NH RWP activity (defined as the mean of the difference between gridded WPA and the minimum tracking threshold, where all values below the threshold are set to zero) by month (October, January, April and July). The general pattern of increasing RWP activity in Boreal winter and nearly zero activity in summer is apparent, but the decrease in activity in the North Pacific during the midwinter months (especially January) and heightened activity in the transition seasons of fall and spring are more apparent here than in Fig. 4.4. This suggests that activity increases in the Pacific during the transition seasons are linked to wave packet intensity, rather than frequency. The other change during the midwinter months is the development of a split storm track near the Tibetan High Plateau, with some RWP activity south of Tibet in January that is not present during other months. This is likely related to the general equatorward drift of the jet stream during winter, as modeled in (Chang and Zurita-Gotor, 2007).

Figure 4.6 spatially examines the monthly climatology of mean WPA for southern hemisphere. Unlike the NH, the SH remains relatively active all year and does not exhibit an equatorward shift of the entire storm track during the winter months. For each month, the most active area for RWP genesis and overall activity is downwind of South Africa. The RWPs are most active around the SH during the Austral Spring (September), but extreme packets are most likely during Austral Fall (April), and, as expected, this means Austral Fall shows an increase in activity. Trenberth (1991) found that the SH storm track became narrow and very focused, with large baroclinic gradients in Austral fall, and that those gradients decreased during winter, as variances in 300 hPa meridional winds increased equatorward while remaining elevated along 50 S. As a result, the only change to the pattern in Austral Winter is a split in RWP activity in the South Pacific basin just south of Australia, which is likely related to the climatologically favored jet that develops downwind of Australia in the winter months (Trenberth, 1991).

4.2) The Climatology of Wave Packet Characteristics

Additional wave packet characteristics such as duration, propagation, speed of movement and size were evaluated. Figure 4.7 shows the duration (days, binned in one-day increments) and propagation (longitude degrees eastward, binned in 60 degree increments beginning at the minimum propagation distance of 40 degrees eastward) of significant RWPs in the NH and SH. NH packets have a shorter typical life span, lasting for an average of 5.8 days and traveling 119 degrees eastward compared to 7.9 days and 152 degrees eastward in the SH, and a bootstrap comparison of NH and SH RWPs using a random sampling of 500 packets from each hemisphere and resampling 10,000 times reveals that, although the difference in duration is not significant, the difference in propagation is (to >90% confidence, see Table 4.1). About 70% of all RWPs last for fewer than 8 days, but longer-lived packets in the NH survived more than 25 and as many as 38 days (such packets occurring about once every other year, and limited to the cool season months) and traveled as far as 800 degrees eastward (over two complete revolutions around the hemisphere), whereas the longest SH packets lasted for up to 49 days (such packets occurring just over once per year and throughout the calendar) and traveled as far as 1500 degree eastward (nearly four complete revolutions). Every long-tracked wave packet in the NH began in the Western North Pacific, but there is no pattern to their formation in the SH.

It is important to note a few differences between this study and the recent climatology of RWPs based on Hovmoller diagrams (Glatt and Wirth, 2013). Glatt found the longest RWP durations between 1957 and 2002 were roughly 30 days, but occurred on the order of once every hundred months, and RWPs with lifetimes of as little as ten days were still uncommon (one every five months). This study finds ten-day RWPs occurring two to three times per month and

packets that lasted thirty days occurring about once every twelve months. This difference is likely caused by the decision of Glatt and Wirth (2013) to use Zimin et al. (2003), rather than Zimin et al. (2006) as their basis for calculating WPA. Glatt and Wirth (2013) noted that areas of large WPA were often erroneously split even within one large RWP due to the presence of broad ridges that caused strong meridional winds to appear in trough/ridge couplets separated by great distances. Tracking WPA using 28-day running mean streamlines corrects for this problem as shown by Zimin et al. (2006).

Figure 4.8 compares the average zonal velocities of RWP centroids (within 10 degrees of a point and for all grid points containing at least 100 observed packet centroids to avoid values heavily biased by a few extreme cases) to the winter (DJF) mean zonal wind speeds at 300 hPa. The regions of highest RWP zonal velocity (25-40 m s^{-1}) are areas just upwind of climatologically favored 300 hPa zonal jets. These storm track entrance regions are frequently associated with the pulse-like movement described in chapter 3 as existing wave packets transfer their EKE into regions favoring rapid cyclogenesis, creating an apparent increase in zonal RWP propagation speed. Outside of these regions where RWPs can be seen to pulse rapidly eastward, RWPs move eastward at 15-25 m s^{-1} in regions collocated with climatologically favored positions of the strongest jets, and slower (10-15 m s^{-1}) at the ends of storm tracks, over large mountain ranges, and in areas that favor blocked flow regimes (e.g. South of Alaska, Greenland, and Australia, over the Rocky Mountains, and just upwind of the Tibetan High Plateau). Overall, RWPs move at about the same speed as the climatological zonal jets.

Figure 4.9 highlights how some of these characteristics of RWPs are related to each other by correlating two characteristics. RWP intensity is correlated with RWP size with a coefficient of 0.75 (Fig. 4.9a), revealing that intense wave packets tend to be larger than weak packets.

RWP duration (in 6-hourly time steps) is correlated with RWP propagation in longitude degrees (Fig. 4.9b), with a statistically significant positive correlation (r = 0.73). The long-lived packets also traveled reliably the furthest east. RWP intensity is correlated with RWP duration (Fig. 4.9c) with a positive correlation (r=0.52), meaning that stronger packets tend to last longer (and by extension travel further). RWP intensity has no correlation with 18-hour-averaged RWP centroid zonal velocity (Fig. 4.9d), suggesting that RWP velocities depend more on the jet wind speed, not on other RWP characteristics.

4.3. Interannual Variability of Wave Packets

Wave packet activity has relatively large interannual variability. Figure 4.10 shows significant and extreme wave packet counts in the NH and SH by year, as well as in the North Atlantic and North Pacific basins. In no region studied has there been any significant trend in the frequency of significant or extreme wave packet formation. Note that the interannual variability in net wave packet activity is as large as 25% of the mean activity value in each basin and in the hemispheres overall. At first glance, there seems to be little pattern in the variability in formation frequency.

To further explore the possible sources of interannual variability in RWPs, figure 4.11 highlights the annual RWP activity volume (found by multiplying each packet's size with its mean WPA magnitude and attributing each packet to a basin based on its centroid position) in the NH, SH, North Pacific (120-240 E, 10-80 N), and North American/Atlantic (240-360 E, 10-80 N) regions during the midwinter months (DJF) and Boreal Winter activity in the Eurasian (0-120 E, 10-80 N), North Pacific and North Atlantic regions. The SH has experienced a steady climb in net RWP activity volume throughout the modern satellite era (a gain of roughly 15% in

average annual activity volume in the 2000s vs. the 1980s); however, it is not clear whether this is due to the increasing reliability of NCAR reanalysis wind speeds(Chang and Guo, 2008), or whether there is some real climate shift in progress in the SH. The lack of a similar gain in activity in the NH casts doubt on the veracity of the SH trend. Figure 4.12 shows a simple correlation between the activity volume values shown in Fig 4.11 and the formation frequencies for significant and extreme RWPs shown in Fig 4.10 for NH and SH RWPs. There is no significant correlation, suggesting that some seasons may produce many weaker packets (and low overall activity volume), while others produce a few stronger packets (and higher activity volume). No region shows any significant correlation to any other region when comparing either activity volume or formation frequency, annually or in just the midwinter months. A further examination of the sources of RWP variability is required.

One theory advanced by previous research (discussed in the introduction to this study) is that large scale flow regimes defined by teleconnective indices might explain some portion of the variability in RWP activity (and vice versa). A manual review of the most and least active seasons revealed no pattern in El Nino Southern Oscillation (ENSO), the Arctic Oscillation (AO), the Quasi-biennial Oscillation (QBO), or the Pacific-North American Pattern (PNA) that reliably explains the variability in RWP formation either regionally or overall. For example, a quick look at the MEI index during the five most and least active NH winter seasons reveals both extreme El Nino (1998, 1987) and extreme La Nina (2000) seasons in the active column, and the same is true of the inactive years (El Nino in 1983, 1993, La Nina in 1999). It is much the same with any other index. The active and inactive seasons cover the entire spectrum of AO outcomes, and can occur during any phase of the QBO. However, two of these possible influences (the AO and ENSO) will be discussed in more detail below.

It is hypothesized that shorter-term variations in the large scale flow regimes are the biggest driver of RWP variability. To test this further, several teleconnective indices are examined in order to determine if there is a common pattern in RWP activity associated with a particular large scale flow regime. The best-known climate signal is ENSO, and Figure 4.13 shows the role of ENSO in varying the distribution of wave packet activity in the NH. The three-month average values of the multivariate ENSO index (MEI) were used to select El Nino and La Nina seasons (MEI exceeding 0.5 or less than -0.5 respectively). 4.13a shows the normal Boreal winter (DJF) RWP activity during ENSO neutral conditions ($-0.5 < MEI < 0.5$). 4.13b shows the difference between ENSO neutral RWP activity and El Nino conditions (positive values are regions where activity increases during El Nino years). Note the increased activity in the southern North Pacific near and east of Hawaii, the slight increase in activity over Canada and Alaska and the general reduction of RWP activity in the rest of the mid-latitude storm track belts. 4.13c is identical to 4.13b except it shows changes in activity during La Nina seasons. The main difference appears to be a general increase in RWP activity throughout the Pacific, and a reduction of activity in much of the Atlantic basin, rather than a shift in the tracks.

Since we could find no reliable connection between the MEI and RWP formation frequency, the two remaining potential explanations for these changes are the intensity of the RWPs and their typical tracks. Clearly, El Nino years induce a more active southern North Pacific storm track, but the main change seems to be a reduction in RWP intensity, since big losses in activity in the storm tracks are not replaced with large gains elsewhere. El Nino favors a split flow regime over the Eastern Pacific, with an active subtropical jet (characterized by frequent weak eddies) and a tendency toward higher than normal heights across much of the North Pacific and Central and Northern North America. This should lead to a decrease in

baroclinicity in the Eastern North Pacific and Atlantic storm tracks, with a corresponding increase in baroclinicity along the subtropical jet, yielding the reduced RWP activity found here in the primary storm tracks and increased activity near Hawaii, as suggested by (Orlanski, 2005). La Nina, meanwhile, produces greatly enhanced activity over the Eastern North Pacific, likely due to a stronger Pacific jet (REF). The same active Pacific jet serves to flood North America with westerly winds and Pacific air, leading to less intrusion of arctic air over Canada and thus robbing the Atlantic storm track of baroclinicity and producing reduced RWP activity.

Another major influence in winter flow regimes and storm activity is the Arctic Oscillation. Using single-point correlation analysis, one can explore the role of the AO in altering the position and intensity of common RWP tracks, and potentially even the role of wave packets in altering the AO. Figure 4.14a shows the significant ($p > 0.95$) correlation between WPA anomaly and the five-day-smoothed daily AO Index (daily AO Index data provided by the University of Washington and smoothed using a running five-day average). To avoid the problem of oversampling covariate data, 750 dates were sampled randomly (out of a possible 7752 days in the cool season of SONDJFMA from 1979-2010). Positive regions indicate positive correlations between the smoothed AO Index and WPA anomaly (meaning that positive AO conditions favor increased WPA). When the AO is positive there is increased activity in the main storm track regions throughout the NH, especially the Pacific and Eurasian regions; however, though the correlations are statistically significant ($p < 0.05$), they are also very low magnitude, explaining between 1 and 5% of the variance in WPA anomaly. When the AO is negative, these regions become less active and regions favoring blocking and wave breaking (e.g. Alaska, Greenland and Siberia) become more active. The linkage between wave packets and changes in the AO was also explored by relating the five-day rate-of-change in the five-day-

smoothed daily AO Index with WPA anomaly (Fig. 4.14b). During periods of rapidly declining AO, the Southern North Pacific near Japan and the region near Greenland become more active, whereas Eurasia and Western North America become more active when the AO is rapidly rising; and, once again, these correlations explain just 1-5% of the variance in WPA anomaly.

In figure 4.15, all events between November and March where the AO Index began at greater than 1.0, fell at least 3 standard deviations within 10 days, and by the 11^{th} day it was below -1.0 were found (56 cases in all). The day where the AO Index declined below zero was the central reference date, and then the WPA and probability of WPA exceeding 14 m s^{-1} were composited. A robust wave packet signal appears in the Central and East Pacific (day -5 from the time of AO transition, as shown in 4.15a) and propagates into the western and northern Atlantic (4.15b) before dissipating in a blocked flow regime (day -1, Fig. 4.15c,d), as shown in the red (probabilities significant increased over NDJFM mean) and blue (probabilities decreased) contours. While not conclusive, this does strongly suggest that wave packets may play an important role in a rapid decrease in the AO, as originally suggested by (Franzke, 2004) for the North Atlantic Oscillation – a teleconnection frequently related to the NAM/AO. To confirm the results of the composite, each event was viewed and the significant RWPs tracked. In 56 cases, an extreme Pacific RWP (>30 m s-1) occurred 29 times within the first five days of the composite. Only 8 cases failed to produce any significant RWP activity in the Pacific, suggesting that the strongest wave packets are the most likely to alter the flow regime and that the flow regime is unlikely to change rapidly without the involvement of RWP activity. A similar composite was also produced for periods where the AO rapidly rose (not depicted), and no robust RWP signal was found.

The AO is not the only regional teleconnection pattern to have a significant impact on RWP tracks. The PNA is also correlated with the WPA anomaly (Fig. 4.16). Here, the PNA was calculated using the varimax-rotated fourth EOF mode drawn from 300 hPa geopotential height anomalies between 1979 and 2010 throughout the entire Northern Hemisphere (this mode reveals all of the known centers of action associated with the PNA). The PNA appears to produce the best correlations in the extreme north and west Pacific and Alaskan regions, as well as Central Europe. Specifically; as the PNA becomes more negative, high latitude blocking increases near Alaska and Siberia, leading to increased RWP activity in those regions, while increased RWP activity is found in Europe during PNA+ conditions.

One final question remains regarding the interannual variability of wave packets. Has there been a significant change in wave packet tracks, intensity or frequency related to longer-term climate shifts or decadal cycles like the Pacific Decadal Oscillation or the Atlantic Multidecadal Oscillation? Figure 4.17 shows the rate of change in mean RWP activity obtained from single-point linear regressions between annual net activity (by grid point) and year taken from 1979-2010. The values plotted are the slope of the regression line at each grid point. A value of 0.1 means that the mean RWP activity has increased by 0.1 m s^{-1} yr^{-1}, meaning that in the thirty years surveyed here, the mean WPA has increased by ~3 m s^{-1}. Given that the standard deviation of mean RWP activity in the storm tracks is 4-5 m s-1, this represents a noticeable shift. There has been a poleward shift in the North Pacific storm track; however, the Atlantic shows no such trend. For both observations, there is an important caveat that this is only 32 years of data. The North Pacific signal, for example, could be related to the warm phase of the Pacific Decadal Oscillation which happened to peak in the 1990s after beginning the common satellite era in the cool phase. Figure 4.17 also makes it clear that there has not been an increase

in the intensity of any of the NH storm tracks, since any positive changes in WPA activity are balanced by negative changes in other parts of the world.

CHAPTER 5: Discussion

Chapter 4 of this thesis described a detailed climatology of RWPs based on a particular track database found using a series of subjective parameters to inform a tracking algorithm. It is necessary to ask: how robust are the results from that climatology to the subjectivity inherent in any algorithm design? From Table 2.1, there are six categories of subjective parameters that impact all tracking methods (other parameters are not common to all methods and such biases would have been revealed in the verification results shown in Chapter 3). Those parameters are: minimum tracking threshold, minimum object size, the spatial and temporal filters used to smooth the WPA data prior to tracking, the size of the box used to detect potential candidates for track continuation and the minimum intensity, propagation distance and duration required for an RWP to count as significant for the climatology. This section explores those six parameters.

The minimum tracking threshold, as noted in the introduction, is necessarily a subjective criterion because no clear physical or statistical reason exists to make the cut between which WPA values represent the RWP signal and which are just noise. Any WPA threshold represents a compromise between one's desire to capture all of the real packets and one's desire not to capture and track WPA maxima that do not propagate like RWPs because they are not real signals. At any given time, roughly two thirds of the grid points in a globally gridded plot of WPA are less than 10 m s^{-1}, and the variations in those low magnitude values do not track coherently. A number of different minimum tracking thresholds were tested before selecting 14 m s^{-1} for use in the climatology. Fig. 5.1 shows the impact of varying the minimum tracking threshold on the climatological distribution of RWP duration. When a minimum tracking threshold of 20 m s^{-1} was used (only the very robust WPA signals were thus being tracked), only

3,756 significant packets were found in the common satellite era, and of those packets, fully 22% lasted just 2-3 days and ~74% of all packets lasted no more than 5 days (average lifespan: 4.0 days). When 10 m s^{-1} was chosen, 6,199 significant packets were found; but those packets tended to last considerably longer on average (8.9 day mean), and only ~51% of all packets found had a lifespan of 5 days or less. With 14 m s-1 as the threshold, 5,929 RWPs were found, lasting an average of 6.7 days, with ~58% lasting five days or less. The hand verification period revealed a mean duration of 6.8 days for hand-tracked dynamic signals and 47 of 96 cases (48%) lasted five days or less, and a similar distribution was found in the calibration period (JAN-MAR, 2009 and JAN 2010).

Using January, 2010 data, one-month verification studies were conducted at 10, 12, 14, 15 and 20 m s^{-1} thresholds. Table 5.1 shows the basic error statistics for this small testing window. In January of 2010, 15 significant wave packets were observed using WPI. At both 10 and 12 m s-1 thresholds, Hybrid 2 tracking found 17 significant wave packets, but in both cases, the common problems were false detection of non-significant packets (lacking WPI signals that would suggest that they were real packets) countered by false merges of unrelated significant packets. At the lowest two tracking thresholds, 5 and 3 false detections were found (for 10 and 12 m s-1 respectively) along with 7 and 4 false merges. These error rates are not acceptable. At the other extreme, when 20 m s-1 was used as a tracking threshold, only 11 significant tracks were found, and even that number is too optimistic, because 3 of those tracks were produced by missed merges for what should have been related objects, where the WPA within the packet dipped below 20 m s-1 for a time while WPI remained elevated. Seven out of 15 tracks were missed entirely. 14 and 15 m s-1 thresholds were not appreciably different, so the lowest threshold was selected in order to capture the most significant packets.

The choice of spatial and temporal filter plays a key role in stabilizing RWP tracks and reducing tracking errors; however, such differences can rarely be seen through an inspection of aggregate climatological statistics (duration, propagation, spatial coverage, formation frequency), as tracking errors tend to occur where wave packets are most likely to form and dissipate, and the track shortening and track lengthening errors tend to cancel each other out to some degree. The best way to evaluate the impact of various spatial WPA filtering techniques on RWP tracking is with hand track verification. Here, JAN-MAR, 2009 WPA data was filtered at four different wavelengths: T15 (very aggressive smoothing), T21, T28 and T42 (very limited filtering). Those verification results may be found in Table 5.2.

During this three month period, there were 47 significant RWPs based on hand tracking of WPI. Using a very aggressive filter (T15), the tendency is toward an increased number of false merges and missed splits, yielding a fairly high (~30%) miss rate, while false detections still occur at normal rates (due to missed merges, primarily). With a very minimal filter (T42), and even a modest (T28) filter, the main issue is too many features being tracked as distinct, yielding too many tracks, and a large number of missed merges and false splits (such track shortening errors leading to 25 and 14 false detections – an unacceptable error rate). This resulted in our selected of T21 as the best spatial filter for the climatology.

The purpose of the temporal filter is to stabilize the internal structures of RWPs so that individual local maxima in WPA propagate more smoothly and are less prone to jumping westward and eastward erratically while the packet, as a whole, moves smoothly eastward. To justify the use of the temporal filter, a correlative study was used to compare a local maximum in WPA with WPI in the same region. A local WPA max and the surrounding grid points within 5 degrees (25 grid points in all) were chosen and the WPA and WPI values averaged. This was

done for WPA and WPI that had a range of temporal filter widths, and the results are shown in Table 5.3. The correlation between WPA and WPI improves with increasing temporal filter width until one reaches 24 hours. After 24 hours, the correlation does not improve. One argument is that RWPs are the result of a cumulative transfer of energy that takes time to impact the meridional wind field. If the goal is to track a variable that best represents the real movement of this energy, then a temporal filter of 24 hours (the least aggressive filter necessary to achieve the best results) is necessary to reflect the cumulative nature of RWP activity.

The parameters used to define which tracked features constitute significant RWPs to be included in the climatology are best explored spatially. Figure 5.3 shows the impact on track density (the frequency of significant track points at every grid point during the common satellite era) of altering the minimum lifetime RWP intensity required for significance. The higher you set the lifetime intensity threshold, the lower are the frequencies, but the spatial patterns do not change appreciably. This implies that using any sort of intensity filter beyond the minimum tracking threshold is likely throwing out real information without also throwing out noise. Figure 5.4 shows the impact on track density of altering the threshold for minimum propagation distance. Although a drop in track density is obvious when a strict (80 degree) threshold is used, the track density climatology does not appear sensitive to the use of a 40 degree filter, as compared to less aggressive trimming of the track data. Given that we're interested in following robust and propagating wave packets, the 40 degree cut-off was chosen for the climatology. Finally, Figure 5.5 shows the impact of altering the duration threshold for significance. There seems to be little change in the track density distribution spatially (other than a general increase in frequency with decreasing duration threshold), suggesting that the climatology results are not sensitive to this parameter, other than altering the number of objects being counted as significant.

The 2-day duration minimum eliminates a mere 19% of the total track points found by Hybrid 2, while eliminating 62% of all distinct RWP tracks. Using a lower threshold can't possibly save much actual data (as not much has been lost), but it can introduce significant clutter into track statistics (especially things like formation and dissipation frequencies). A one-day minimum produces track formations all over the storm tracks, as shown in Figure 5.6, comparing formation frequencies with 1-day and 2-day minimum tracking thresholds, implying that we're not adding more useful data by allowing shorter tracks.

A final note is required regarding the minimum object size used in tracking and the size of the box used for track continuity checks. The vast majority of all local maxima in WPA above the minimum tracking threshold belong to continuous objects that are very large (many hundreds of grid points). Simply removing all objects that do not reach at least 200 grid points in areal coverage yields only a 2% reduction in the total number of track points identified by the Hybrid significant object detection algorithm. A change this small cannot significantly impact the climatology, and no justification exists for removing objects any larger than 200 grid points. We therefore conclude that the climatology is not sensitive to the minimum object size, and use a very liberal threshold of 40 grid points to remove very small objects that do not need to be tracked. As for the continuity search box, it is entirely possible that further study on the impacts of this parameter might reveal a more ideal alignment. A manual review of the calibration period showed very obvious error patterns using other configurations, but no rigorous testing has yet been done to confirm the search box parameter as optimized.

CHAPTER 6: Conclusions

This research began with several motivating questions, the first and foremost among them being whether it was possible to reliably track wave packets and form a robust climatological database of those tracks. In chapter 3 of this thesis, it was proven that wave packets could be reliably tracked when the right combination of calibrated assumptions and tracking techniques were applied to WPA data. It was found that tracking based on a hybrid of existing object and point-based techniques significantly outperformed point-based tracking alone, producing 40% fewer false track detections, yielding less error-prone formation and dissipation points (error showing significantly less case by case spread) and better estimates of a track's longevity and propagation distance. Using either hybrid tracking algorithm produces ~90% detection success, with ~20% false alarm rates, largely from missed track merges and false track splitting. The second hybrid tracking scheme was found to be more conservative in its estimates of track duration when examining cases of extreme (> 25 day) duration. While both hybrid schemes perform well with normal packets, H2 is less likely to evince track lengthening errors that lead to overestimates of track duration in extreme cases. H2 finds about 80% of all hand-verified long tracked events, and over 90% of the events it does find are verified. H1 has a similar detection rate, but more than half (15 out of 27) of the tracks it finds that H2 does not are not verified.

RWPs were found to be tightly linked to climatologically favored storm track belts in the North Pacific, North Atlantic, and East of South Africa in the SH. The NH seasonal cycle was found to be more significant than the SH seasonal cycle, as RWP activity in the NH almost completely vanishes during the summer months (JJA), while RWPs continue forming regularly

in the SH summer (DJF) due to the constant presence of the circumpolar jet near Antarctica. Extreme RWPs (> 30 m s^{-1} maximum lifetime intensity) peak in November and January in the NH and April in the SH, with the bimodal distribution of NH extreme RWPs likely related to peaks in the two different ocean basins. The North Pacific sees a peak in activity in November and March/April, with a mid-winter suppression of RWP activity present in December and January, while the North Atlantic hits peak RWP activity in January. In the SH, RWPs are most frequent in September, and the South Pacific storm track splits into a Northern and Southern branch downwind of Australia during Austral summer.

The characteristics of RWPs were also studied and compared. RWPs were found to have a range of intensities showing a significant right skew with a mean centroid intensity of 22 m s^{-1}, but peak intensities as high as 50 m s^{-1} possible in rare cases. RWPs last an average of 5.8 days in the NH and 7.8 days in the SH, traveling 119 degrees eastward (NH) and 151 degrees (SH) respectively. The difference in propagation distance was found to be statistically significant after bootstrapping. RWPs in the SH travel faster than their NH counterparts overall, with typical speeds of 20-25 m s^{-1} in the SH and 15-20 m s^{-1} in the NH. However, in both hemispheres, the fastest moving packets were found just upstream of jet entrance regions, where RWP energy can be seen to rapidly pulse eastward when it encounters new cyclogenesis. Typical RWP zonal velocities were found to be in line with the mean zonal winds at 300 hPa. It was found that intense wave packets also tended to be larger than weak packets, long lived packets tended to travel the furthest eastward and intense packets tended to last the longest, all with statistically significant positive correlations. On the other hand, no relationship between RWP zonal velocity and any of the other physical parameters was found, suggesting that RWPs move at speeds governed by the large scale flow, not by their internal structure.

RWPs were also found to have significant interannual variability, with RWP activity volume ranging by as much as 25% from year to year. This variability was not readily explained by seasonal teleconnective indices like ENSO, the AO or the PNA. However, each of those teleconnection patterns were found to have a statistically significant correlation with spatial changes in RWP activity in the NH winter months. El Nino winters were found to suppress RWP activity in the primary storm tracks while not suppressing RWP formation frequency, suggesting that packets were simply weaker (by as much as 1 m s^{-1} on average). El Nino conditions also favored a slight increase in activity near Alaska in the North and Hawaii in the South, hinting at the tendency for the Pacific jet to become split with an active, but mostly zonal southern jet, and higher than normal heights across northern North America. La Nina winters also suppressed the North Atlantic storm track, especially north of 40 N, however, they significantly enhanced the North Pacific storm track. The AO, as expected, plays a key role in RWP activity in the storm tracks, with positive AO conditions favoring high activity in all of the storm tracks, while negative AO conditions favor increased RWP activity in regions connected with high amplitude blocking (Greenland, Alaska and Siberia, e.g.). The PNA was more of a local influence, primarily modulating RWP tracks in the NW Pacific (Siberia and Alaska). PNA- conditions favored increased RWP activity in those regions, while PNA+ conditions favored increased activity over Central Europe.

The question has also been asked: do RWPs play any role in changing the large scale flow regime? The AO was used to illustrate that RWPs do indeed play a key role in regime change. The 56 events where the AO rapidly dropped from a high of greater than 1 standard deviation above normal to a low of greater than 1 standard deviation below normal in ten days or less were composited, centered around the date where the AO cross the zero line, yielding very

interesting results. A robust (statistically significant) RWP-like enhancement in the probabilities of WPA exceeding the minimum tracking threshold can be seen to propagate from the eastern Pacific (day -5) to the Western Atlantic and SE US (day -3) to the North Atlantic (in the form of an apparent blocking regime at day -1). In fact, of 56 cases, 29 included extreme RWPs somewhere in the Pacific basin at day -5, while only 9 were devoid of any significant RWPs. This strongly suggests that a rapid drop in the AO is, at the very least, unlikely without the involvement of RWP activity in the Pacific, and is more likely with more intense RWPs.

This research also demonstrates, using a variety of sensitivity tests and short verification studies, that the climatological findings in chapter 4 are very robust to the subjective criteria used to inform the hybrid tracking technique. The basic parameters used to build the hybrid algorithm, including the 14 m s-1 minimum tracking threshold, the 40 grid point minimum object size, the T21 spectral filtering and 24-hour temporal filter used to smooth the raw WPA data, and the minimum propagation and duration requirements for a track to count as significant toward the climatology, when combined, capture about 80% of all significant WPA maxima within a significant wave packet. Changes in those variables yielded minimal changes in the distribution of RWP tracks globally, unless those constraints were made too strict. A minimum tracking threshold higher than 15 m s-1 appears to deny good track data without significantly reducing noise, and the same pattern holds true for the minimum duration, propagation and lifetime packet intensity criteria. High confidence may be placed in the spatial tracking data, the data on RWP formation, dissipation, duration, and propagation, including the interannual variability, seasonal cycles and relationships between RWPs and teleconnection patterns.

The next logical step for modelers and dynamicists would be to apply similar tracking techniques to RWPs forecasted by GCMs and NWP models to investigate the similarities and

differences between the observed RWP climatology and RWPs produced in the modeled world. Preliminary research has strongly suggested that model resolution is very important in RWP forecasting, with the GEFS doing far worse probabilistically immediately after the resolution in the model is dropped at day 8 in the forecast period. Given the importance of RWPs to the inherent predictability of cyclones, it is incumbent in the modeling community to use this research to better understand the strengths and limitations of current NWP models and GCMs.

REFERENCES

Altenhoff, A.M., Martius, O., Croci-Maspoli, M., Schwierz, C. and Davies, H.C., 2008. Linkage of atmospheric blocks and synoptic-scale Rossby waves: A climatological analysis. Tellus Series a-Dynamic Meteorology and Oceanography, 60(1): 1053-1063.

Anderson, J.R. and Graykum, J.R., 1989. A Diagnostic Study of Pacific Basin Circulation Regimes as Determined from Extratropical Cyclone Tracks. Monthly Weather Review, 117(12): 2672-2686.

Anwender, D., Harr, P.A. and Jones, S.C., 2008. Predictability Associated with the Downstream Impacts of the Extratropical Transition of Tropical Cyclones: Case Studies. Monthly Weather Review, 136(9): 3226-3247.

Archambault, H.M., Keyser, D. and Bosart, L.F., 2010. Relationships between Large-Scale Regime Transitions and Major Cool-Season Precipitation Events in the Northeastern United States. Monthly Weather Review, 138(9): 3454-3473.

Arnaud, Y., Desbois, M. and Maizi, J., 1992. Automatic Tracking and Characterization of African Convective Systems on Meteosat Pictures. Journal of Applied Meteorology, 31(5): 443-451.

Blackmon, M.L., Lee, Y.H. and Wallace, J.M., 1984. Horizontal Structure of 500 mb Height Fluctuations with Long, Intermediate and Short Time Scales. Journal of the Atmospheric Sciences, 41(6): 961-980.

Brennan, M.J. and Lackmann, G.M., 2005. The Influence of Incipient Latent Heat Release on the Precipitation Distribution of the 24–25 January 2000 U.S. East Coast Cyclone. Monthly Weather Review, 133(7): 1913-1937.

Cassity, M.M. and Colgan, S.G., 1973. An Automated Objective Technique For Constructing Tropical Cyclone Best Tracks. Monthly Weather Review, 101(11): 824-829.

Chang, E.K.M., 1999. Characteristics of wave packets in the upper troposphere. Part II: Seasonal and hemispheric variations. Journal of the Atmospheric Sciences, 56(11): 1729-1747.

Chang, E.K.M., 2001. The structure of baroclinic wave packets. Journal of the Atmospheric Sciences, 58(13): 1694-1713.

Chang, E.K.M., 2005. The role of wave packets in wave-mean flow interactions during Southern Hemisphere summer. Journal of the Atmospheric Sciences, 62(7): 2467-2483.

Chang, E.K.M. and Guo, Y., 2008. Impacts of Assimilation of Satellite and Rawinsonde Observations on Southern Hemisphere Baroclinic Wave Activity in the NCEP–NCAR Reanalysis. Journal of Climate, 21(13): 3290-3309.

Chang, E.K.M. and Orlanski, I., 1993. On the Dynamics of a Storm Track. Journal of the Atmospheric Sciences, 50(7): 999-1015.

Chang, E.K.M. and Zurita-Gotor, P., 2007. Simulating the Seasonal Cycle of the Northern Hemisphere Storm Tracks Using Idealized Nonlinear Storm-Track Models. Journal of the Atmospheric Sciences, 64(7): 2309-2331.

Charles, M.E. and Colle, B.A., 2009a. Verification of Extratropical Cyclones within the NCEP Operational Models. Part I: Analysis Errors and Short-Term NAM and GFS Forecasts. Weather and Forecasting, 24(5): 1173-1190.

Charles, M.E. and Colle, B.A., 2009b. Verification of Extratropical Cyclones within the NCEP Operational Models. Part II: The Short-Range Ensemble Forecast System. Weather and Forecasting, 24(5): 1191-1214.

Cordeira, J.M. and Bozart, L.F., 2011. Cyclone Interactions and Evolutions during the "Perfect Storms" of Late October and Early November 1991. Monthly Weather Review, 139(6): 1683-1707.

Davis, C., Brown, B. and Bullock, R., 2006. Object-based verification of precipitation forecasts. Part I: Methodology and application to mesoscale rain areas. Monthly Weather Review, 134(7): 1772-1784.

Endlich, R.M. and Wolf, D.E., 1981. Automatic Cloud Tracking Applied to Goes and Meteosat Observations. Journal of Applied Meteorology, 20(3): 309-319.

Everson, P.D., Gan, M.A. and Rao, V.B., 2008. An Objective Study of 500-hPa Moving Troughs in the Southern Hemisphere. Monthly Weather Review, 136(6): 2186-2200.

Feldstein, S.B. and Franzke, C., 2006. Are the North Atlantic Oscillation and the Northern Annular Mode Distinguishable? Journal of the Atmospheric Sciences, 63(11): 2915-2930.

Franzke, C., 2004. Is the North Atlantic Oscillation a Breaking Wave? Journal of the Atmospheric Sciences, 61(2): 145-160.

Froude, L.S.R., 2009. Regional Differences in the Prediction of Extratropical Cyclones by the ECMWF Ensemble Prediction System. Monthly Weather Review, 137(3): 893-911.

Glatt, I. and Wirth, V., 2013. Identifying Rossby Wave Trains and Quantifying their Properties. Quarterly Journal of the Royal Meteorological Society, 139(January, 2013): Accepted for Publication.

Hakim, G.J., 2003. Developing wave packets in the North Pacific storm track. Monthly Weather Review, 131(11): 2824-2837.

Haraguchi, P.Y., 1967. Accuracy of Weather Satellite Estimates of Tropical Cyclone Locations and Maximum Wind Speeds in the Western Pacific. Journal of Applied Meteorology, 6(4): 731-739.

Harr, P.A. and Dea, J.M., 2009. Downstream Development Associated with the Extratropical Transition of Tropical Cyclones over the Western North Pacific. Monthly Weather Review, 137(4): 1295-1319.

Hodges, K., 1994. A General Method for Tracking Analysis and its Application to Meteorological Data. Monthly Weather Review, 122(11): 2573-2586.

Holton, J., 2004. An Introduction to Dynamic Meteoroogy. Elsevier Academic Press, Seattle, WA.

Hoskins, B.J. and Hodges, K.I., 2002. New perspectives on the Northern Hemisphere winter storm tracks. Journal of the Atmospheric Sciences, 59(6): 1041-1061.

Hoskins, B.J. and Hodges, K.I., 2005. A new perspective on Southern Hemisphere storm tracks. Journal of Climate, 18(20): 4108-4129.

Hovmoller, E., 1949. The Trough-and-Ridge Diagram. Tellus Series a-Dynamic Meteorology and Oceanography, 1: 62-66.

Kalnay, E. et al., 1996. The NCEP/NCAR 40-year reanalysis project. Bulletin of the American Meteorological Society, 77(3): 437-471.

Kaspi, Y. and Schneider, T., 2011. Downstream Self-Destruction of Storm Tracks. Journal of the Atmospheric Sciences.

Ko, K.-C. and Hsu, H.-H., 2010. Downstream Development of the Summertime Tropical Cyclone/Submonthly Wave Pattern in the Extratropical North Pacific. Journal of Climate, 23(8): 2223-2229.

Lee, S. and Held, I.M., 1993. Baroclinic Wave-Packets in Models and Observations. Journal of the Atmospheric Sciences, 50(10): 1413-1428.

Lombardo, K. and Colle, B.A., 2010. The Spatial and Temporal Distribution of Organized Convective Structures over the Northeast and Their Ambient Conditions. Monthly Weather Review, 138(12): 4456-4474.

Machado, L.A.T., Rossow, W.B., Guedes, R.L. and Walker, A.W., 1998. Life Cycle Variations of Mesoscale Convective Systems over the Americas. Monthly Weather Review, 126(6): 1630-1654.

Majumdar, S.J., Sellwood, K.J., Hodyss, D., Toth, Z. and Song, Y.C., 2010. Characteristics of Target Areas Selected by the Ensemble Transform Kalman Filter for Medium-Range Forecasts of High-Impact Winter Weather. Monthly Weather Review, 138(7): 2803-2824.

Martius, O., Schwierz, C. and Davies, H.C., 2007. Breaking waves at the tropopause in the wintertime Northern Hemisphere: Climatological analyses of the orientation and the theoretical LC1/2 classification. Journal of the Atmospheric Sciences, 64: 2576-2592.

Martius, O., Schwierz, C. and Davies, H.C., 2010. Tropopause Level Waveguides. Journal of the Atmospheric Sciences, 67(3): 866-879.

Nakamura, H., 1992. Midwinter Suppression of Baroclinic Wave Activity in the North Pacific. Journal of the Atmospheric Sciences, 49(17): 1629-1642.

Orlanski, I., 2005. A New Look at the Pacific Storm Track Variability: Sensitivity to Tropical SSTs and to Upstream Seeding. Journal of the Atmospheric Sciences, 62(5): 1367-1390.

Orlanski, I. and Katzfey, J., 1991. The Life Cycle of a Cyclone Wave in the Southern Hemisphere. Part I: Eddy Energy Budget. Journal of the Atmospheric Sciences, 48(17): 1972-1998.

Reviere, G. and Orlanski, I., 2007. Characteristics of the Atlantic storm-track eddy activity and its relation with the North Atlantic Oscillation. Journal of the Atmospheric Sciences, 64(1): 241-266.

Strong, C. and Magnusdottir, G., 2008. Tropospheric Rossby Wave Breaking and the NAO/NAM. Journal of the Atmospheric Sciences, 65(9): 2861-2876.

Trenberth, K.E., 1991. Storm Tracks in the Southern Hemisphere. Journal of the Atmospheric Sciences, 48(19): 2159-2178.

Wang, X.L., Swail, V.R. and Zweiss, F.W., 2006. Climatology and Changes of Extratropical Cyclone Activity: Comparison of ERA-40 with NCEP–NCAR Reanalysis for 1958–2001. Journal of Climate, 19(13): 3145-3166.

Woollings, T., Hoskins, B.J., Blackburn, M. and Berrisford, P., 2008. A new Rossby wave–breaking interpretation of the North Atlantic Oscillation. Journal of the Atmospheric Sciences, 65(2): 609-626.

Zimin, A.V., Szunyogh, I., Hunt, B.R. and Ott, E., 2006. Extracting envelopes of nonzonally propagating Rossby wave packets. Monthly Weather Review, 134(4): 1329-1333.

Zimin, A.V., Szunyogh, I., Patil, D.J., Hunt, B.R. and Ott, E., 2003. Extracting envelopes of Rossby wave packets. Monthly Weather Review, 131(5): 1011-1017.

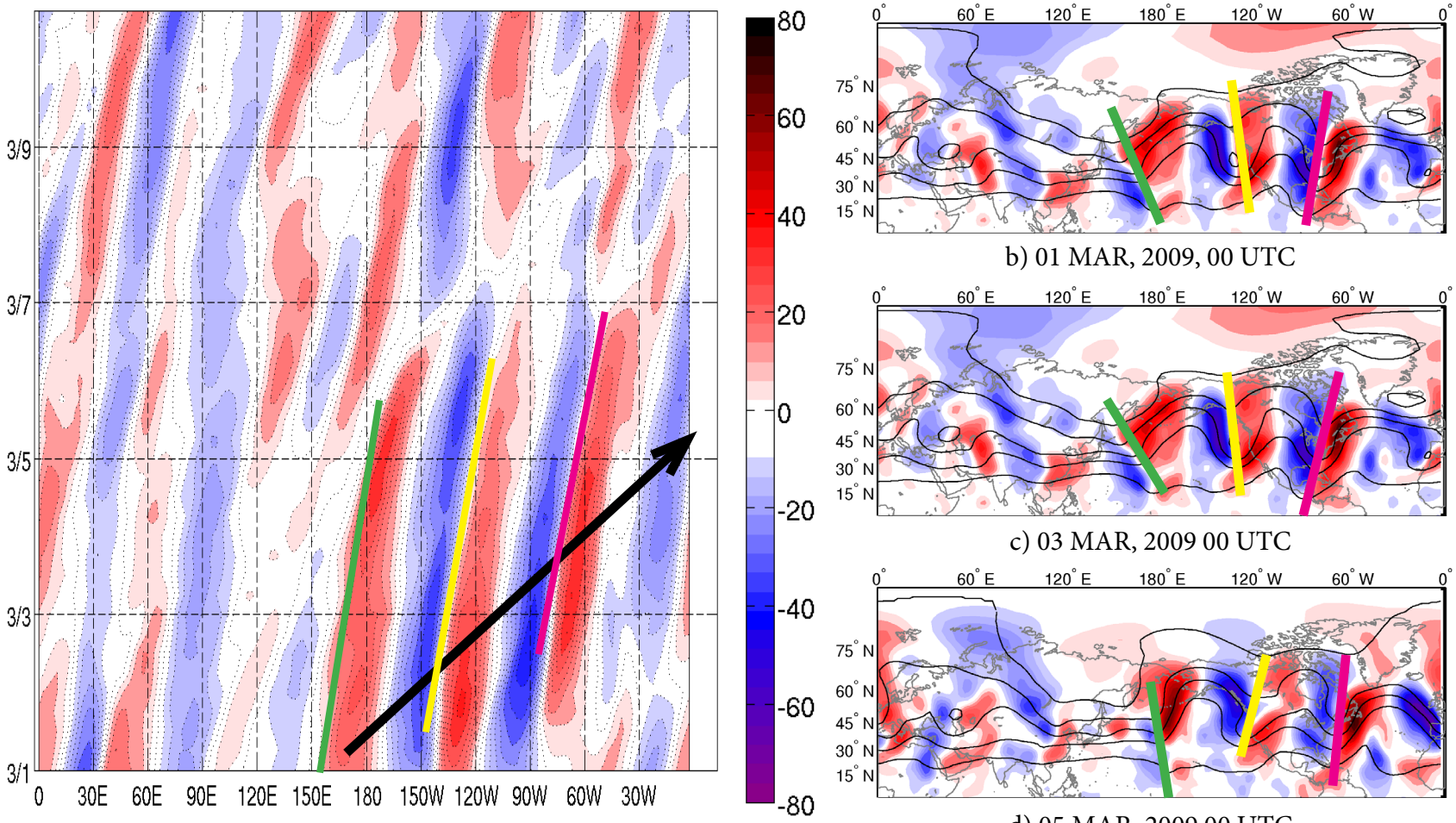

a) Hovmoller Diagram of 300 hPa V

b) 01 MAR, 2009, 00 UTC

c) 03 MAR, 2009 00 UTC

d) 05 MAR, 2009 00 UTC

Fig. 1.1 - The evolution of an intense Rossby wave packet (RWP) over North America between MAR 01 and MAR 09, 2009 as shown by (a) a Hovmoller diagram of 300 hPa meridional wind, and (b-d) spatial maps of meridional wind and height and 300 hPa from 00 UTC on MAR 01, MAR 03 and MAR 05 respectively. The positions of invidual troughs are labeled and the group velocity of the RWP is shown in (a) with a black arrow.

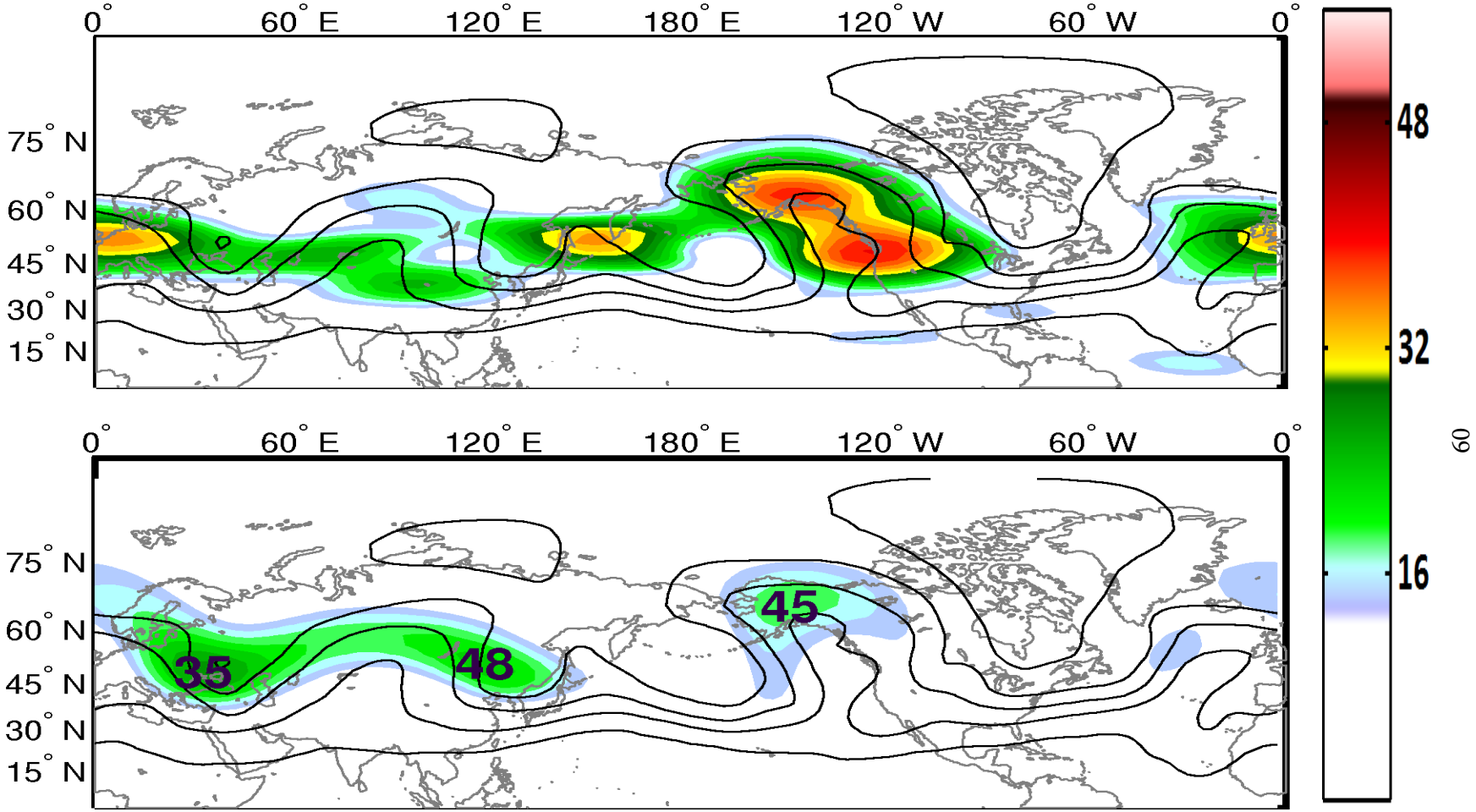

Fig 1.2 - Two methods for finding the wave packet envelope amplitude are compared on 31 JAN, 2007 (00 UTC). In (a), a complex demodulation technique is used, and in (b) a Hilbert transform technique along a time-averaged streamflow technique is applied as in Zimin (2006).

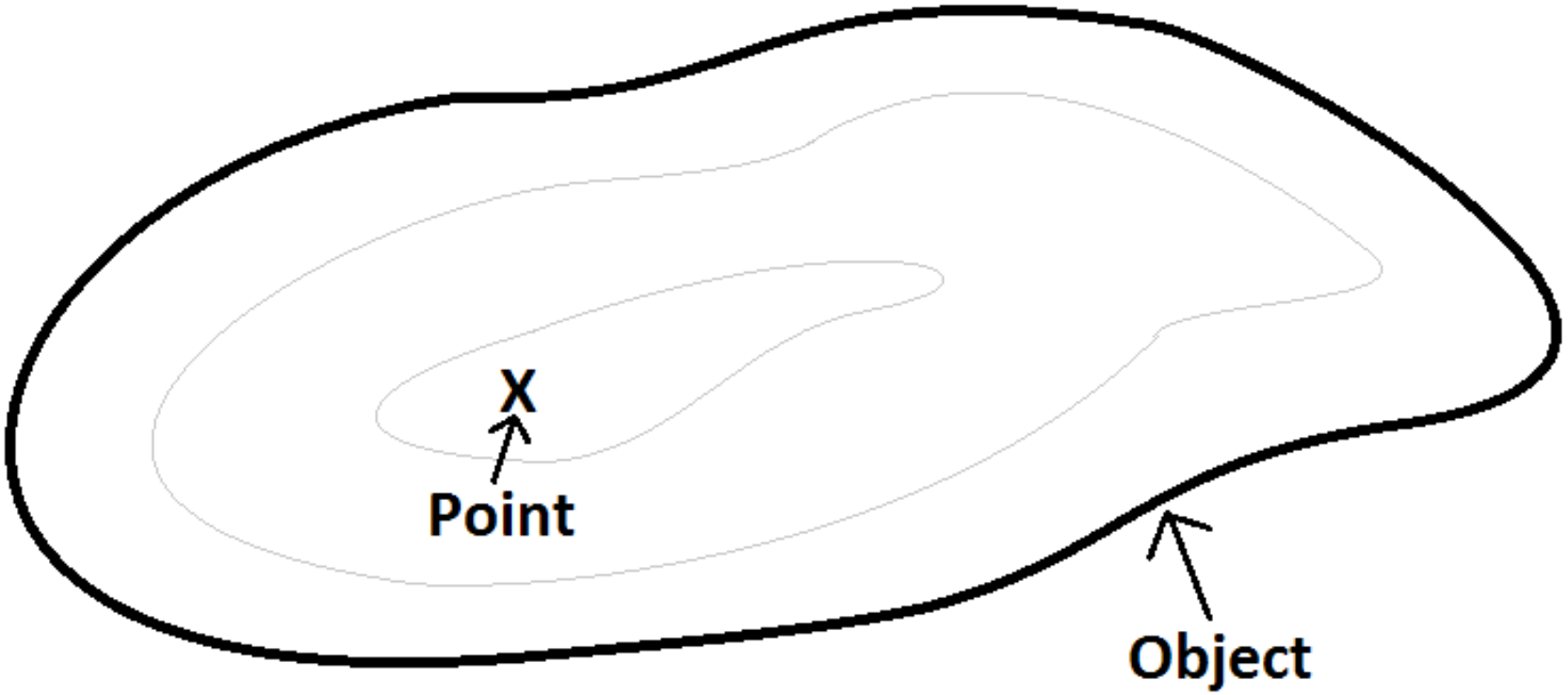

Fig 1.3 - Schematic diagram demonstrating the difference between point and object tracking - in the former, only a point feature is used in tracking, but in the latter, everything inside the heavy objet outline would be followed and used in decisionmaking.

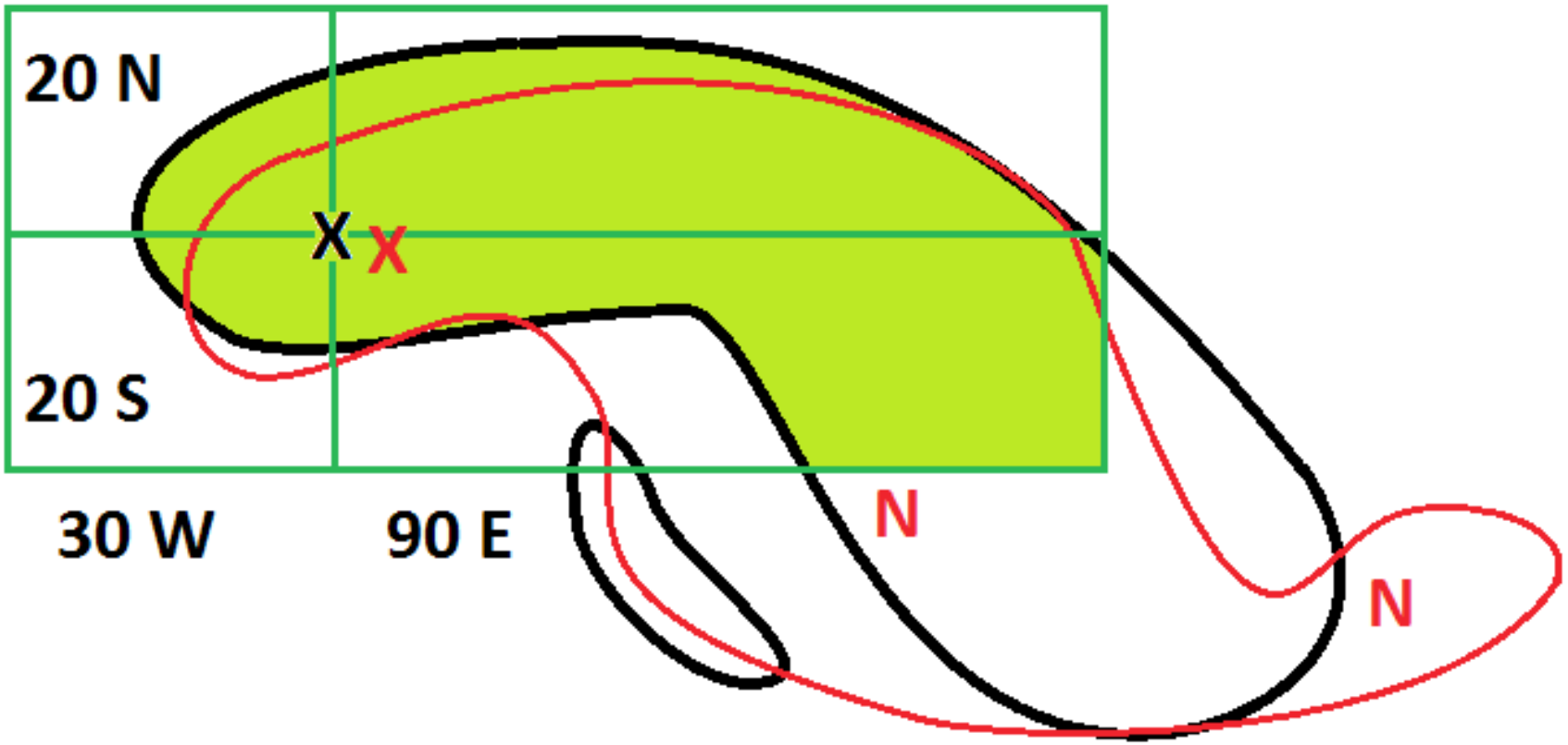

Fig 2.1 - Schematic diagram clarifying the role of the search box in decisions regarding the continuation of active tracks in time. The track being continued is marked with a black X. Black contours represent the object boundaries defined by the minimum tracking threshold at the active time, and red contours represent the next time in sequence. The red markers represent candidates for track merging - the X is a valid continuation, and the Ns are not valid. The highlighted region is the valid search range defined by the search box and the active object boundary

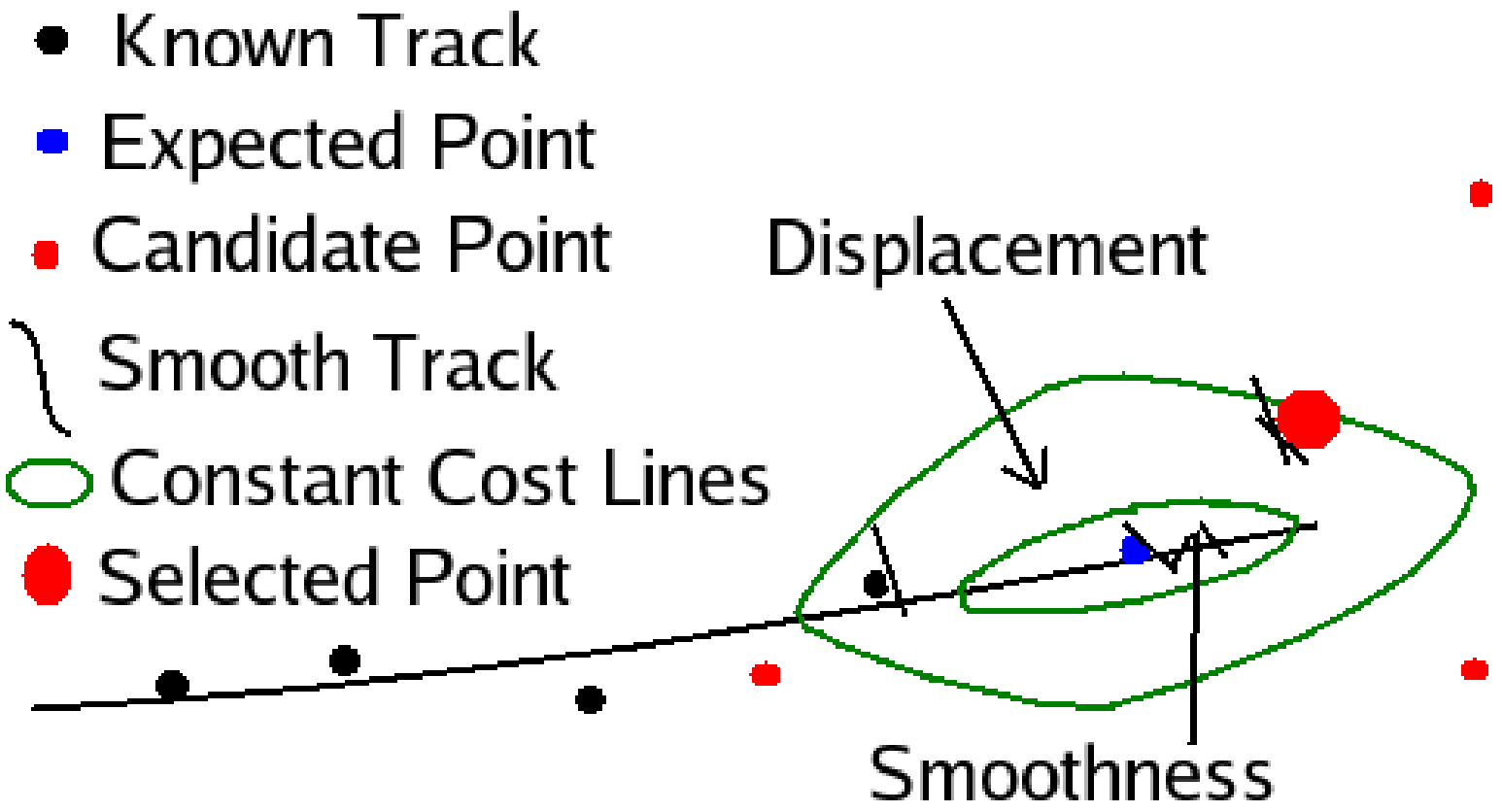

Fig 2.2 - Schematic diagram describing tracking methods used by Hodges' TRACK algorithm. The last four track points in an active track are considered - the feature's average velocity is used to make a prediction as to where the next track point should be, and adaptive tracking constraints are used to set the parameters of a cost optimization function designed to find a likelihood that any candidate point is in fact the next point in the active track.

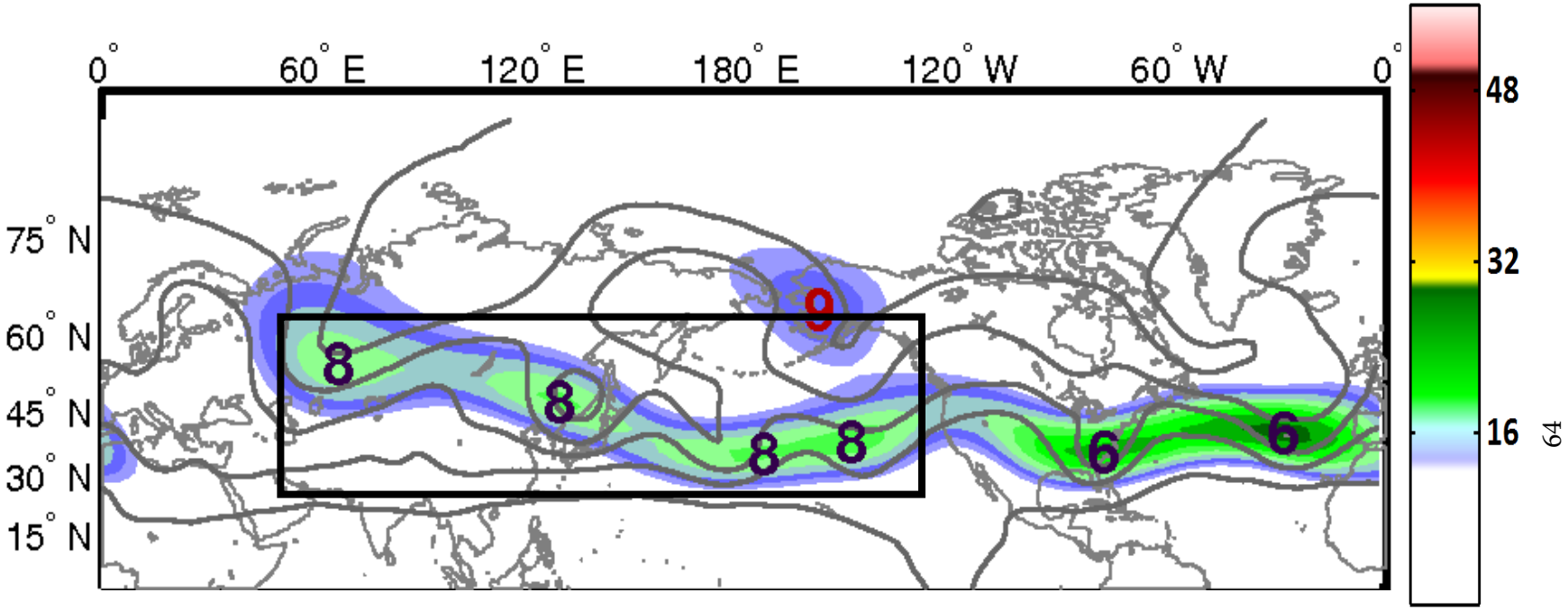

Fig. 2.3 - Multiple examples of non-significant WPA maxes that are related to nearby (more intense) maxima and should not be separately tracked. WPA (shaded and contoured every 2 m s^{-1} beginning at 14 m s^{-1}, and 300 hPa geopotential height (contoured in black every 30 dam) are shown, as well as the ID markers for all features pinpointed by the TRACK algorithm on 08 JAN, 1996 (12 UTC). At this time, a weak packet over Russia (labeled 8 at the far left) has become erroneously linked with two non-significant WPA maxima downstream and this has forced a renaming of a significant maximum south of Alaska.

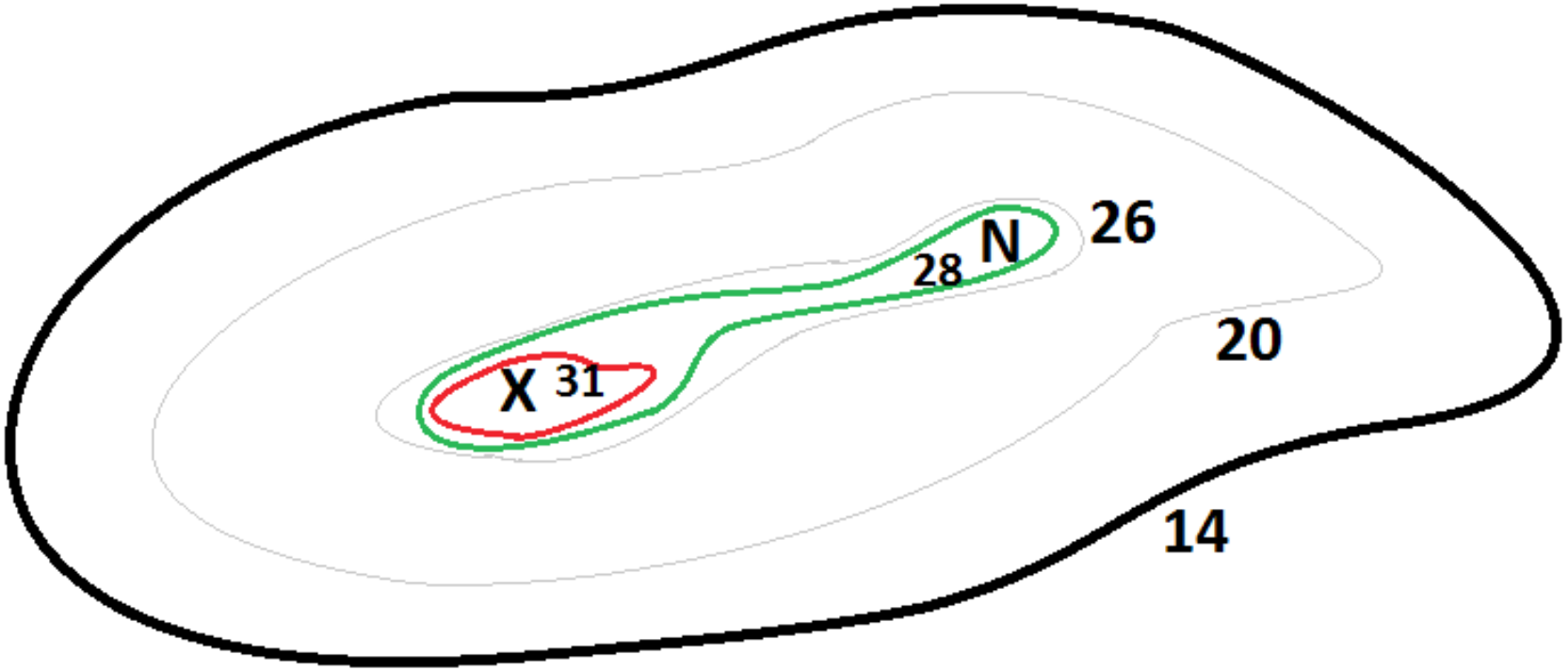

Fig. 2.4 - Schematic diagram of the 95% prominence rule in practice. The object bounded by the heavy black contour contains two local maxima in WPA of relatively similar intensity. The green contour is the WPA 95% as high as the right (weak) feature, and the red contour is at 95% the value of the left (strong) feature. The left feature (X) is ruled significant, since its 95% contour does not enclose any local maxima of greater intensity, but the right feature (N) is not signfiicant, since its 95% contour encloses the left feature, a stronger WPA max.

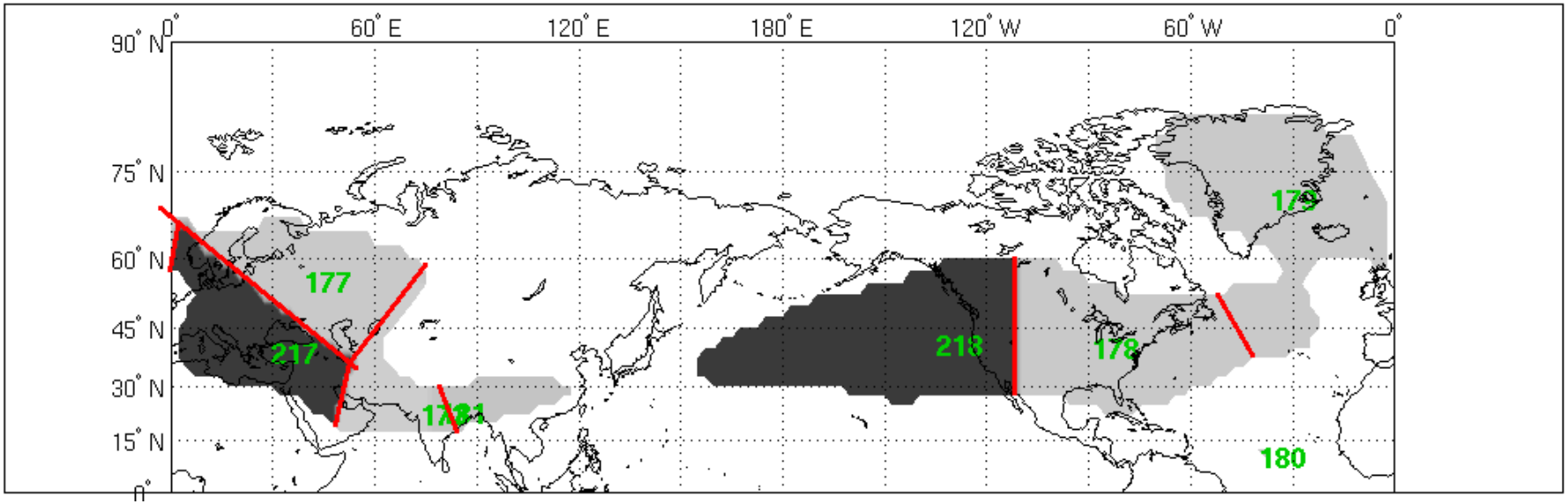

Fig. 2.5 - A demonstration of the results of nearest neighbor searching as a means for attributing objects to local maxes in WPA. Shaded regions have WPA exceeding 14 m s^{-1}, and local maxima in WPA are labeled with the ID markers from the TRACK method. Object boundaries found by nearest neighbor searching are marked with red lines. The data is taken form 03 MAR, 2009 (00 UTC).

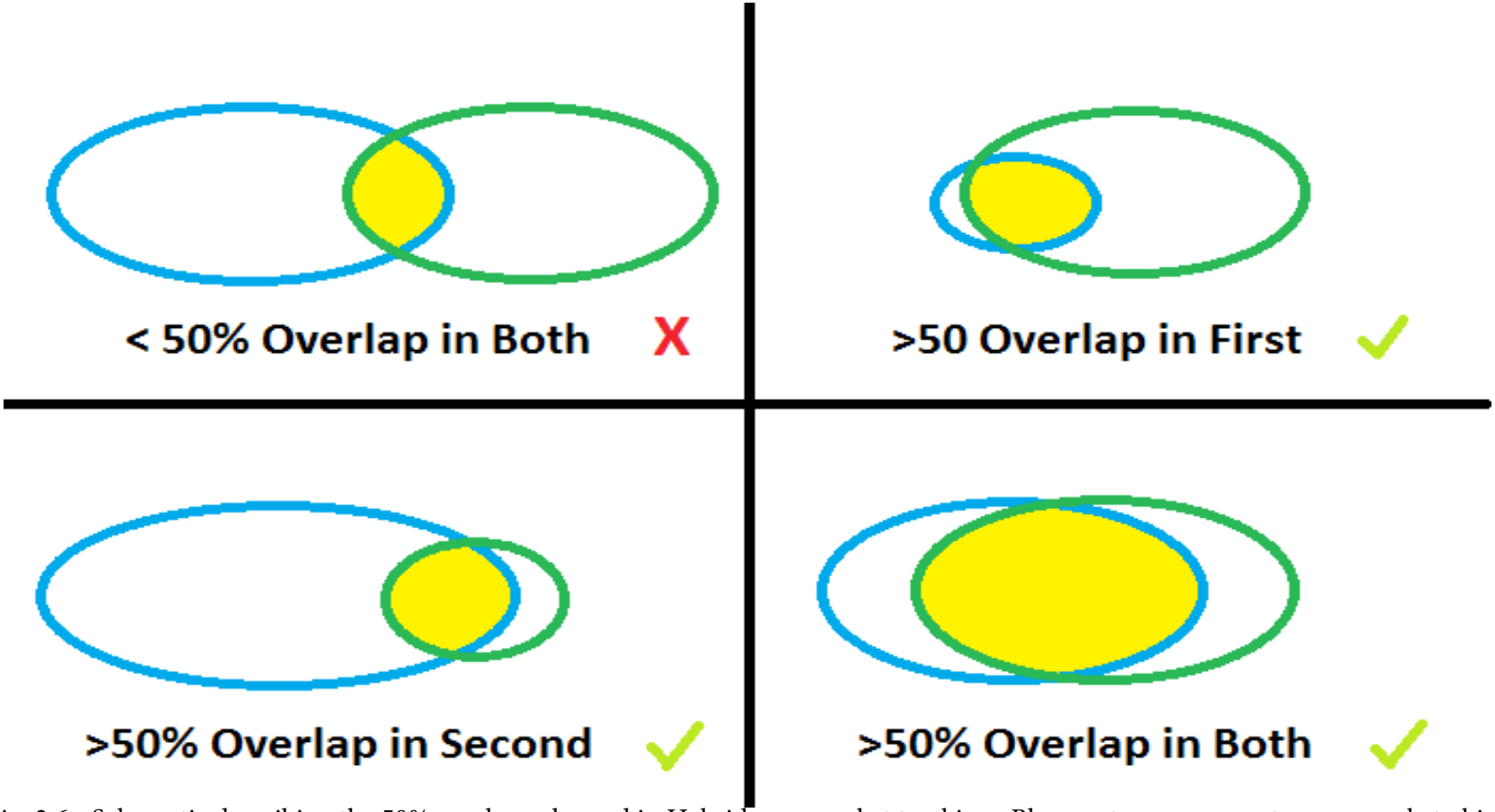

Fig. 2.6 - Schematic describing the 50% overlap rule used in Hybrid wave packet tracking. Blue contours represent a wave packet object as it exists in the first time step being compared, and the green contours represent wave packet objects in the next time step. The yellow highlighted region represents the overlap region. If 50% of either the first or next object is occupied by the overlap region, the objects are considered valid candidates for track continuation.

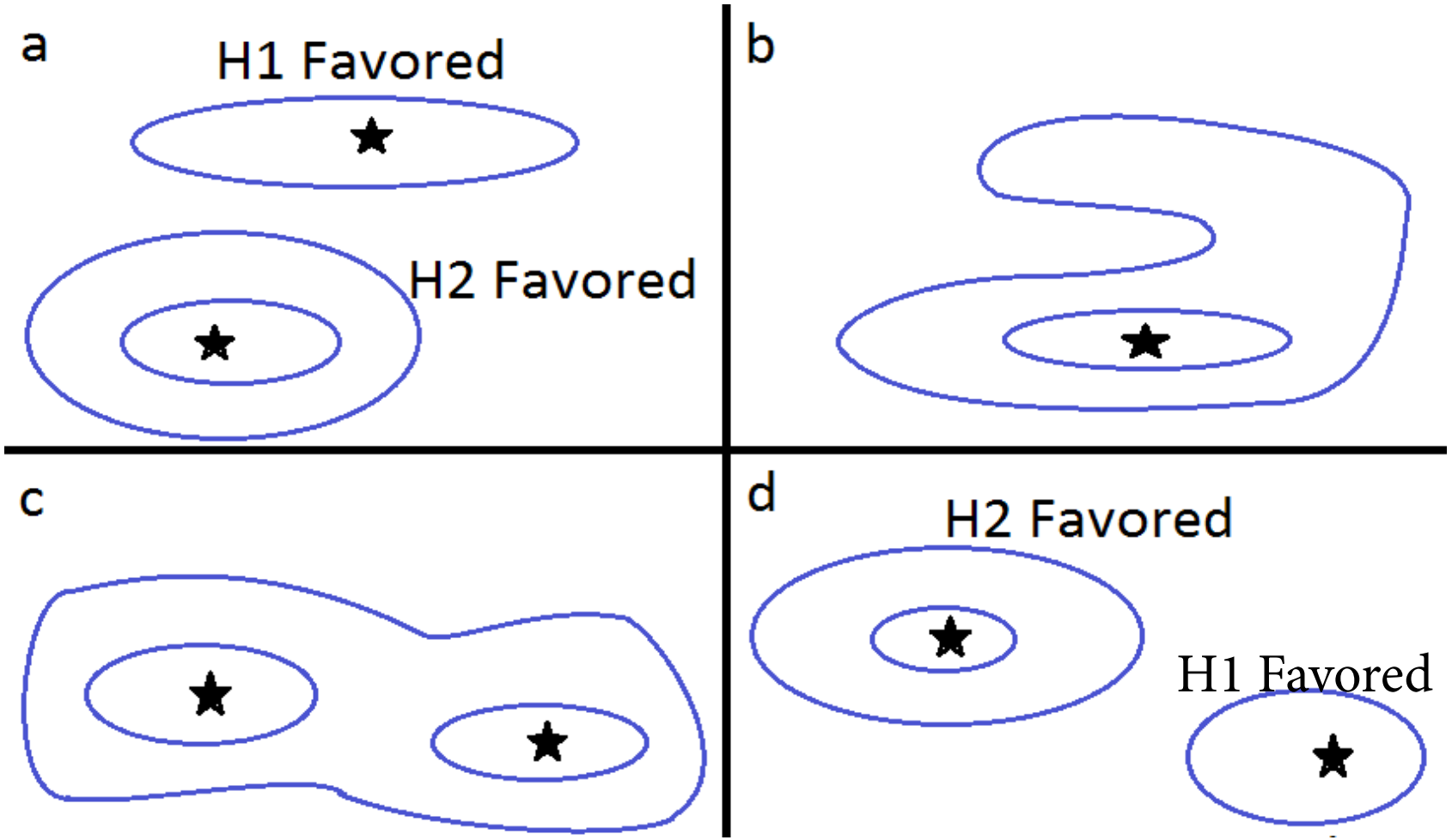

Fig. 2.7 - Schematic describing the differences between H1 and H2 when resolving tracking conflicts. In (a) and (b), a typical split flow wave packet merger is shown at an earlier and later time step. Both tracked objects (marked with stars) in (a) have a claim on the merged object in (b). The track that continues depends on whether you favor the object that is furthest east (H1), or largest/most intense (H2). In (c) and (d) a typical leading split is shown. Either tracked maximum in (d) could claim to be the correct continuation of the joined object in (c) with the other object obtaining a new name. H1 favors the furthest east object for continuing the previous track and H2 favors the most intense.

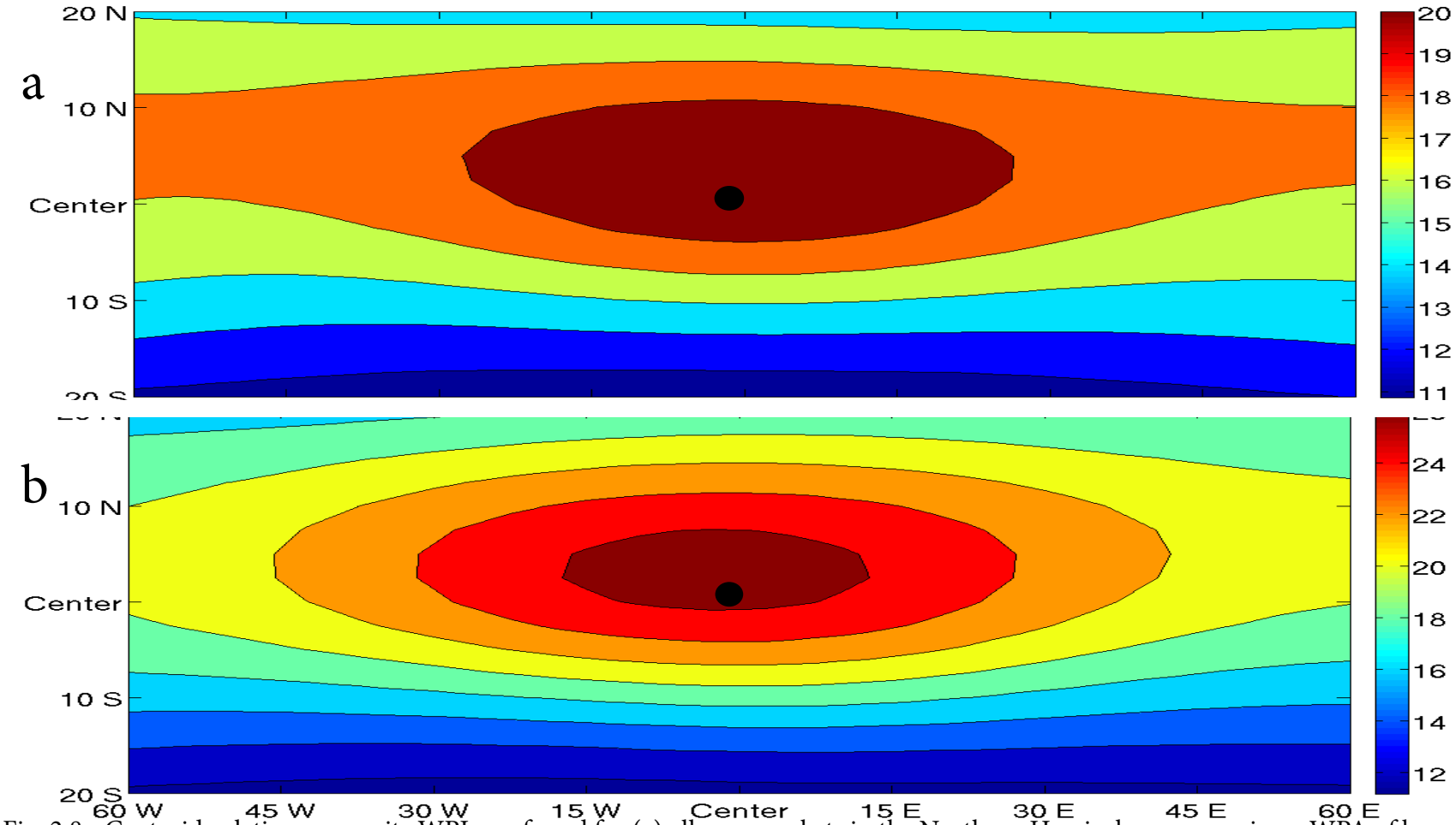

Fig. 2.8 - Centroid-relative composite WPI was found for (a) all wave packets in the Northern Hemisphere possessing a WPA of between 14 and 16 m s-1 and (b) the first eight time steps for all significant wave packets of any intensity. Both (a) and (b) are contoured every 2 units of WPI beginning at 12. The position of the centroid is marked with a black circle. WPI values at the core of the composite represent the typical dynamic energy associated with wave packet propagation. The low estimate found of 18 in (a) is taken as the minimum WPI plotted for hand verification and the higher estimate of 25 in (b) is taken as the minimum WPI required for at least 24 hours to count a packet as significant.

Rule Category	Specification	Test Range
Minimum WPA Tracking Threshold	14 m s^{-1}	10 to 20 m s^{-1}
Spatial Data Filter (Cholesky Smoothing)	T21 Resolution	T15 to T42 Resolution
Temporal Smoothing Algorithm	24 hr Running Average	No Smoothing to 48 hr Average
Object Size	40 (2.5 degree) Grid Points	No Minimum to 200 Grid Points
Search Box	20 degrees N/S	15-30 degrees N/S
	30 degrees W	0-45 degrees W
	90 degrees E	45 degrees E to No Eastward Limit
Significant Track Minimum Duration	2 days	1 to 3 days
Significant Track Minimum Propagation	40 degrees East	No Minimum to 90 degrees East
Significant Track Minimum Intensity	14 m s^{-1}	14 to 20 m s^{-1}

Table 2.1 - Summary of General Tracking Rules

Rule Category	TRACK	H1	H2
Valid Next Track Point	Cost Optimization	50% Object Overlap	50% Object Overlap
Time Comparison	Current to Next	Current to Next	Prior to Current
Maximum Displacement	30 Great Circle Degrees	Search Box Bounded	Search Box Bounded
Track Smoothness	Adaptive Tracking	N/A	N/A
Significant Local Maximum Detection	All Maxes Significant	95% Prominence Rule	95% Prominence Rule
Object Attribution	N/A	Nearest Neighbor	Nearest Neighbor
Disputed Merge Candidates - 1st Rule	Longest Lived	Longest Lived	Largest Area
Disputed Merge Candidates - 2nd Rule	Closest to Active Track	Resulting in Most Eastward Move	Most Intense
Runaway Merge Prevention	Object Boundary	120 degree E/W Max Separation	Contour Split Method
Runaway Track Continuity	Longest Lived	Furthest West	Most Intense

Table 2.2 - Tracking Rules Specific to One Method

Displacement (deg.)	Smoothness Parameter
1	0.7
2	0.6
4	0.5
8	0.4
15	0.2
30	0.1

Table 2.3 - Adaptive Tracking Constraints used in TRACK for the purpose of adjusting the sensitivity of the cost optimization algorithm to changes in the direction of movement of the RWP being tracked

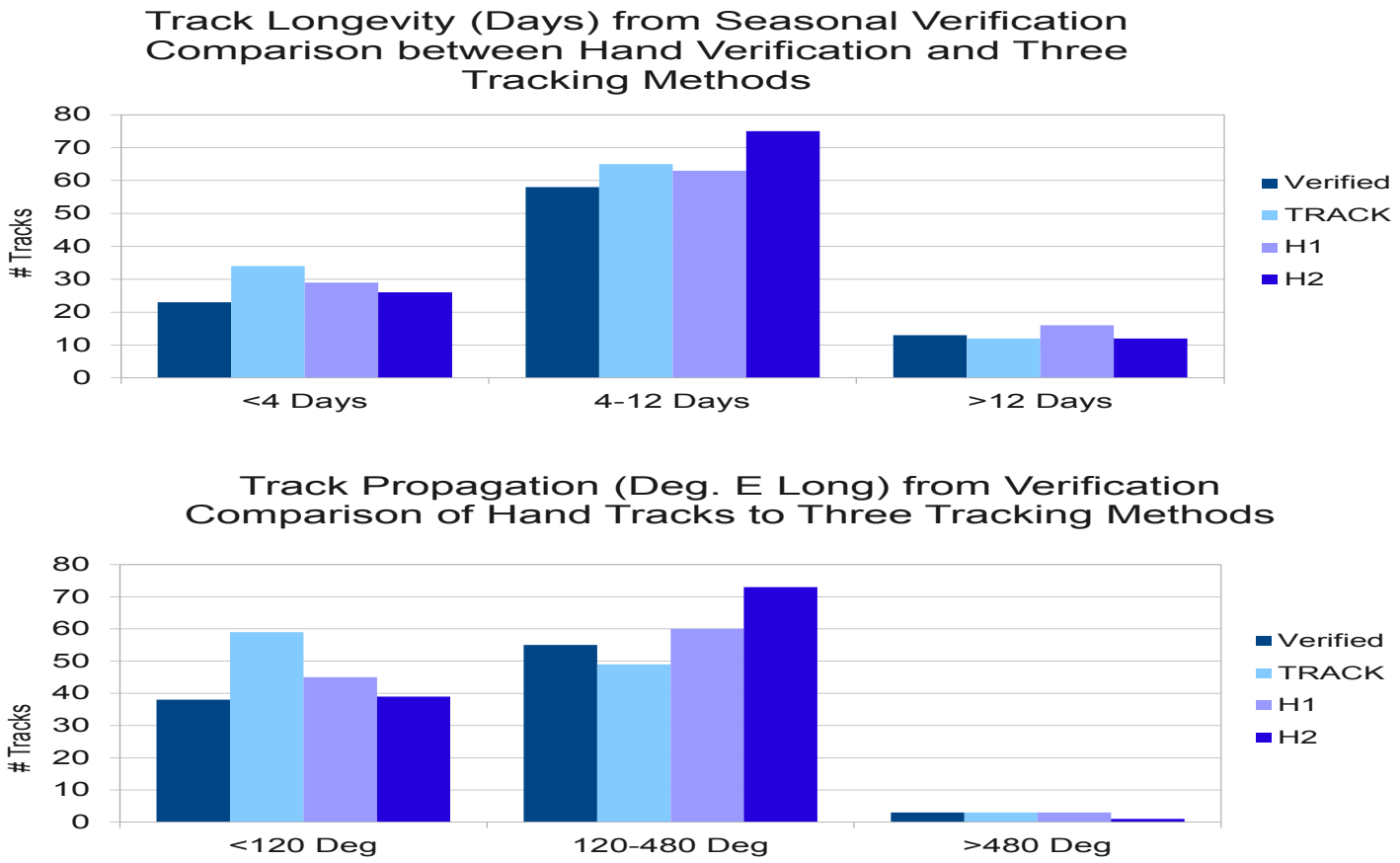

Fig. 3.1 - Verification (a) Track duration and (b) track propagation frequencies, broken out into three ranges each for increased pattern recognition and displayed for each tracking method and for hand tracking over the seasonal verification period.

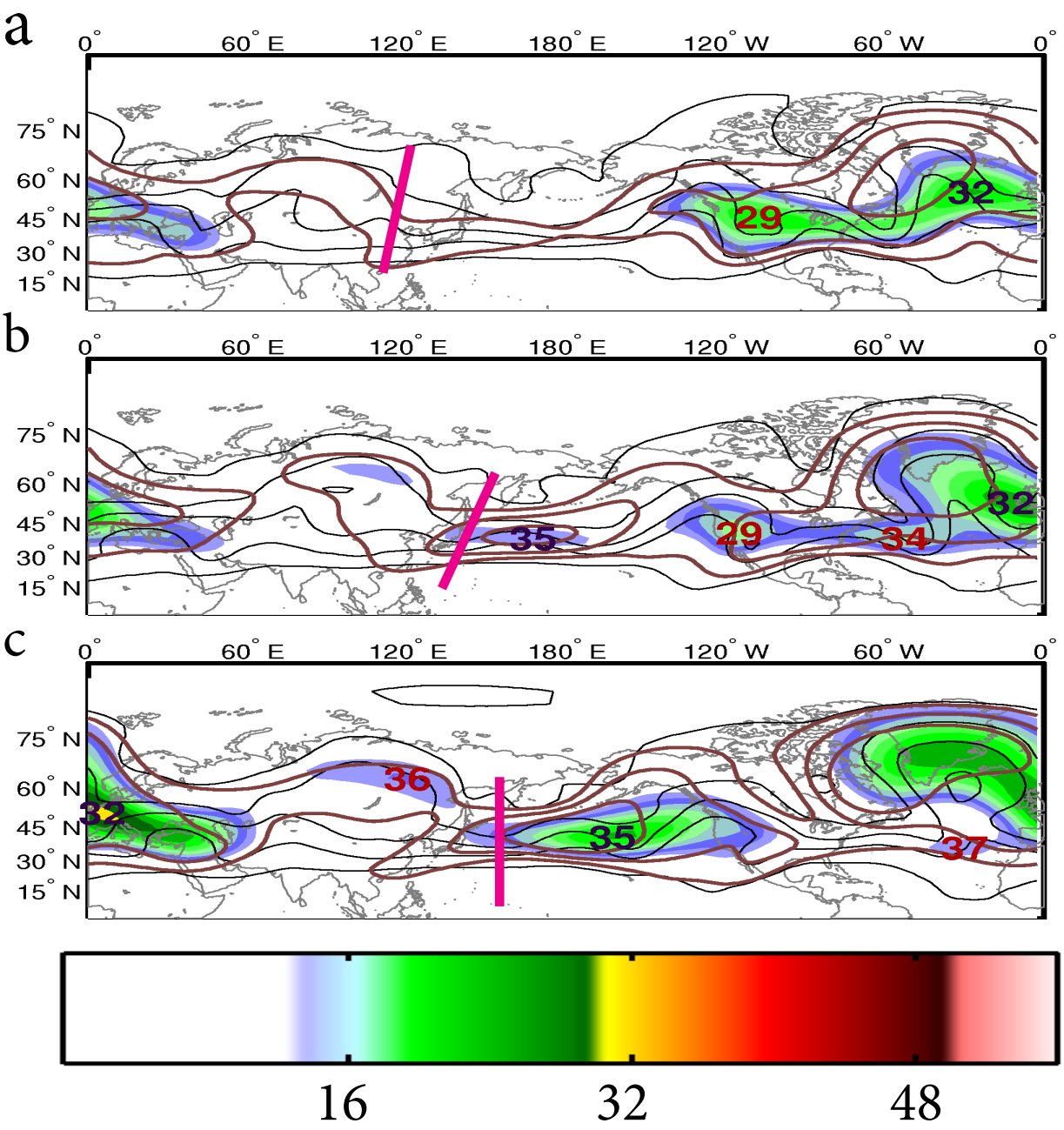

Fig. 3.2 - Example of a locally forced RWP from late January of 2007 showing WPA (shaded), WPI (contoured at 18, 25, 35, and 55 in brown), and 300 hPa geopotential height (contoured every 30 dam beginning at 970) (a) one day before, (b) at the time of and (c) one day after wave packet initiation. The packet formed at 06 UTC on 22 JAN, 2007/ The pink lines represent the axis of the short wave trough that initiated wave packet development.

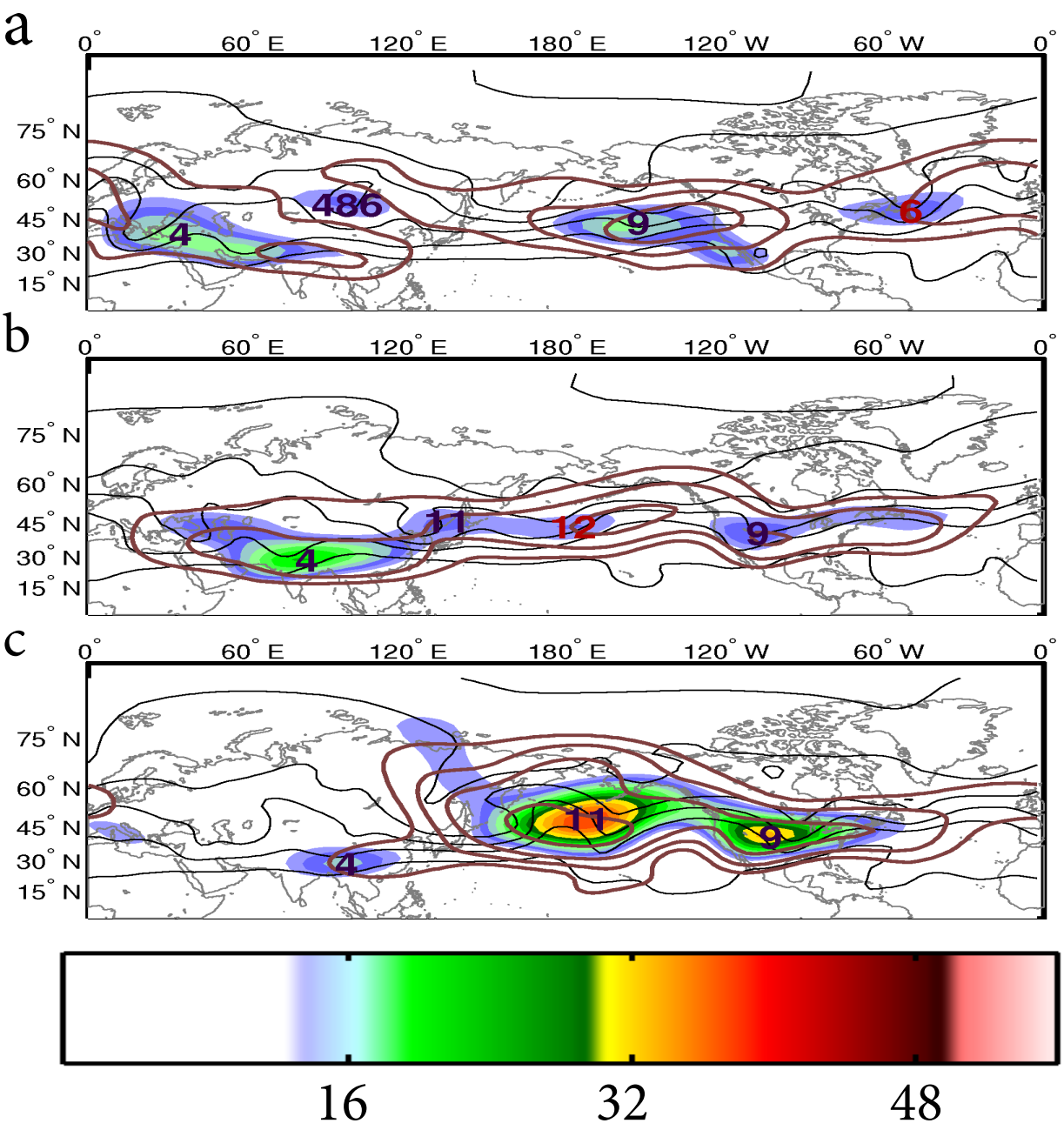

Fig. 3.3 - Example of an upstream seeded RWP development - identical to fig. 3.2 except that in this case, a dissipating wave packet in (a) creates a cut-off low which, after encountering a strong waveguide, develops a new RWP (b) two days later, and two days later (c) this wave packet has become robust. The upstream seeded wave packet initiated at 00 UTC on 06 JAN, 2007.

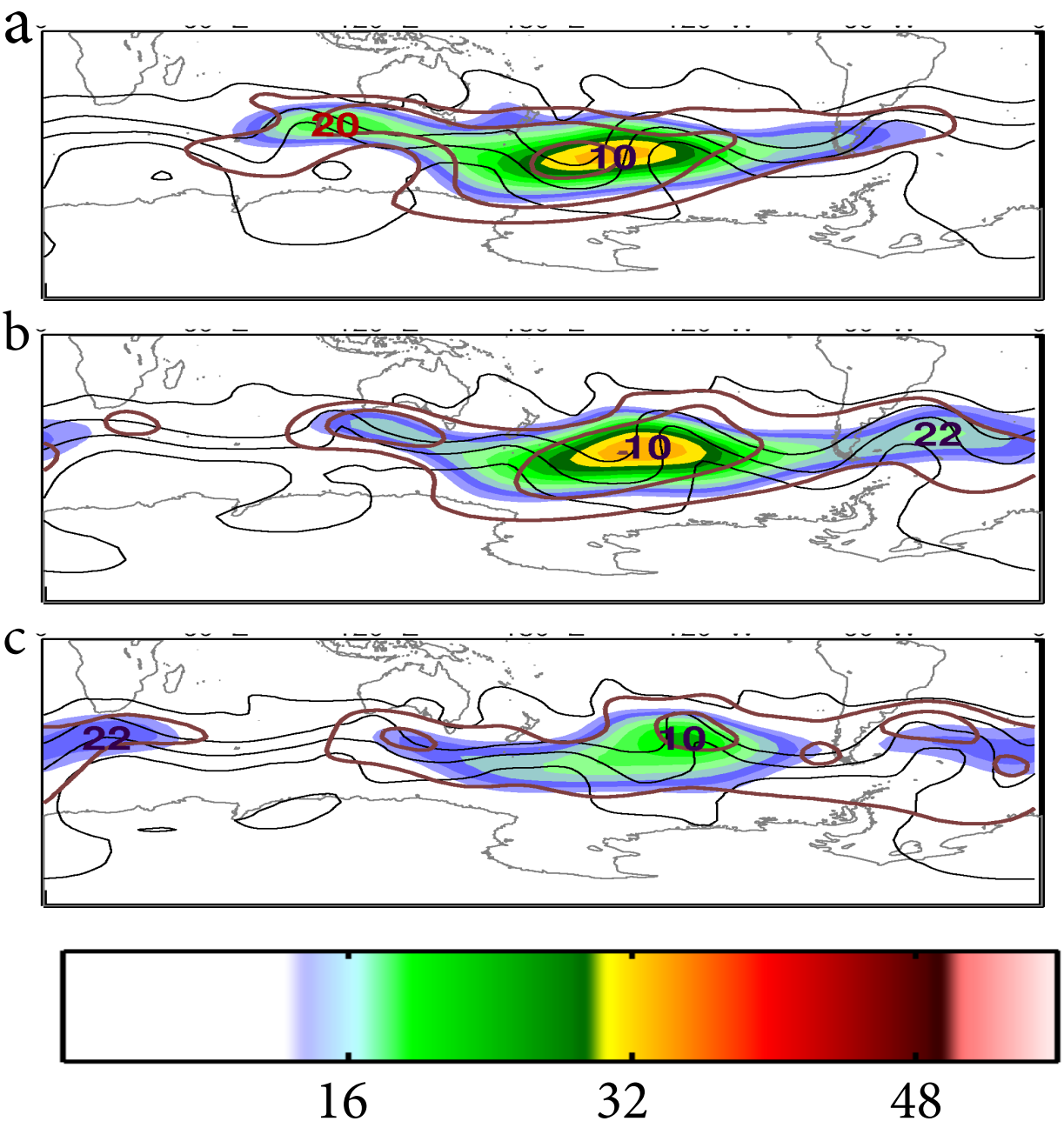

Fig. 3.4 - Example of a wave packet formation caused by the splitting of one packet into two at the packet's leading edge, as sho0wn in figure 3.2. The splits occurred at 18 UTC on the 14th (shown in b) and one day prior (a) and one day after (c) the split are also shown for context.

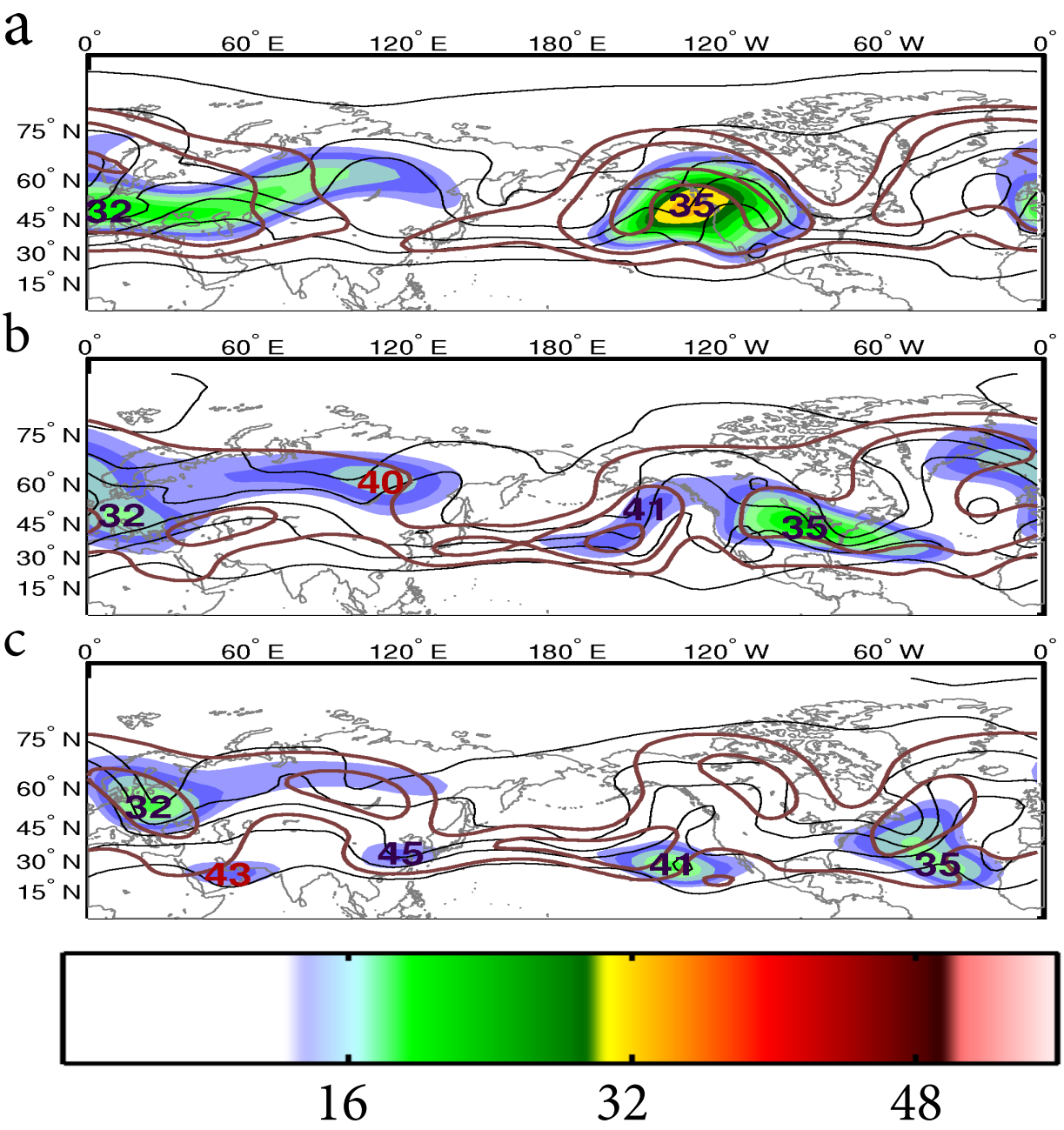

Fig. 3.5 - Example of a wave packet formed by the splitting of an existing packet at its trailing edge - identical to figure 3.5 except that this event occurred at 06 UTC on 26 JAN, 2007 (shown in b), and 36 hours prior to (a) and 36 hours after (c) the split formation are shown for context.

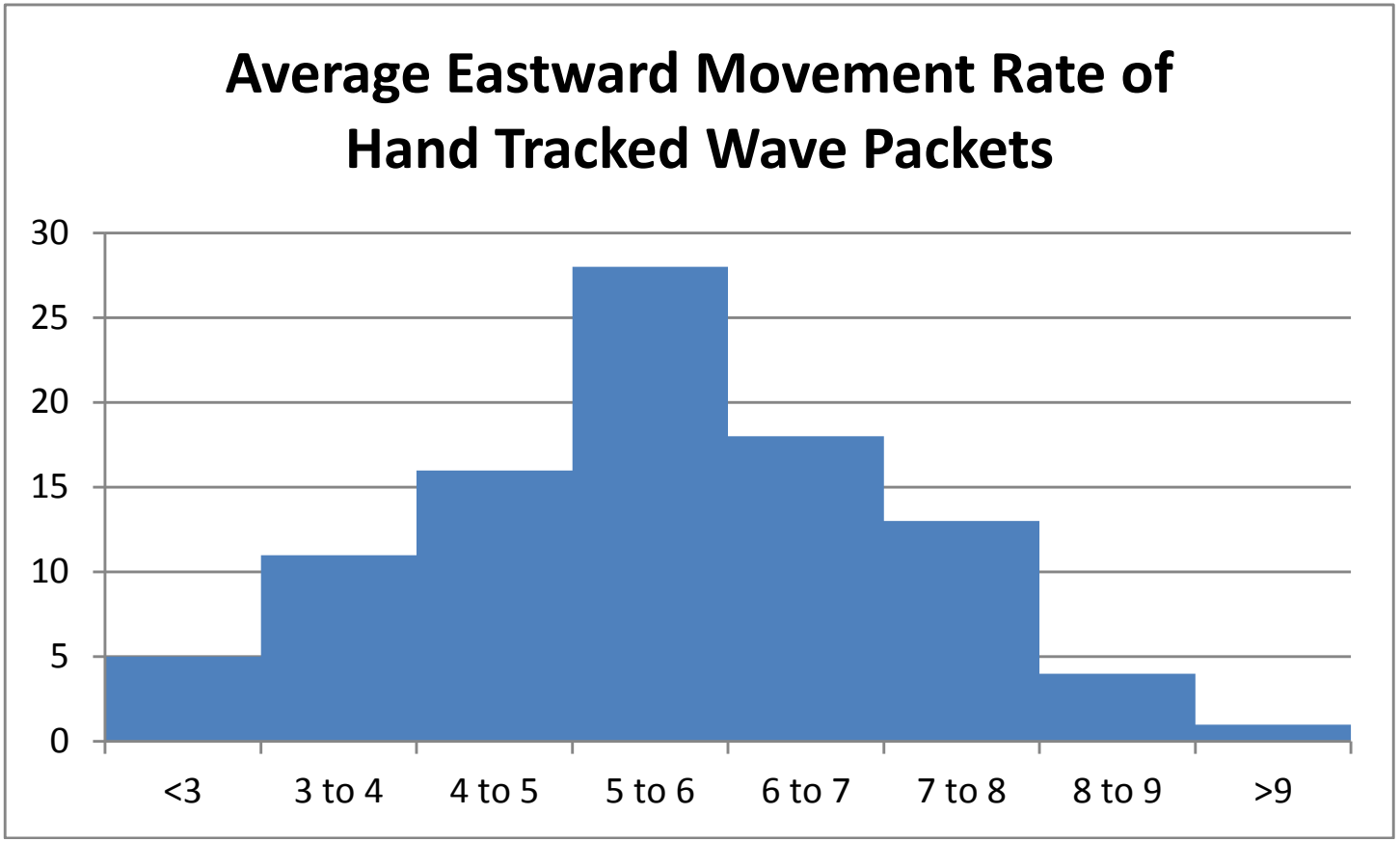

Fig. 3.6 - Frequency of wave packets in the seasonal hand tracking period moving at various eastward rates (degrees 6 hr^{-1}) - the rate was found by dividing the total eastward propagation of each packet (in longitude degrees) by the total duration (in 6-hr time steps).

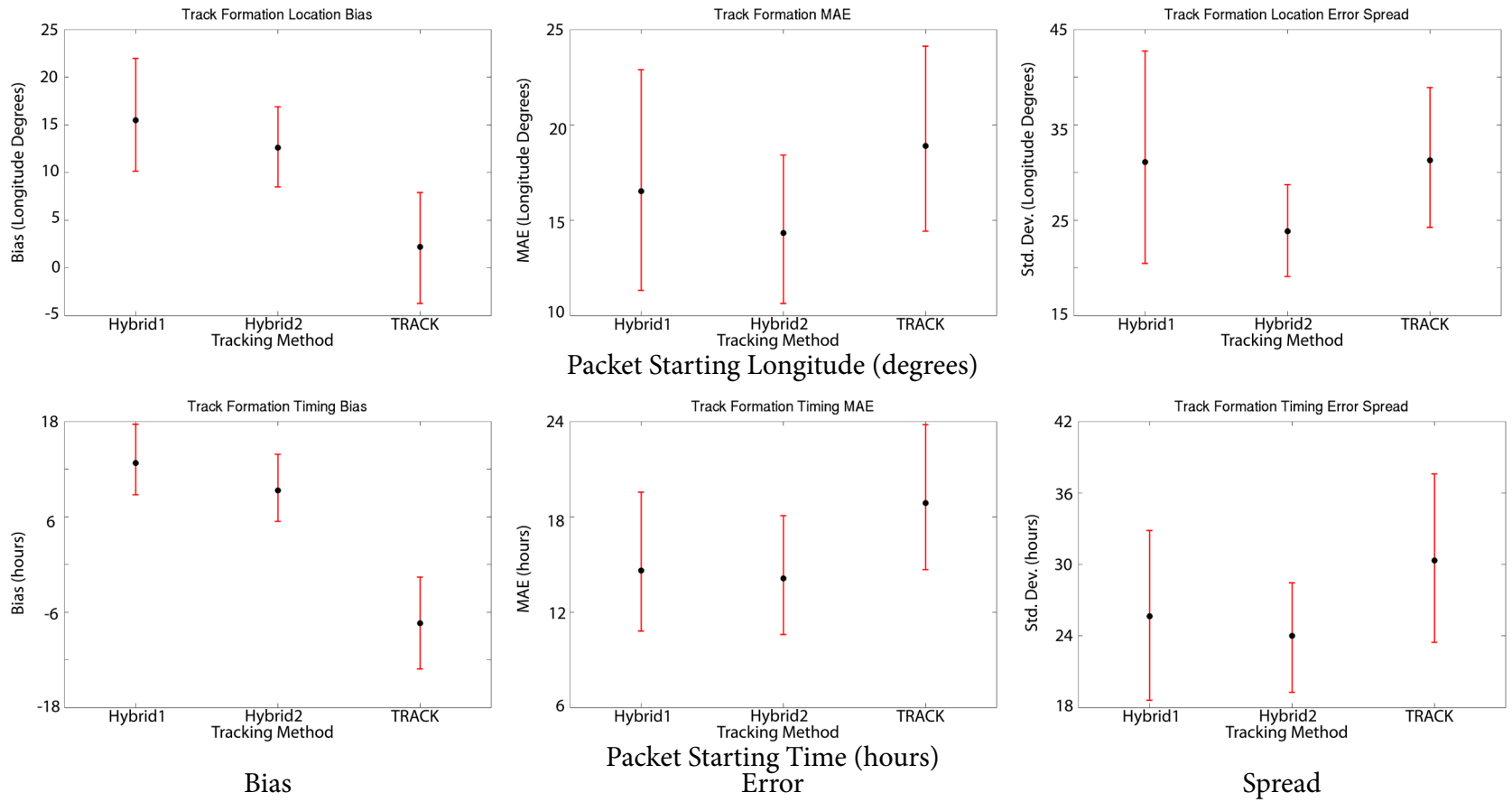

Fig. 3.7 - Statistics governing the performance of each tracking method relative to hand tracking regarding the starting location (TOP) and time (BOTTOM) of wave packets in the seasonal verification period. Bootstrapping was performed on bias (mean error), error (mean absolute error) and error spread (standard deviation of error) in order to obtain 90% confidence intervals (shown in red whiskers).

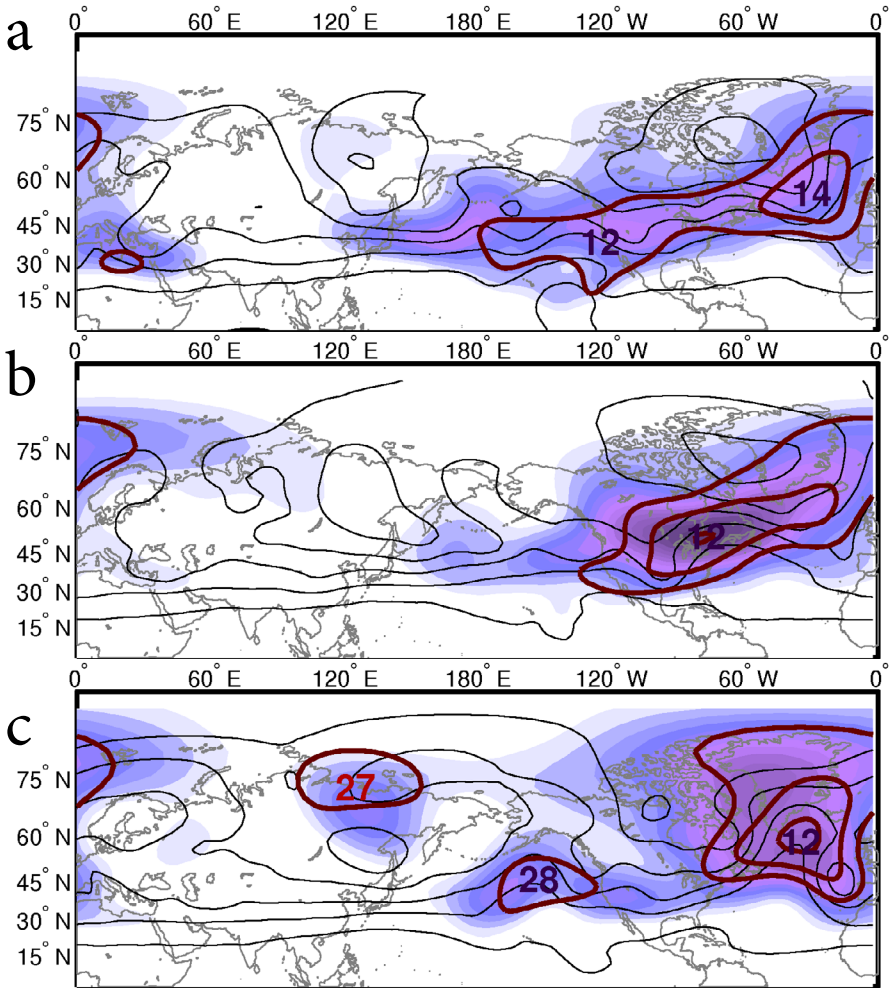

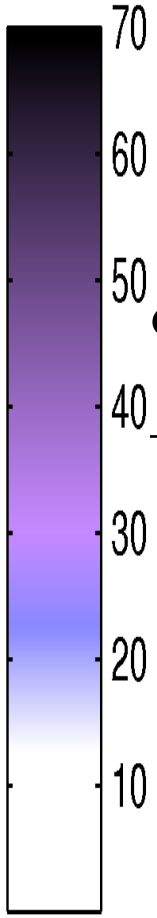

d

Phase	WPA (m s-1)	WPI	E. Movement (deg. day-1)
Weakening	18.6	22.5	7.3
Pulsing	25.7	39.0	20.4
Maturing	26.9	34.9	24.1

Fig. 3.8 - WPI (shaded), WPA (contoured in red every 8 m s^{-1}) and 300 hPa geopotential height (contoured in black every 30 dam) for (a) 17 JAN, 1996 (12 UTC), (b) 19 JAN, 1996 (00 UTC), and (c) 20 JAN, 1996 (12 UTC), representing a typical period of wave packet weakening, pulsing and maturing, respectively. In panel d are some facts regarding the mean WPA, WPI, and eastward movement rate during each period of a pulse recorded during hand tracking.

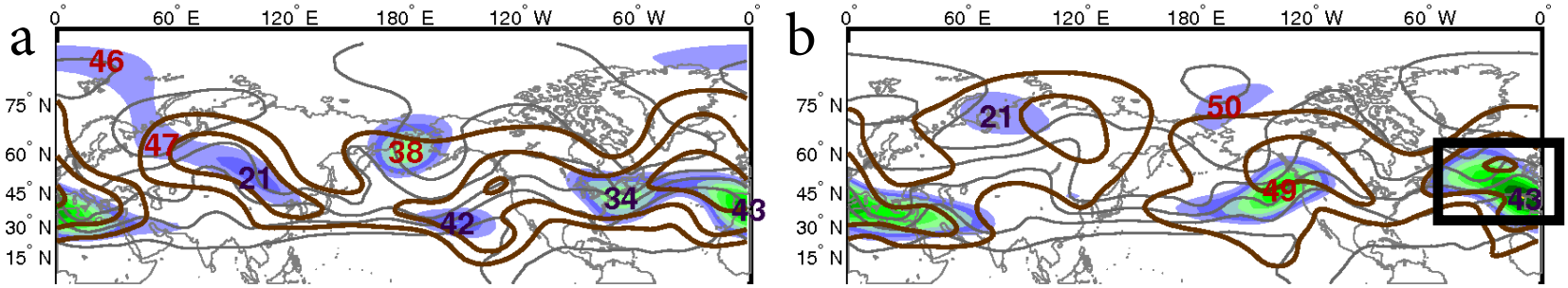

Consumption Merge Failure (lead packet continues erroneously at the expense of progressive trailing packet)

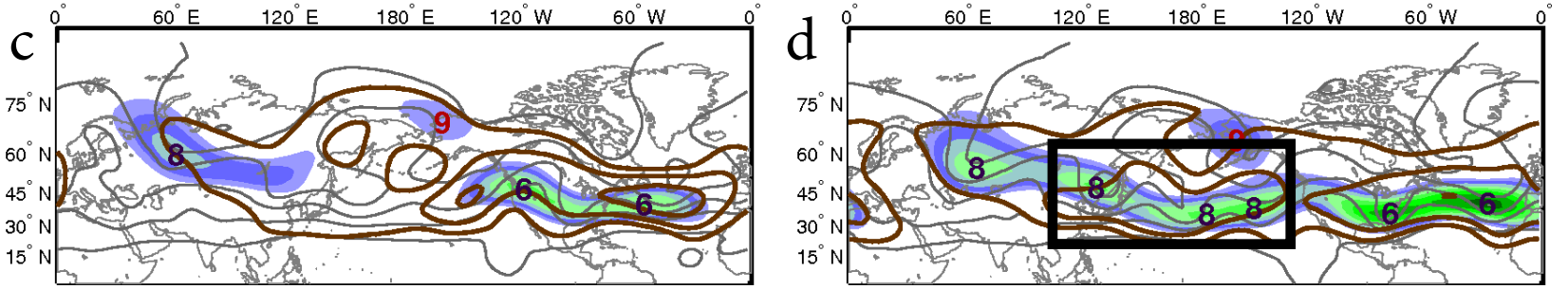

False Feature Identification (Excessive feature selection causing problems with track merging algorithm)

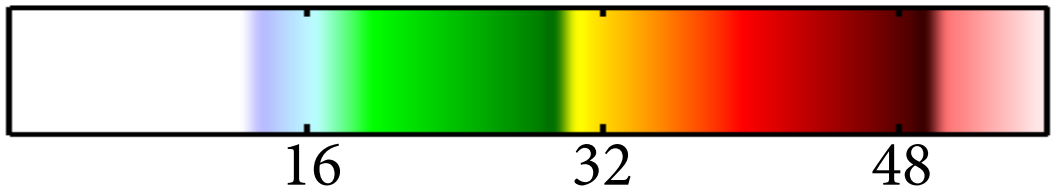

Fig. 3.9 - Examples of common tracking errors found during verification of TRACK - WPA (shaded), WPI (contourd in brown at 18, 25, 35 and 55), and 300 hPa geopotential height (contoured in black every 30 dam) shown for (a) 07 FEB, 1996 and (c) 07 JAN, 1996 respectively. (b) and (d) are taken from 24 hours after (a) and (c) respectively, and the error is highlighted with a black box. In (b), #34 has continued east, but #43 incorrectly claims credit for the object. In (d) a series of non-significant WPA maxima create a missed wave packet developing over the Pacific that incorrectly takes ID #8, rather than being asigned a new track number. #8 remains over Russia.

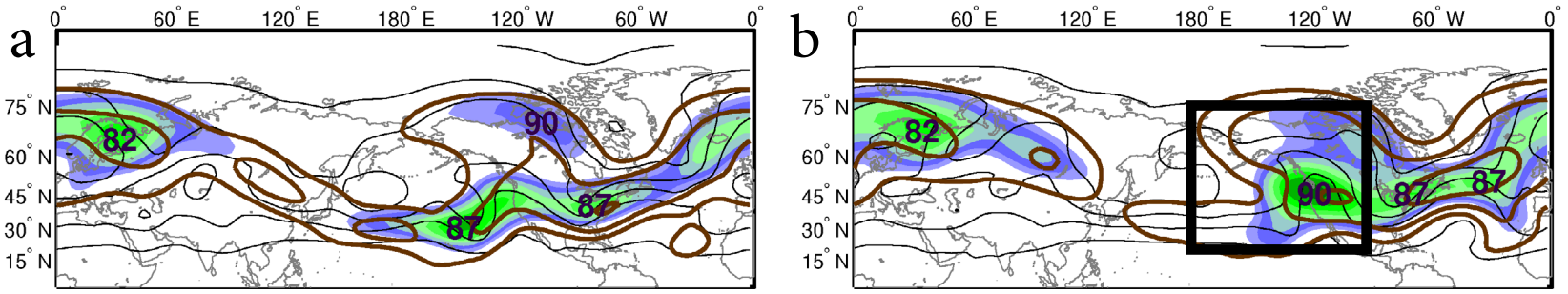

Split flow merge error (in split flow regime, the wrong packet given continuity after a merger)

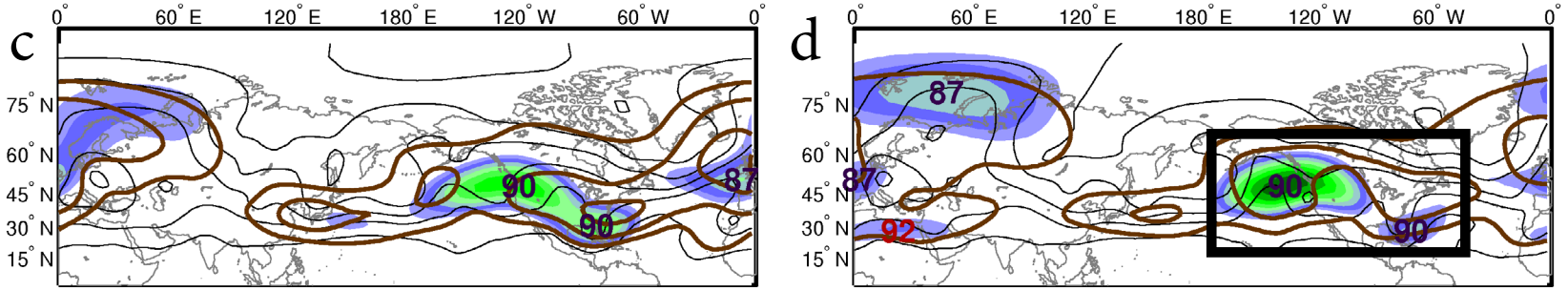

Missed trailing split formation (a trailing split is observed, but the existing packet erroneously claims trailing energy)

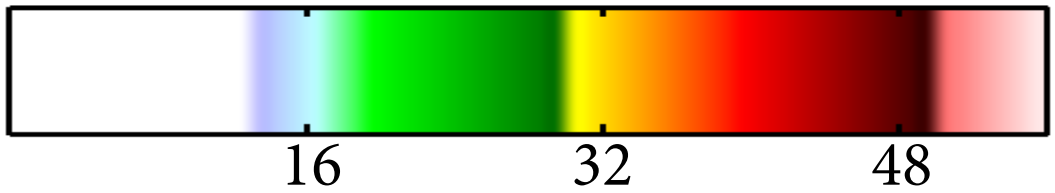

Fig. 3.10 - Examples of common tracking errors found during verification of H1 and H2 - WPA (shaded), WPI (contourd in brown at 18, 25, 35 and 55), and 300 hPa geopotential height (contoured in black every 30 dam) shown for (a) 08 MAR, 1996 and (c) 11 MAR, 1996 respectively. (b) and (d) are taken from 24 hours after (a) and (c) respectively, and the error is highlighted with a black box. In (b) #87 should have continued east but has been co-opted by non-significant #90 while its leading edge maintains #87, when it should be splitting to form a new object. In (d) a trailing split occurs, but #90 claims both pieces of the packet.

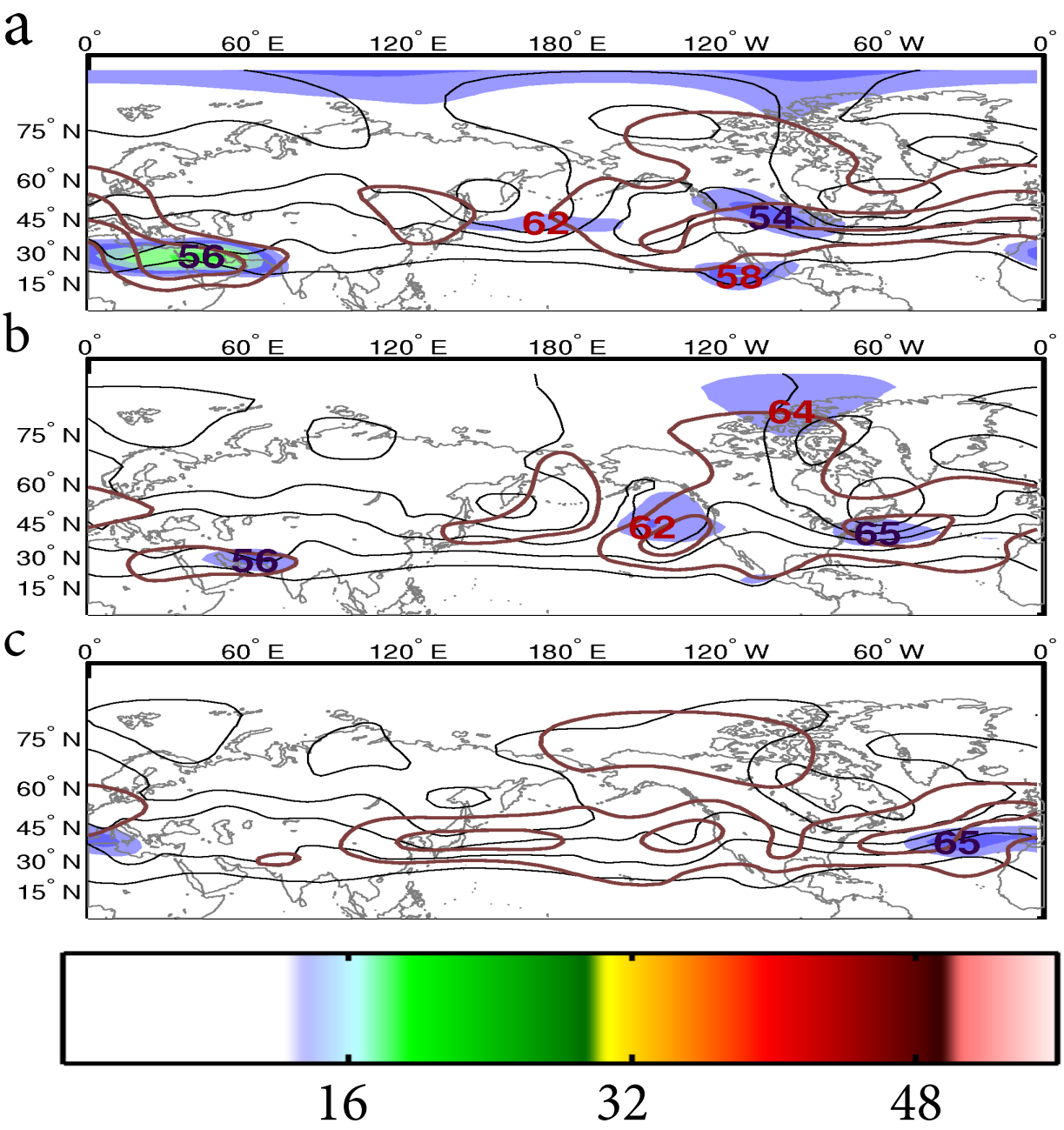

Fig. 3.11 - WPA (shaded), WPI (contoured at 18, 25, 35 and 55 in brown) and 300 hPa geopotential height (contoured every 30 dam starting at 970 in black) for a typical example of wave packet total dissipation that occurred over Europe 09 FEB, 2007 (12 UTC). One day prior to the final track point (a), the final track point (b) and one day after dissipation (c) are shown.

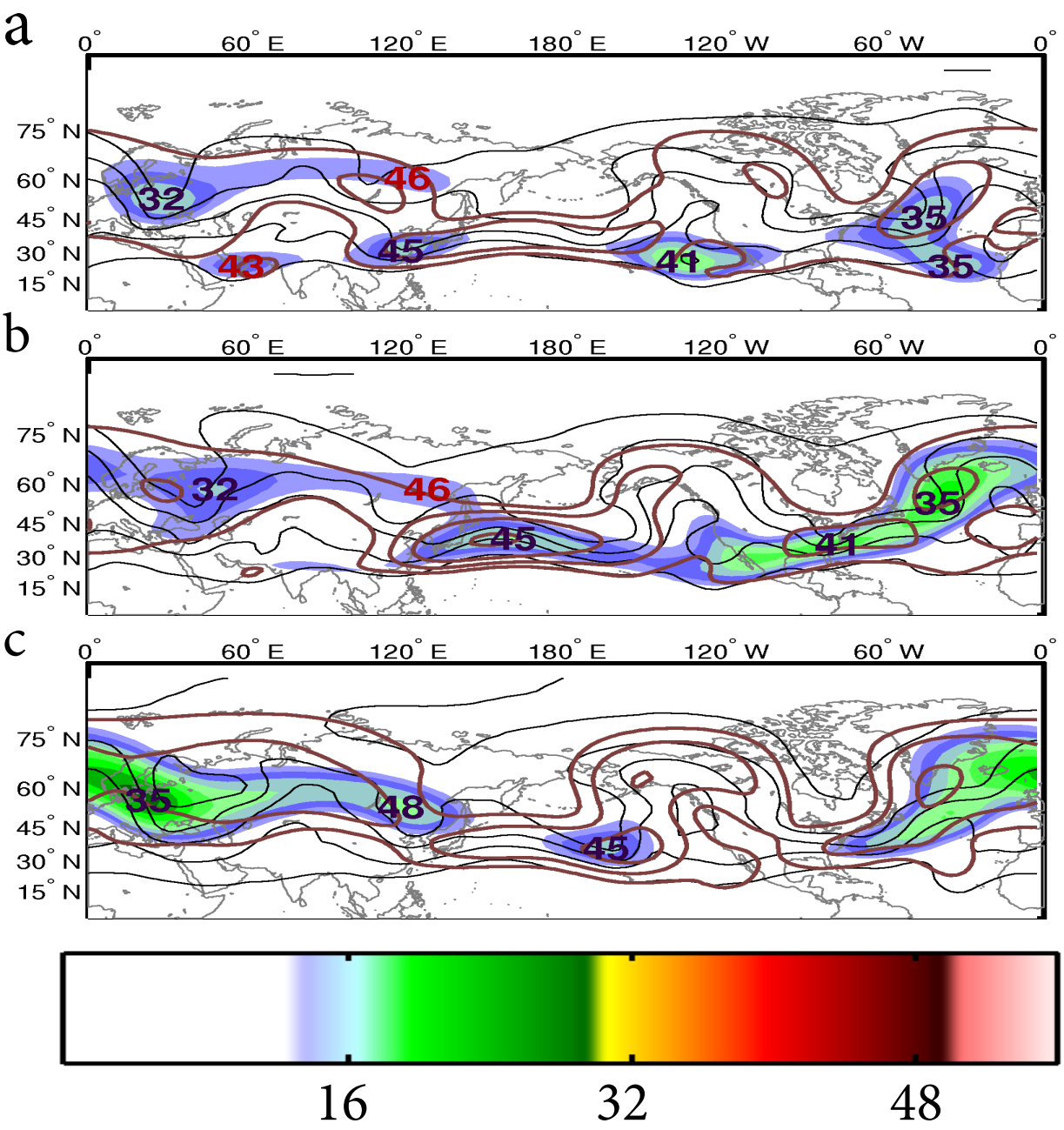

Fig. 3.12 - WPA (shaded), WPI (contoured at 18, 25, 35 and 55 in brown) and 300 hPa geopotential height (contoured every 30 dam starting at 970 in black) for a typical example of a wave packet merging event that occurred over the Atlantic Basin 29 JAN, 2007 (00 UTC). One day prior to the final track point (a), the final track point (b) and one day after dissipation (c) are shown.

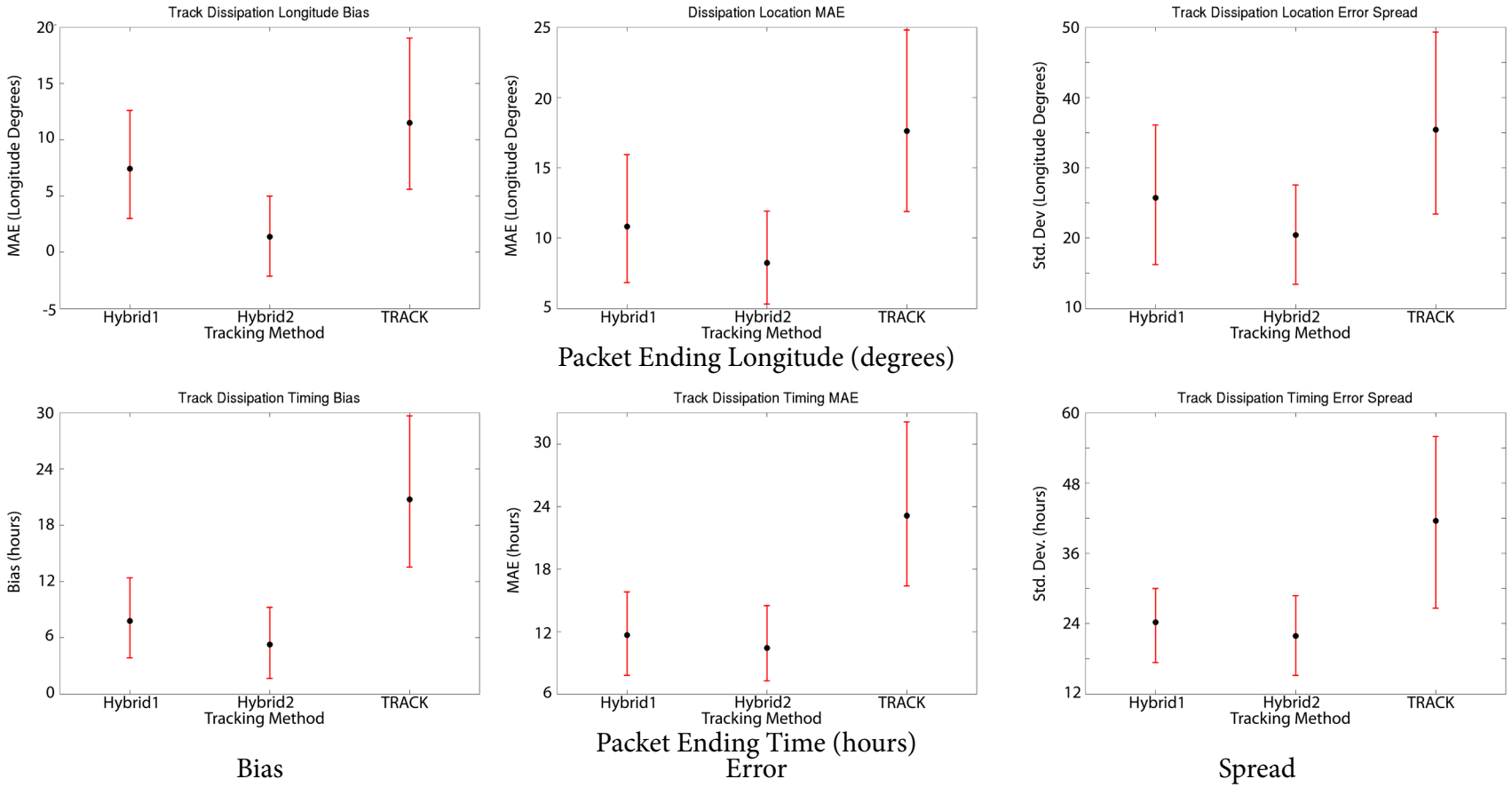

Fig. 3.13 - Statistics governing the performance of each tracking method relative to hand tracking regarding the ending location (TOP) and time (BOTTOM) of wave packets in the seasonal verification period. Bootstrapping was performed on bias (mean error), error (mean absolute error) and error spread (standard deviation of error) in order to obtain 90% confidence intervals (shown in red whiskers).

Method	#T	Missed Tracks			
		Total	Miss Detection	Failed Split	False Merge
TRACK	111	21	1	2	18
Hybrid1	108	9	2	0	7
Hybrid2	113	6	2	2	2
Hand	96	0	0	0	0

Method	#T	False Tracks			
		Total	False Detection	False Split	Failed Merge
TRACK	111	36	14	19	3
Hybrid1	108	21	6	11	4
Hybrid2	113	23	8	9	6
Hand	96	0	0	0	0

Method	Bias	%Det	%False
TRACK	1.16	78.1	32.4
Hybrid1	1.13	90.6	19.4
Hybrid2	1.18	93.8	20.4
Hand	1.00	100.0	0.0

Table 3.1 - Seasonal Verification Track Statistics by Method: data taken from seasonal verification of wave packet tracks (JAN-MAR, 1996 and JAN-MAR, 2007) - %Det = 100*((hand tracks - missed tracks) / hand tracks). %False = 100*(False Tracks/Total Tracks Detected by Method)

Pulses	Frequency	Mean Duration (6-hr intervals)	Mean Propagation (deg. East)
1	42	18.8	107.9
2	38	33.9	176.7
3	9	53.0	308.9
4	5	61.8	367.5
5	1	87.0	390.0
6	0	N/A	N/A
7	1	146.0	1030.0

Table 3.2 - Pulse Statistices from Hand Tracking

Pulse Time	West	Overhead	East
Formation	16	72	8
All	24	129	28

Table 3.3 - Centroid-relative Pulse Location

All data taken from hand verified wave packet tracks from the seasonal verification period and gathered visually. A pulse was recorded if the packet maximum WPA was seen to weaken by at least 5 m s-1 prior to a reintensification with WPI increasing by at least 5 or at wave packet formation. Pulse time refers to when during the life cycle of a wave packet the pulse was recorded. Pulses were said to be west (east) of the packet centroid if the local maximum in WPI associated with the pulse was at least 30 degrees west (east) of the packet centroid, and overhead otherwise.

Table 3.4 - Long Track Cases

H	Start Date	Start Long.	Duration (days)	Propagation (Longitude)	H1	H2
S	11/6/1993	340	55.8	1670	X	X
N	3/17/1998	125	47.5	990	X	X
S	1/7/2004	240	44.3	1120	X	
S	7/24/2003	10	44.3	1315	X	
S	3/20/1984	15	43.5	1305	X	X
S	2/22/1996	265	40.0	1080	X	X
S	6/3/2003	330	38.0	865	X	
S	5/20/2008	0	37.8	1055	X	X
S	7/7/2002	320	37.8	1240	X	
S	8/22/1999	260	36.5	940	X	X
S	5/13/1990	205	35.8	515	X	X
N	1/4/2003	160	34.5	585	X	X
N	9/12/2004	20	34.5	825	X	
S	1/10/2001	35	33.5	1000	X	X
N	9/25/1996	185	33.3	520	X	X
S	6/25/1998	20	33.3	595	X	X
N	3/20/1982	175	31.0	510	X	X
S	12/5/1983	135	30.8	785		X
S	1/8/1994	245	30.3	1030	X	X
S	12/19/1987	195	29.8	735	X	X
N	2/5/1985	180	29.8	845	X	
S	12/21/1990	185	29.5	535		X
S	4/6/1992	15	29.0	620	X	X
S	7/10/1992	60	29.0	510	X	X
S	5/10/1993	0	29.0	505	X	X
S	10/24/2001	190	29.0	1045	X	X
S	1/9/1989	320	28.3	805	X	X
S	11/29/1996	335	28.0	765		X
S	1/27/2002	310	28.0	950		X
S	7/16/1987	200	28.0	535	X	X
S	9/12/1996	220	27.5	560		X

Table 3.4 - Long Track Cases

H	Start Date	Start Long.	Duration (Days)	Propagation (Longitude)	H1	H2
S	2/25/1992	335	27.5	620		X
S	9/2/2005	350	27.3	765		X
S	5/26/2000	40	27.3	770	X	
N	1/8/1988	180	27.0	625	X	X
S	3/29/1991	90	27.0	705		X
S	3/7/1987	250	27.0	725	X	X
S	7/25/1987	185	26.8	505		X
S	1/14/1982	345	26.8	930	X	X
N	10/25/1991	210	26.8	615	X	X
N	2/17/1989	150	26.8	540	X	X
S	6/12/2005	290	26.3	605		X
S	3/31/1995	330	26.3	480	X	X
S	4/27/2004	60	26.3	670	X	X
S	3/3/2006	260	26.3	755	X	X
N	3/31/1995	15	26.0	455	X	X
S	11/19/2005	5	26.0	725	X	X
S	5/15/1980	355	25.8	720	X	X
S	7/30/1994	0	25.8	695	X	
S	1/30/1999	305	25.5	835	X	X
N	3/5/2000	90	25.5	575	X	
N	2/11/2008	210	25.5	655	X	
S	1/21/1995	300	25.3	845	X	X
N	10/3/1999	155	25.3	610	X	X
S	12/31/1998	35	25.3	680	X	
S	7/19/1984	320	24.5	575	X	
S	5/7/1998	145	23.8	455	X	
N	11/4/1981	250	23.5	200	X	
S	3/1/2004	210	23.0	690	X	
S	12/28/2002	45	23.0	555	X	
S	4/2/1987	65	22.3	560		X
S	5/8/2003	0	21.8	470	X	

Table 3.4 - Long Track Cases

H	Start Date	Start Long.	Duration (Days)	Propagation (Longitude)	H1	H2
N	12/1/2008	75	21.0	465	X	
S	5/18/1986	120	20.5	270	X	
N	3/16/1989	105	20.0	460	X	
S	11/8/1979	215	19.8	475	X	
S	10/18/2007	50	19.3	535	X	
N	12/23/1982	315	17.8	430	X	
N	2/18/1997	50	17.5	495	X	
S	12/18/1992	270	17.0	390	X	X
S	5/8/1999	190	17.0	270	X	
S	6/10/1991	300	15.3	330	X	
N	4/2/1986	120	13.5	215	X	X
N	11/4/1997	30	13.5	365	X	
N	11/6/1989	120	13.3	220		X

Method	Long Tracks	Verified	Verification Rate	Detection Rate
Hybrid1	63	45	0.71	0.82
Hybrid2	48	44	0.91	0.80
Both	75	55	0.73	1.00

Method	Track Lengthening Errors		Track Shortening Errors		Total Errors	Error Rate
	False Merge	Failed Split	Failed Merge	False Split		
Hybrid1	45	14	24	0	83	1.32
Hybrid2	21	0	30	13	64	1.33

Table 3.5 - Verification of Long (>25-day) Tracks

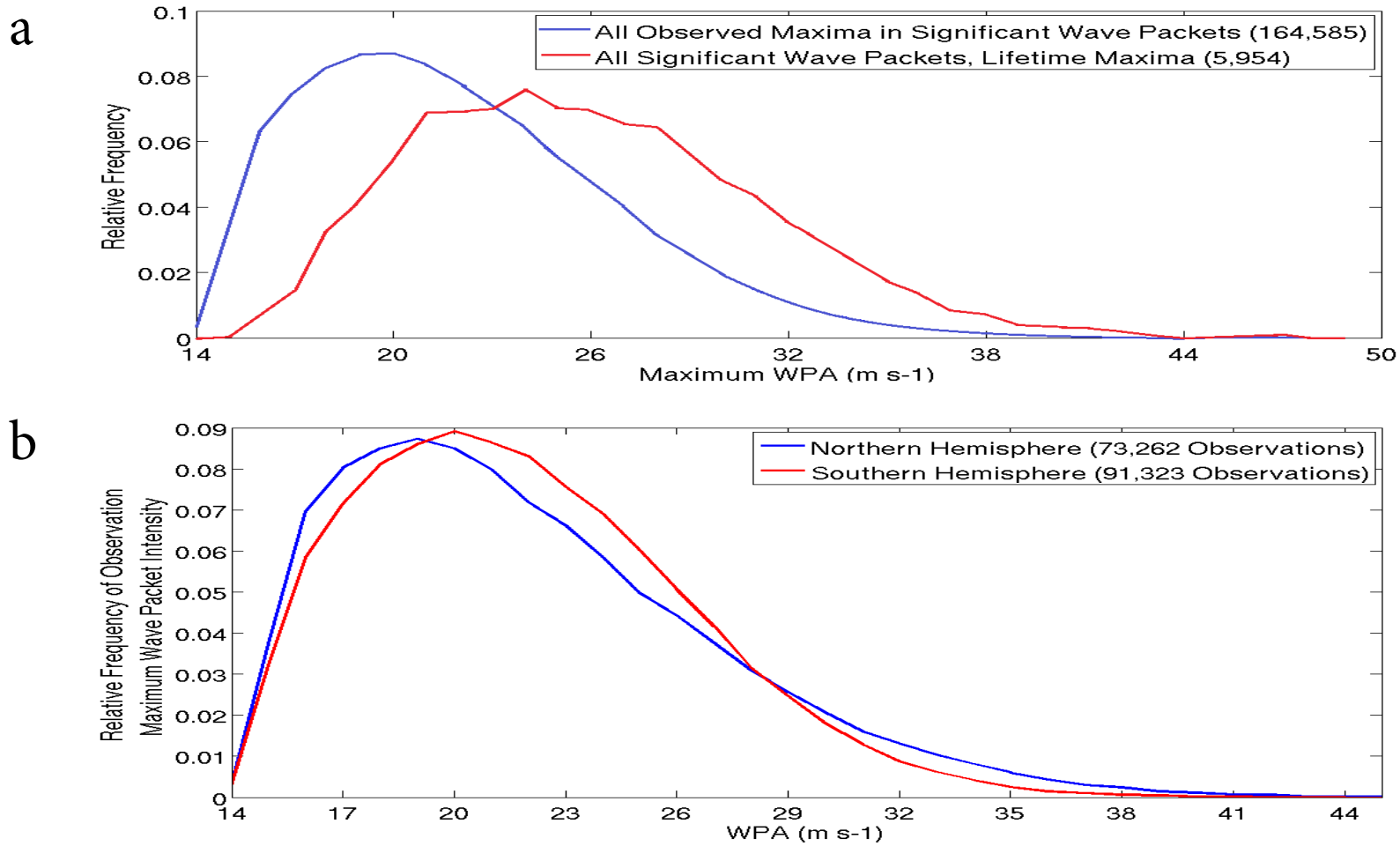

Fig. 4.1 - Relative frequency distributions of WPA (m s^{-1}) for (a) all wave packet centoirds (global) and the maximum intensity of all significant wave packets (global) and (b) all wave packet centroids in the NH and SH

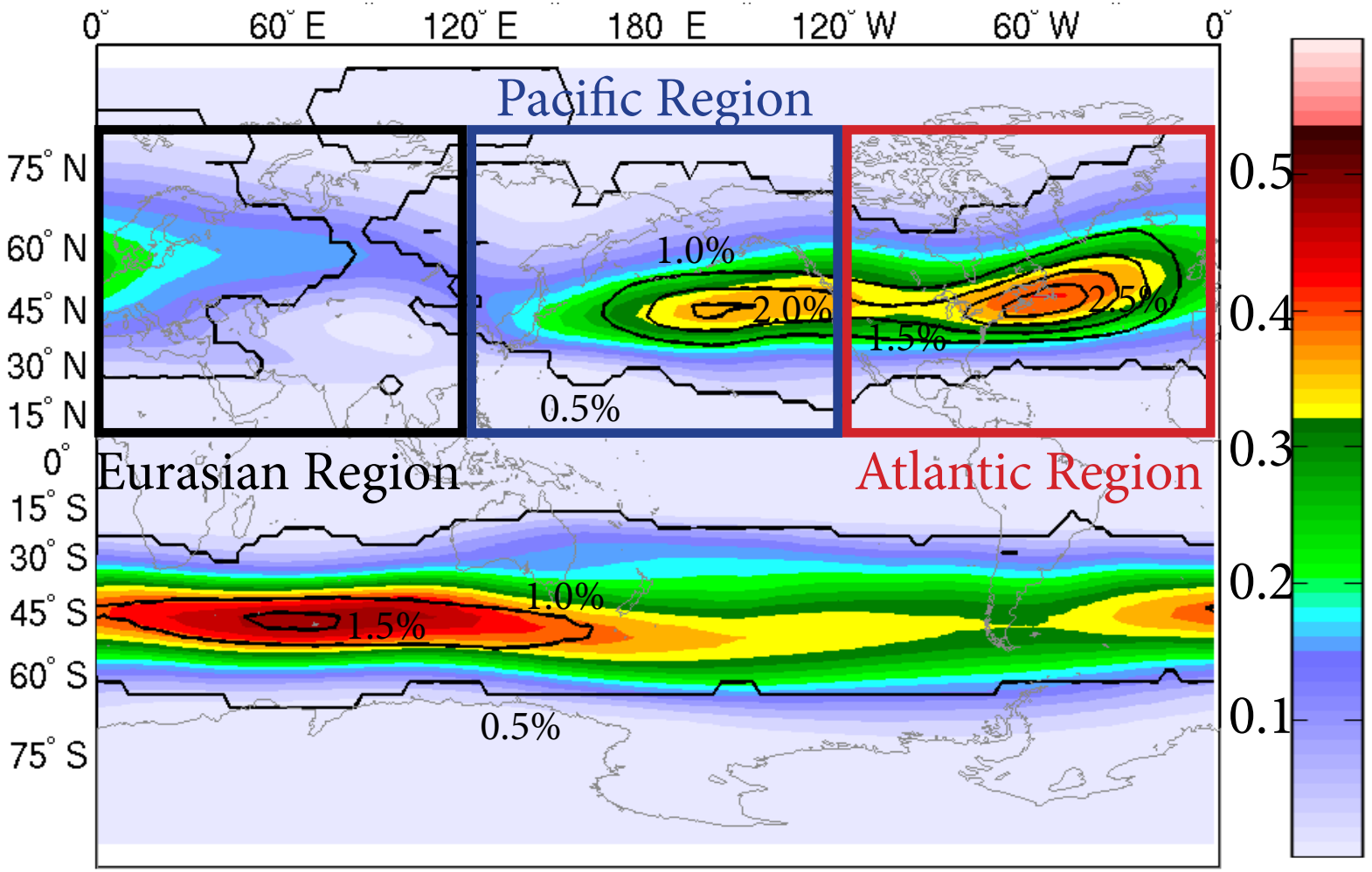

92

Fig. 4.2 - The annual probability of WPA within significant wave packet objects exceeding 14 m s^{-1} (shaded) and 30 m s^{-1} (contoured every 0.005, beginning at 0.005). For future reference, the three major regions of the Northern Hemisphere are also marked and labeled.

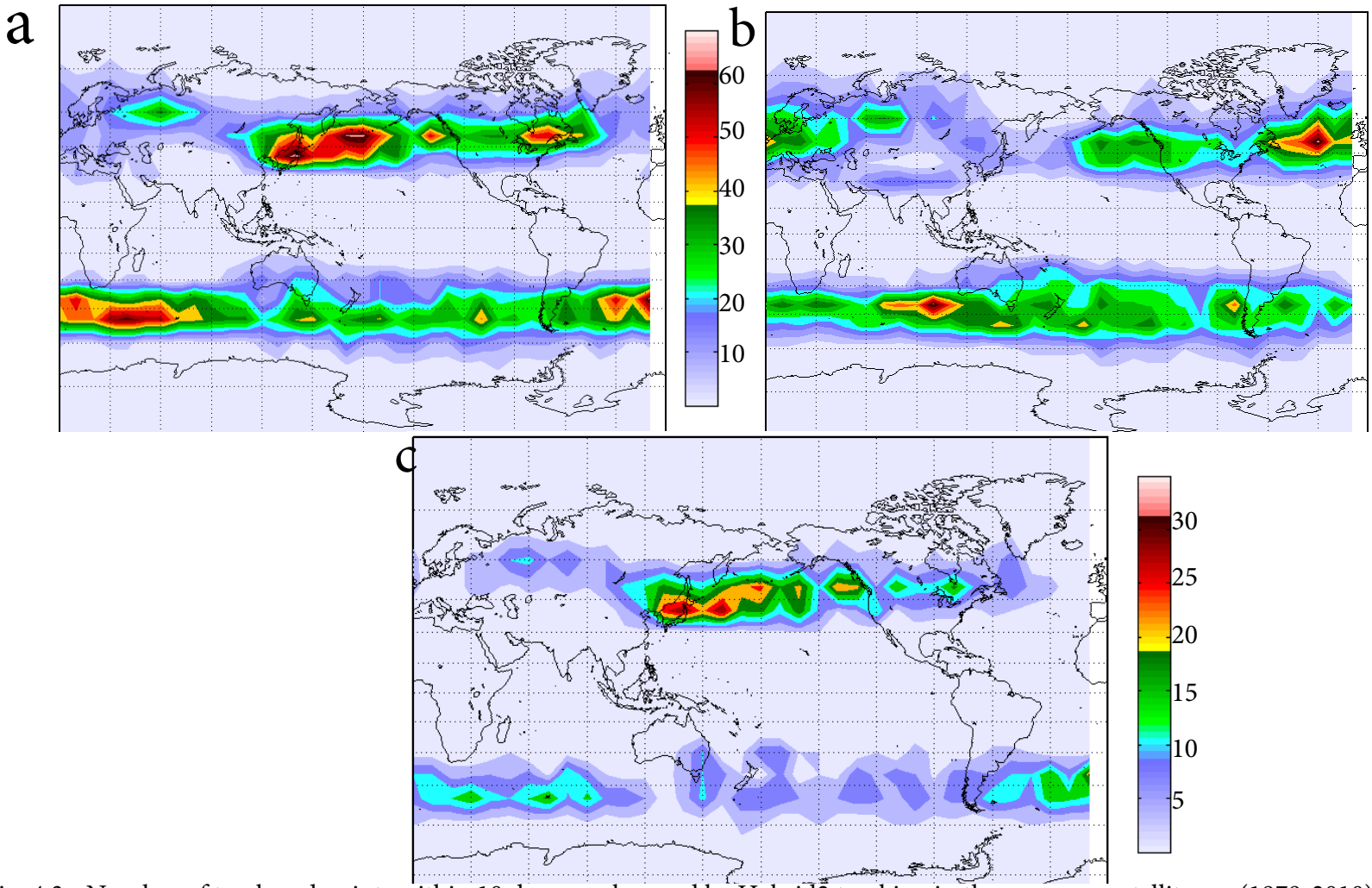

Fig. 4.3 - Number of track end points within 10 degrees observed by Hybrid2 tracking in the common satellite era (1979-2010) for (a) all significant track formations, (b) all significant track dissipations and (c) all track formations for extreme wave packet events (>30 m s^{-1} maximum lifetime intensity)

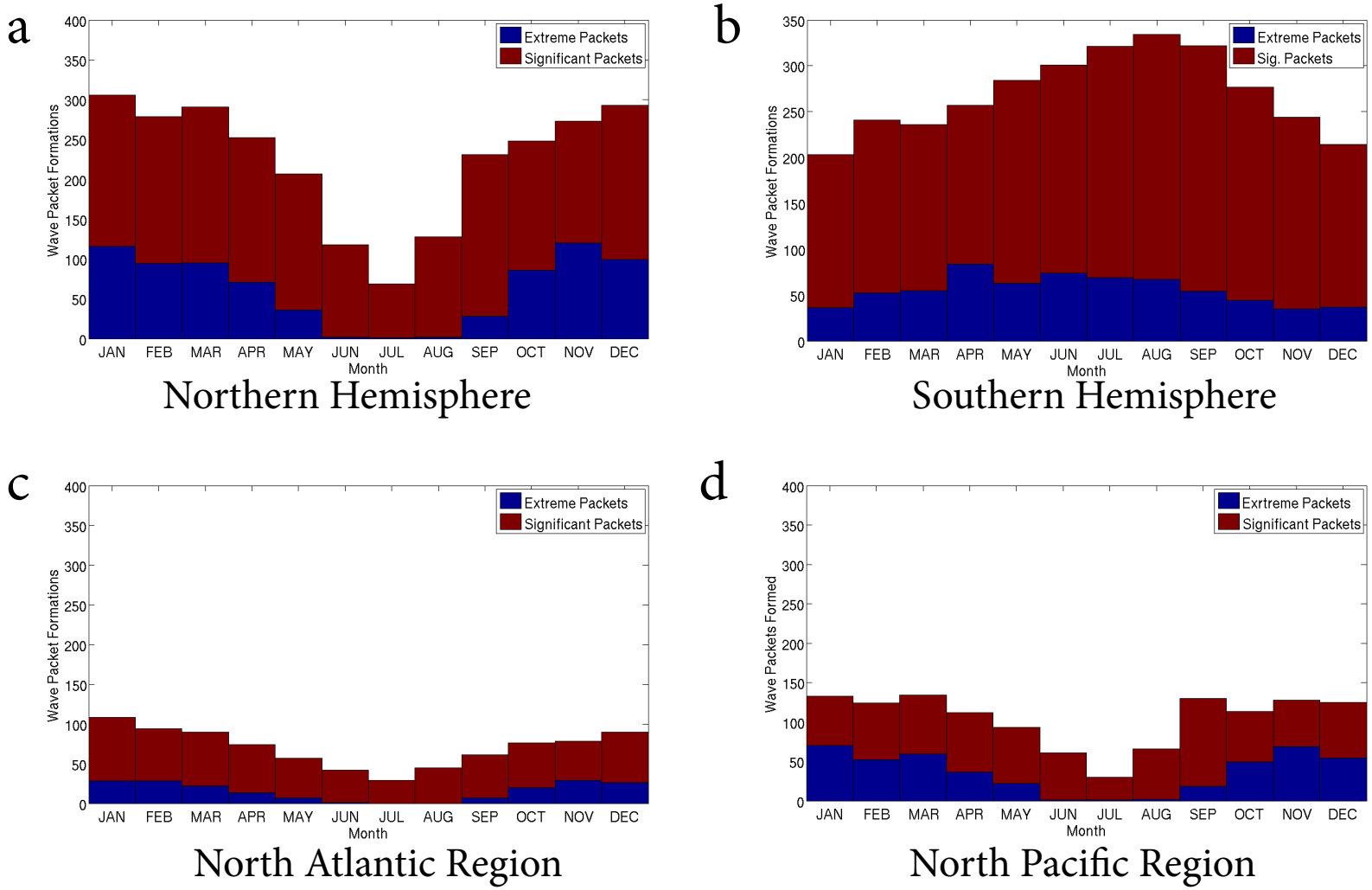

Fig. 4.4 - Number of significant (red) and extreme (blue) wave packets forming in each calendar month in (a) the entire NH (b) the entire SH, the North Atlantic storm track belt (240-360 E, 10-80 N) and (d) the Noth Pacific storm track belt (120-240 E, 10-80 N)

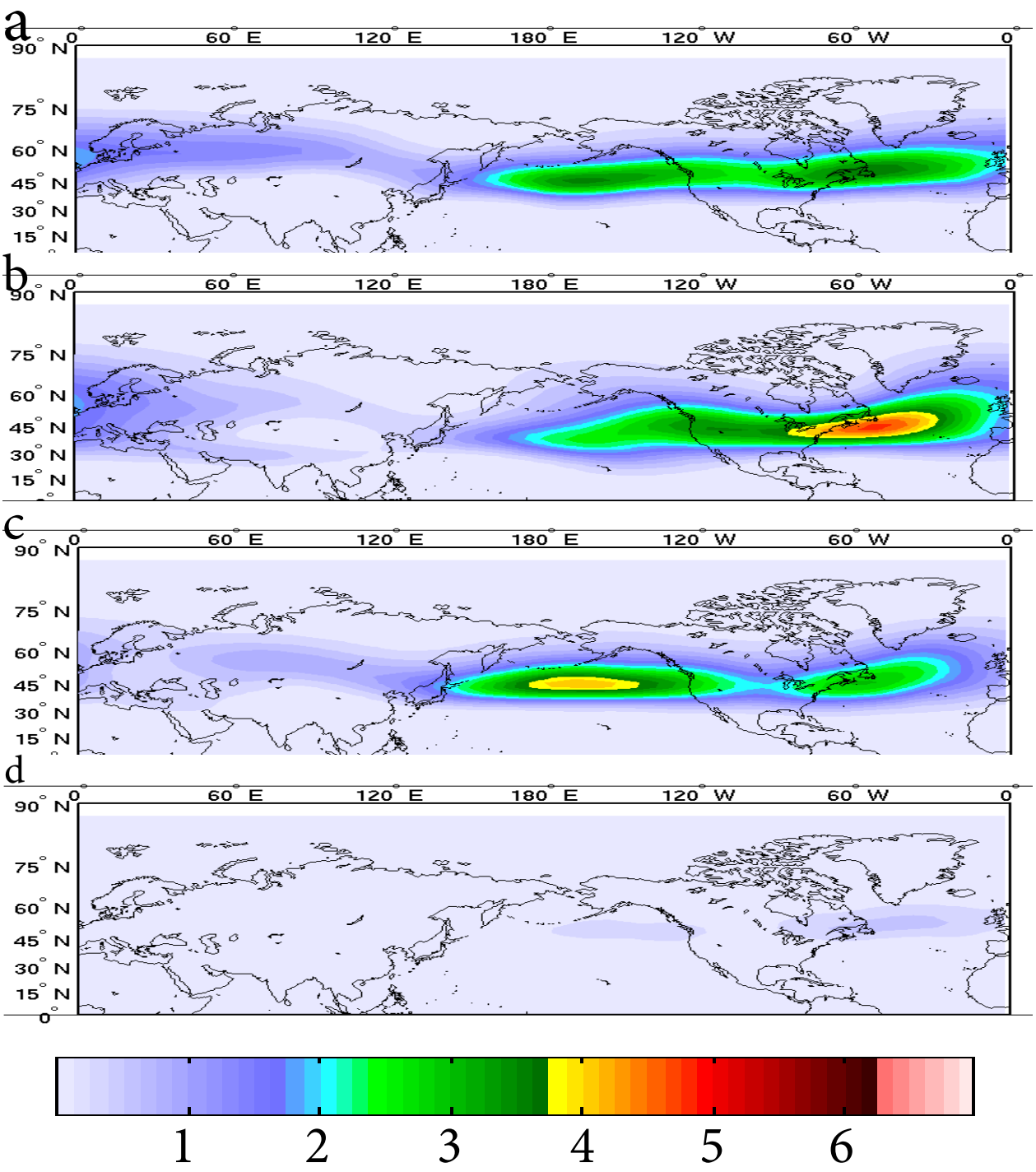

Fig. 4.5 - Monthly average wave packet activity (m s^{-1} 6 hr^{-1}) for (a) October, (b) January, (c) April and (d) July in the Northern Hemisphere - obtained by calculating the WPA at each grid point and each time step in the common satellite era in excess of the minimum tracking threshold (14 m s-1), with all lesser values counting for zero and dividing by the number of time steps in each month.

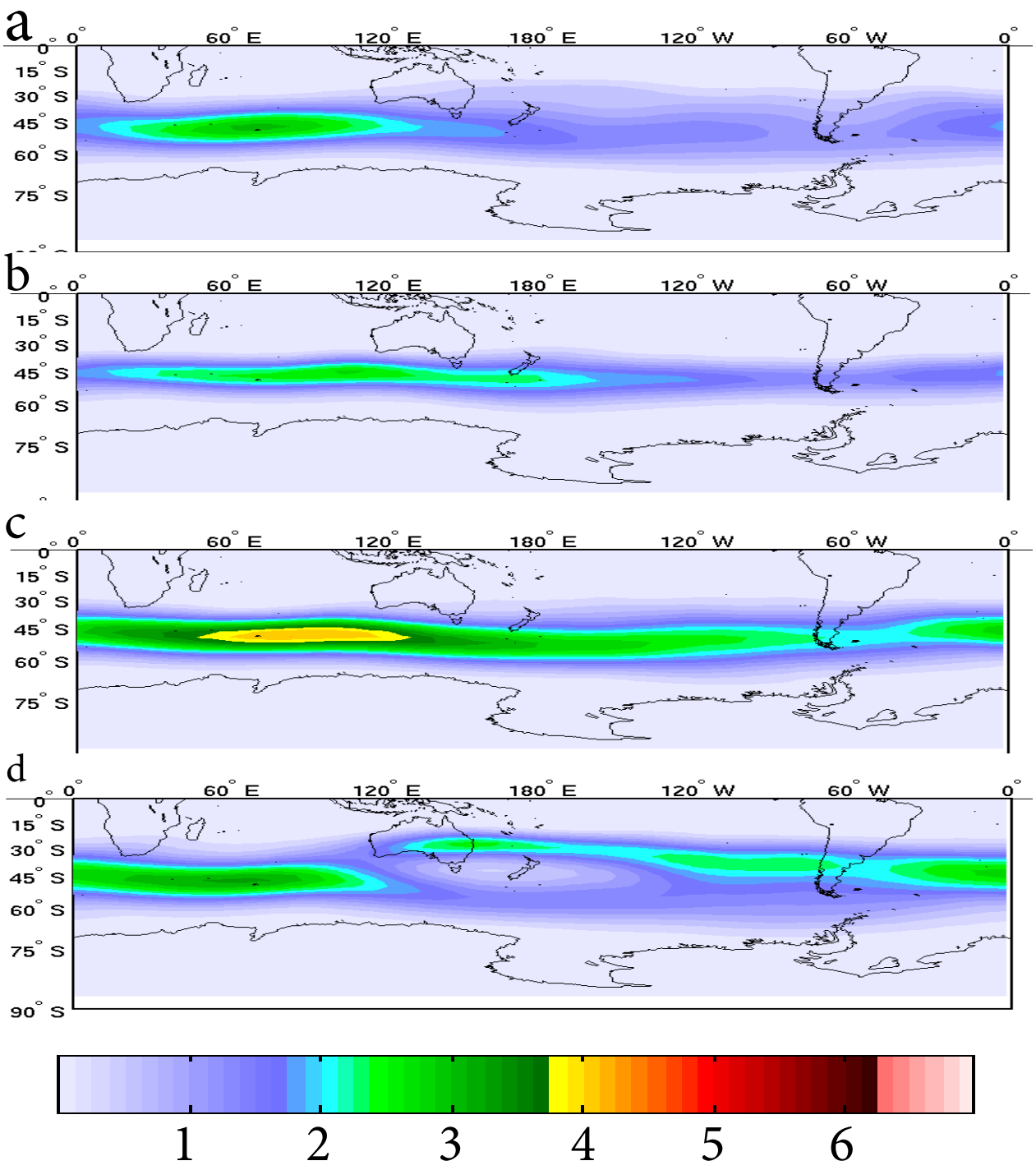

Fig. 4.6 - Monthly average wave packet activity (m s^{-1} 6 hr^{-1}) for (a) October, (b) January, (c) April and (d) July in the Southern Hemisphere - obtained by calculating the WPA at each grid point and each time step in the common satellite era in excess of the minimum tracking threshold (14 m s-1), with all lesser values counting for zero and dividing by the number of time steps in each month.

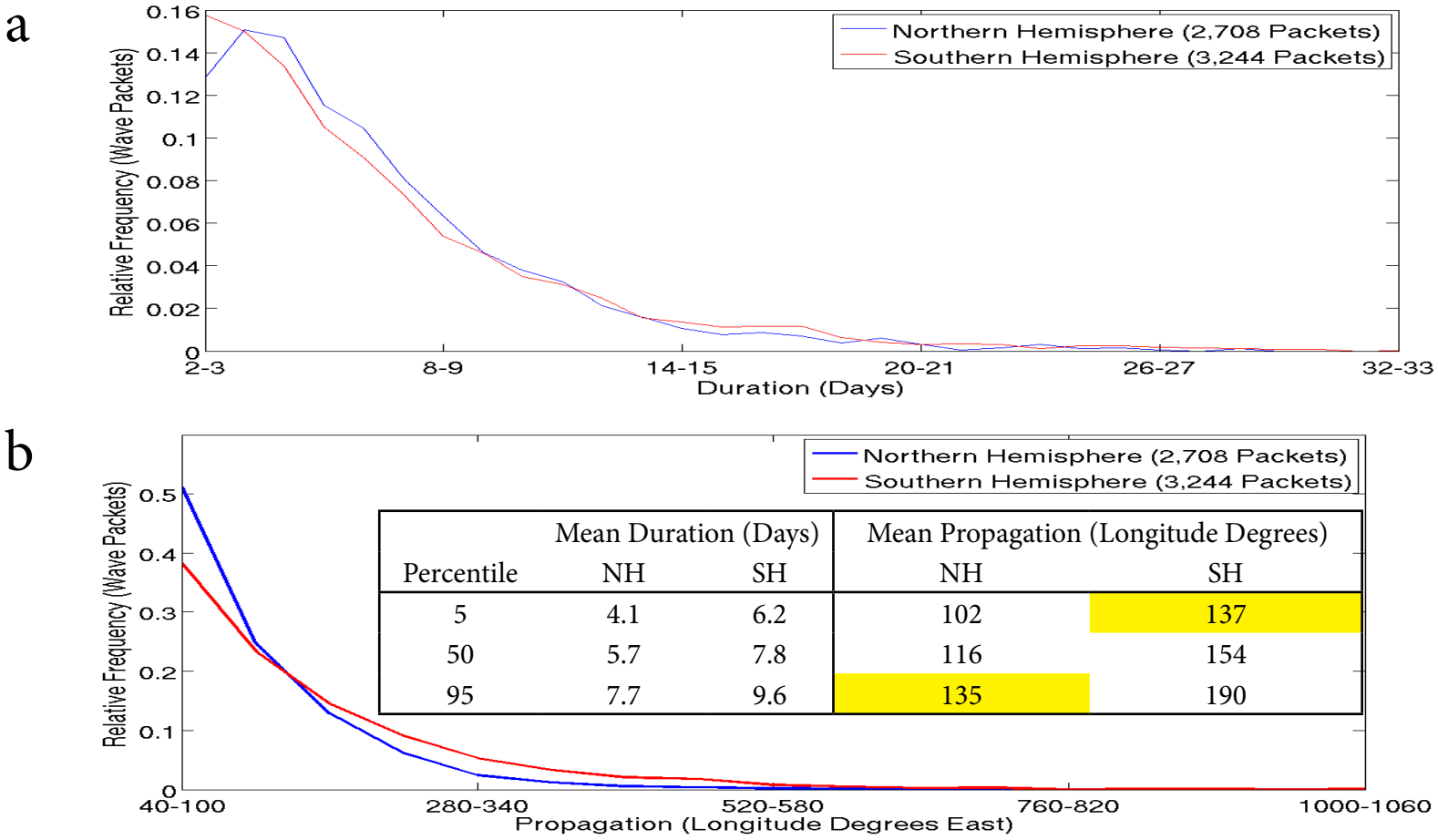

	Mean Duration (Days)		Mean Propagation (Longitude Degrees)	
Percentile	NH	SH	NH	SH
5	4.1	6.2	102	137
50	5.7	7.8	116	154
95	7.7	9.6	135	190

Fig. 4.7 - Relative frequency distributions of significant RWP (a) duration (days) and (b) eastward propagation (longitude degrees) in each hemisphere. The inset chart reveals the results of bootstrapping for propagation and duration averages from 500 packet samples drawn randomly 10,000 times.

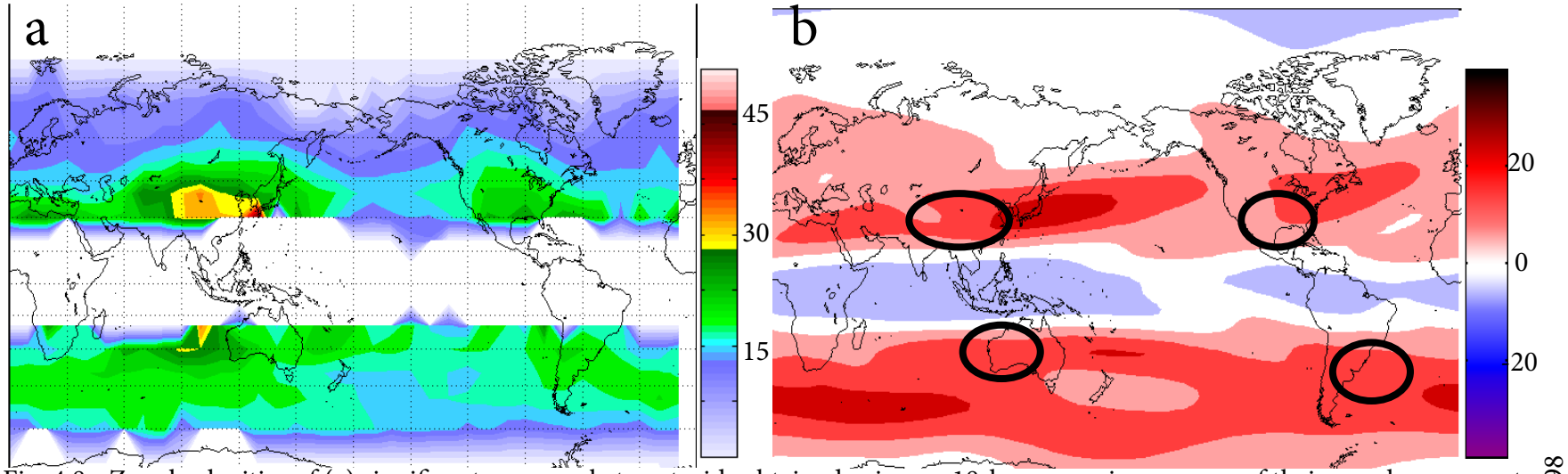

Fig. 4.8 - Zonal velocities of (a) significant wave packet centroids obtained using an 18-hour running average of their zonal movements and averaging all centroids within 10 degrees of a given grid point, masking out all grid points for which fewer than 25 observations can be found and (b) annual average 300 hPa zonal wind (both in m s^{-1}) as a point of comparison. Regions circled in black represent areas of enhanced RWP zonal velocity and are colocated with the entrance regions of the climatologically favored jet streams.

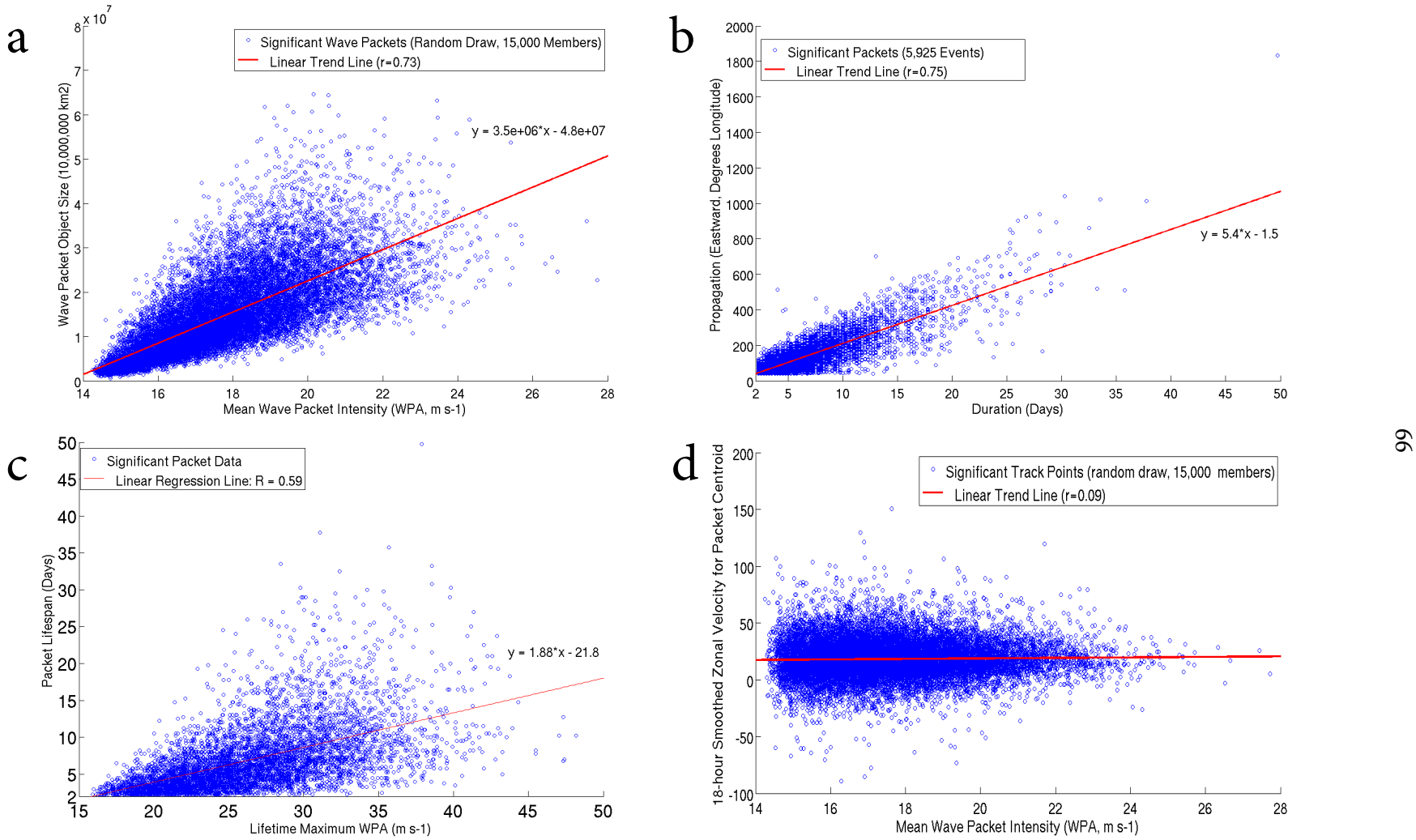

Fig. 4.9 - Scatter plots (with linear regression lines) relating (a) RWP centroid intensity (m s^{-1}) with RWP size (10^7 km^2) (b) RWP duration (6 hr) with RWP propagation (longitude degrees) (c) RWP centroid intensity with duration and (d) RWP centroid intensity with 18-hour averaged centroid velocity (m s^{-1}).

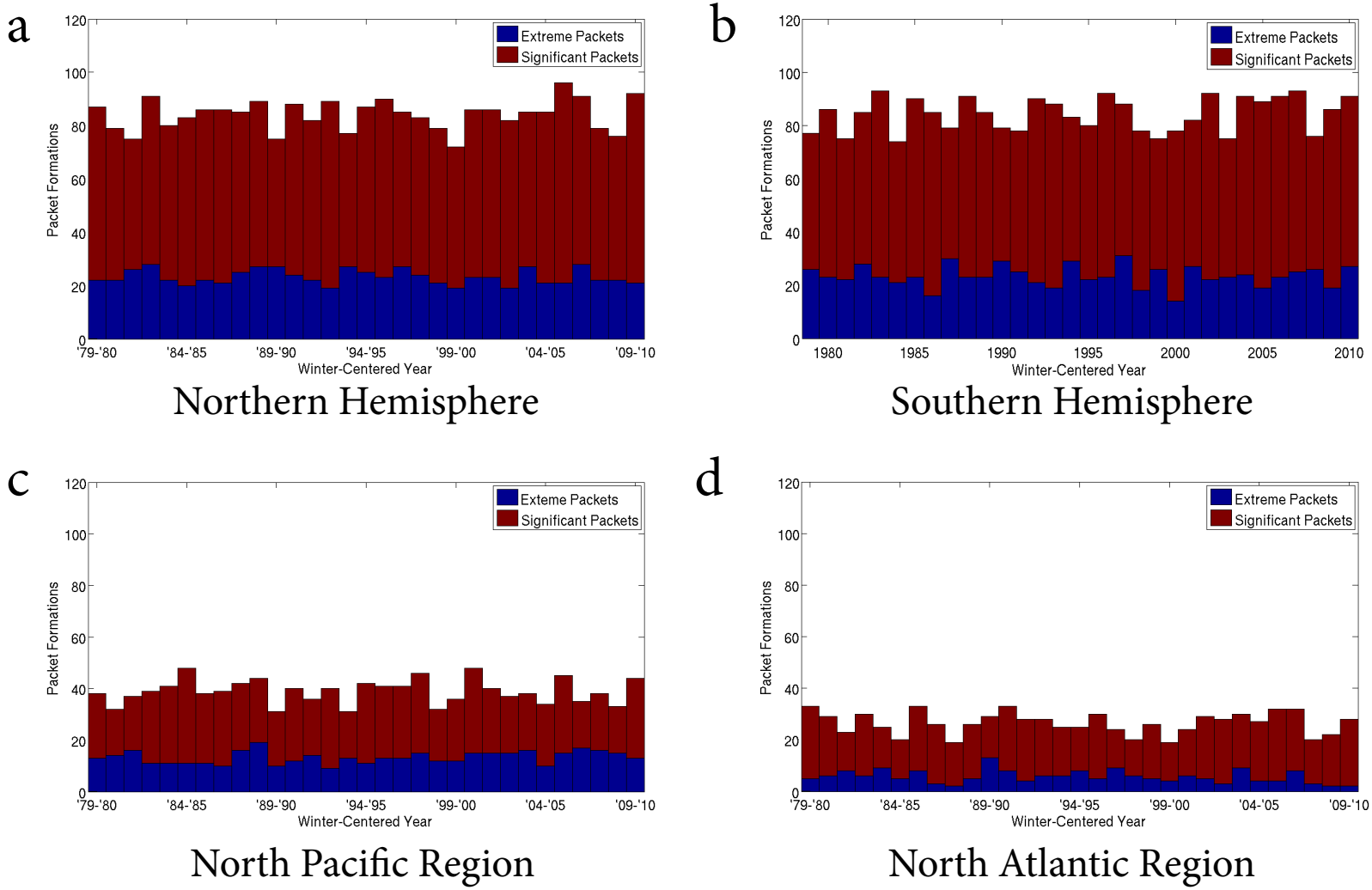

Fig. 4.10 - RWP formations by winter-centered year (NH: JUL-JUN, SH: JAN-DEC), listed as the year of the final month for (a) the entire NH, (b) the entire SH, (c) the North Pacific (120-240 degrees E) and (d) North Atlantic (240-360 degrees E) regions.

a

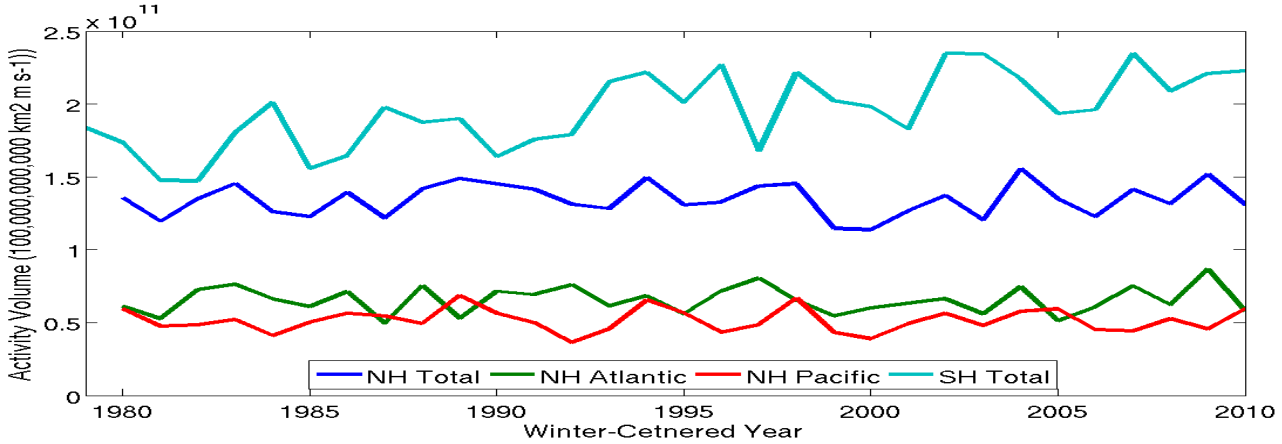

b

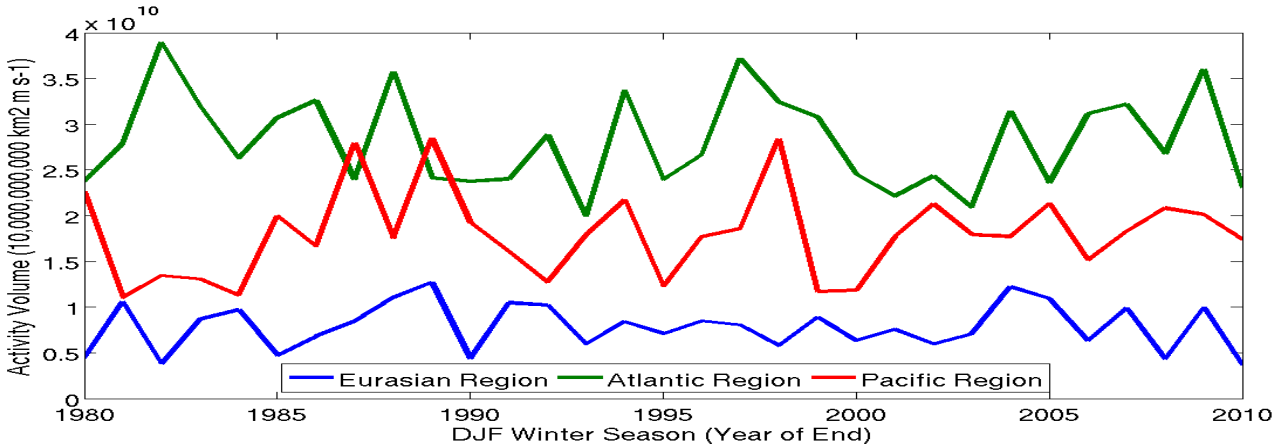

Fig. 4.11 - Interannual variability in RWP activity volume obtained by multiplying the mean WPA above the minimum tracking threshold of 14 m s-1 for a given packet by its areal coverage and then summing over the specified region based on the locations of the packet centroids. In (a) activity volume (in 10^{11} km^2 m s^{-1}) is summed over the entire winter-centered year for each of four regions and in (b) activity volume (in 10^{10} km^2 m s^{-1}) is summed over just the months of DEC-FEB.

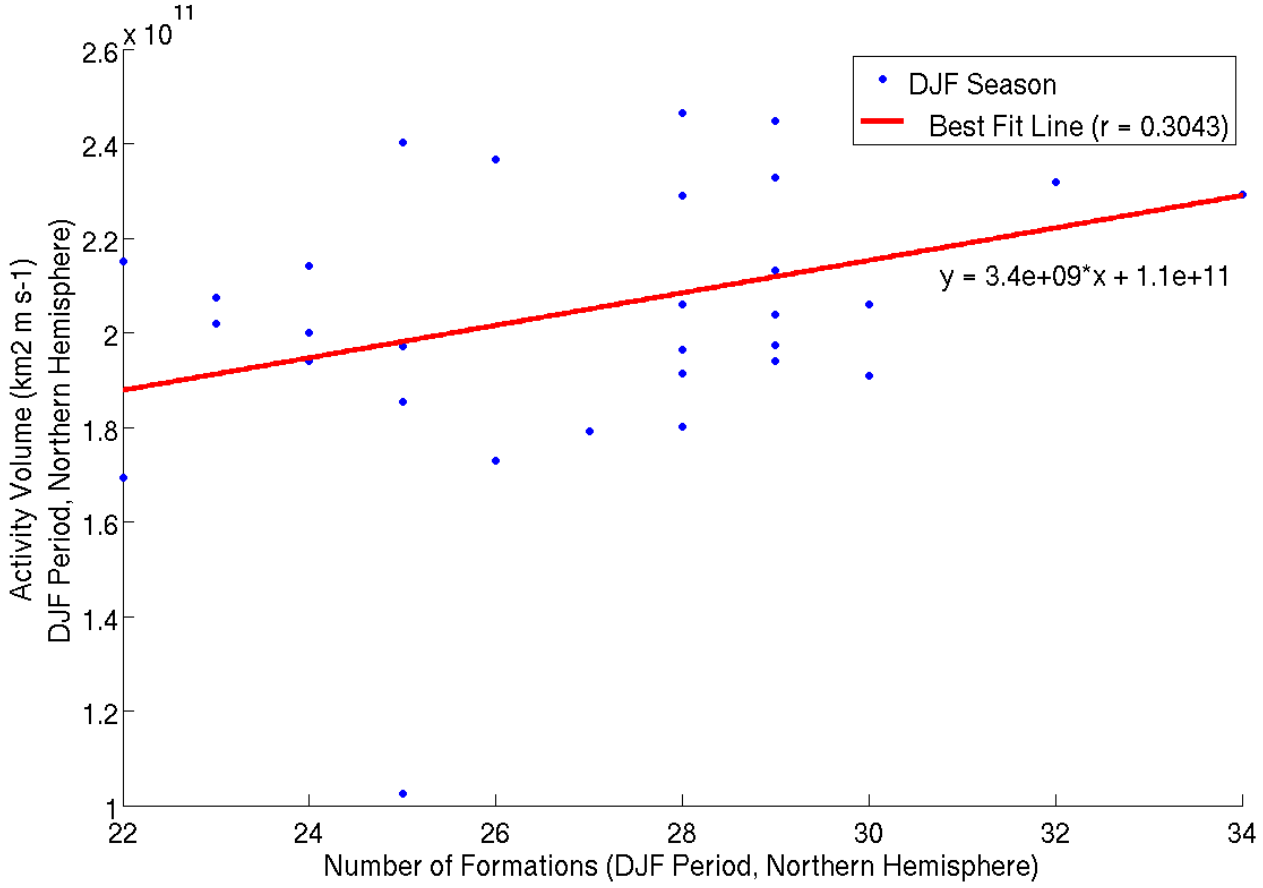

Fig. 4.12 - Linear correlation test between the frequency of formation in the Northern Hemisphere winter (DJF) months and the net RWP activity volume as defined in Fig. 4.11 in the NH winter months.

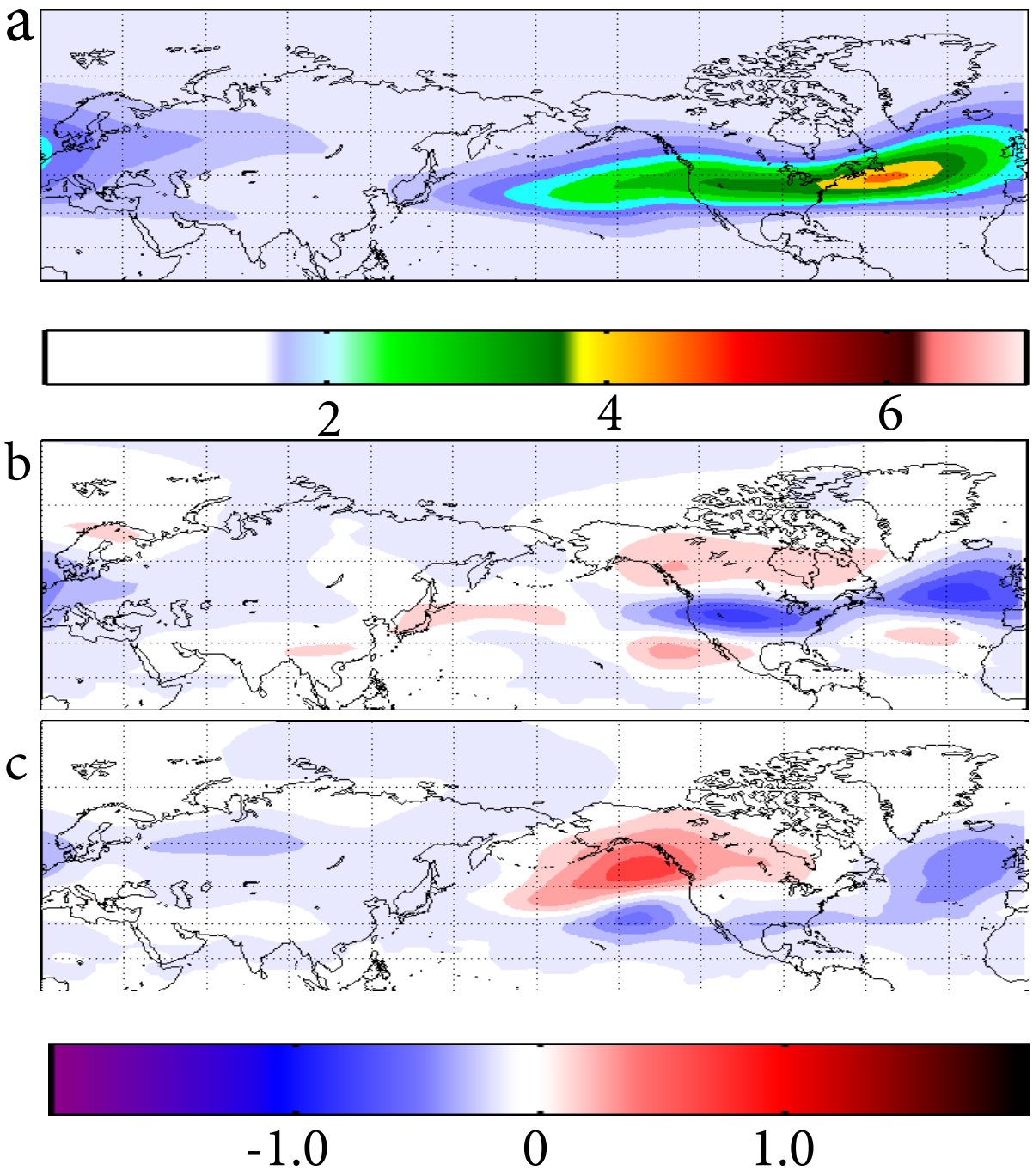

Fig. 4.13 - A comparison of average RWP activity (m s^{-1} 6 hr^{-1}) in varying states of ENSO as measured by the multivariate ENSO index (MEI). In (a) the RWP activity is shown for ENSO neutral winter (DJF) seasons. In (b) and (c) the difference is shown between RWP activity in El Nino (b) and La Nina (c) seasons. El Nino is defined as any year in which the winter mean MEI is greater than 0.5, and a La Nina is defined as any year in which the winter mean MEI is less than -0.5/ (a) is contoured every 0.5 m s^{-} 6 hr^{-1}, and (b) and (c) are contoured every 0.2 m s^{-1} 6 hr^{-1}.

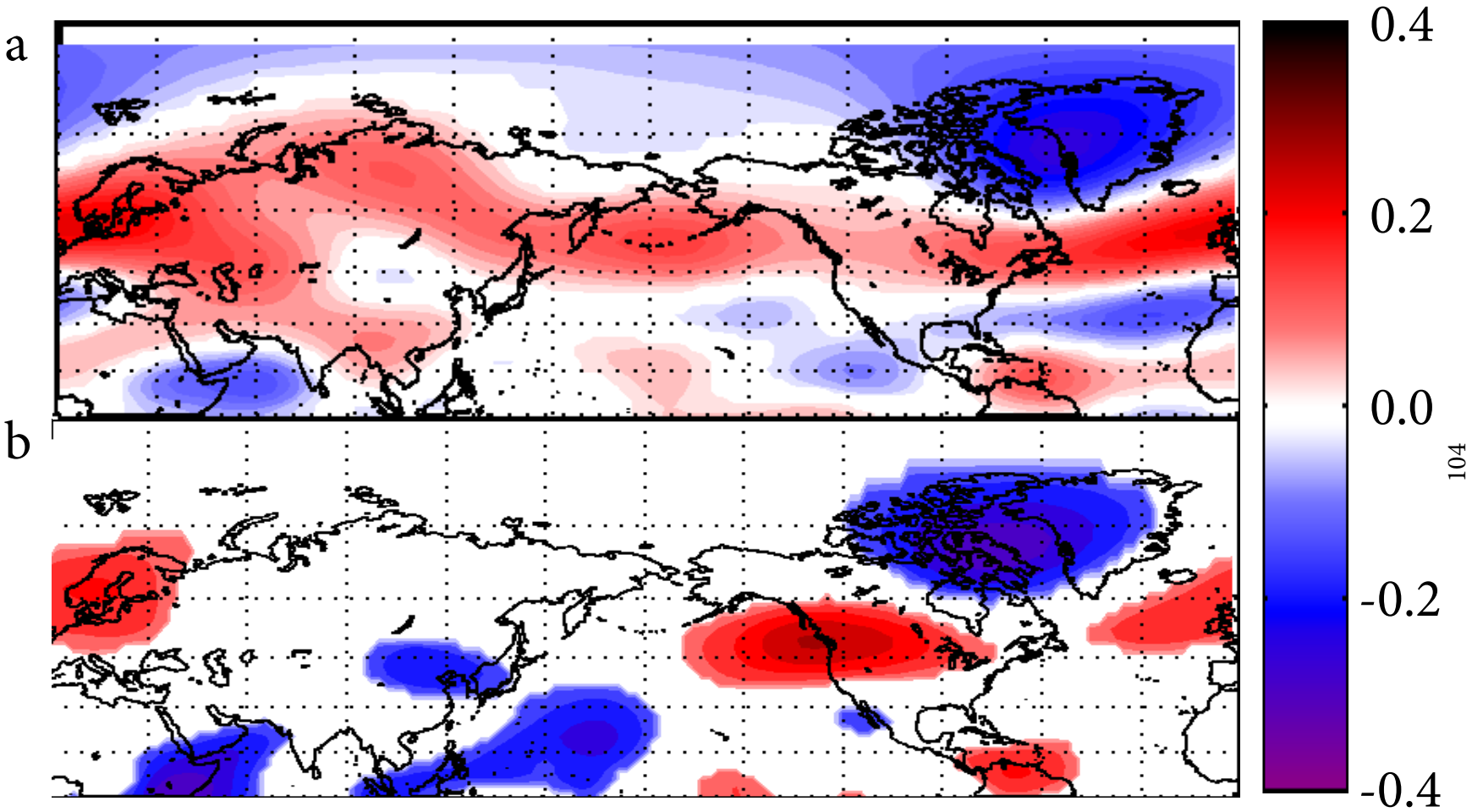

Fig. 4.14 - Single point correlation analysis relating WPA anomaly (the difference between the WPA values at each grid point and the climatological average for the time being measured) with (a) the 5-day-smoothed AO daily AO Index value (contoured every 0.02) and (b) the rate of change in the 5-day-smoothed AO Index value (contoured every 0.05). In each figure, the data was randomly drawn from all cool season (SONDJFMA) days such that the total sample being analyzed was 1/10th the size of the available data set to avoid interdependence, and the correlation coefficients which were not statistically significant with a p-value of >0.95 were masked out.

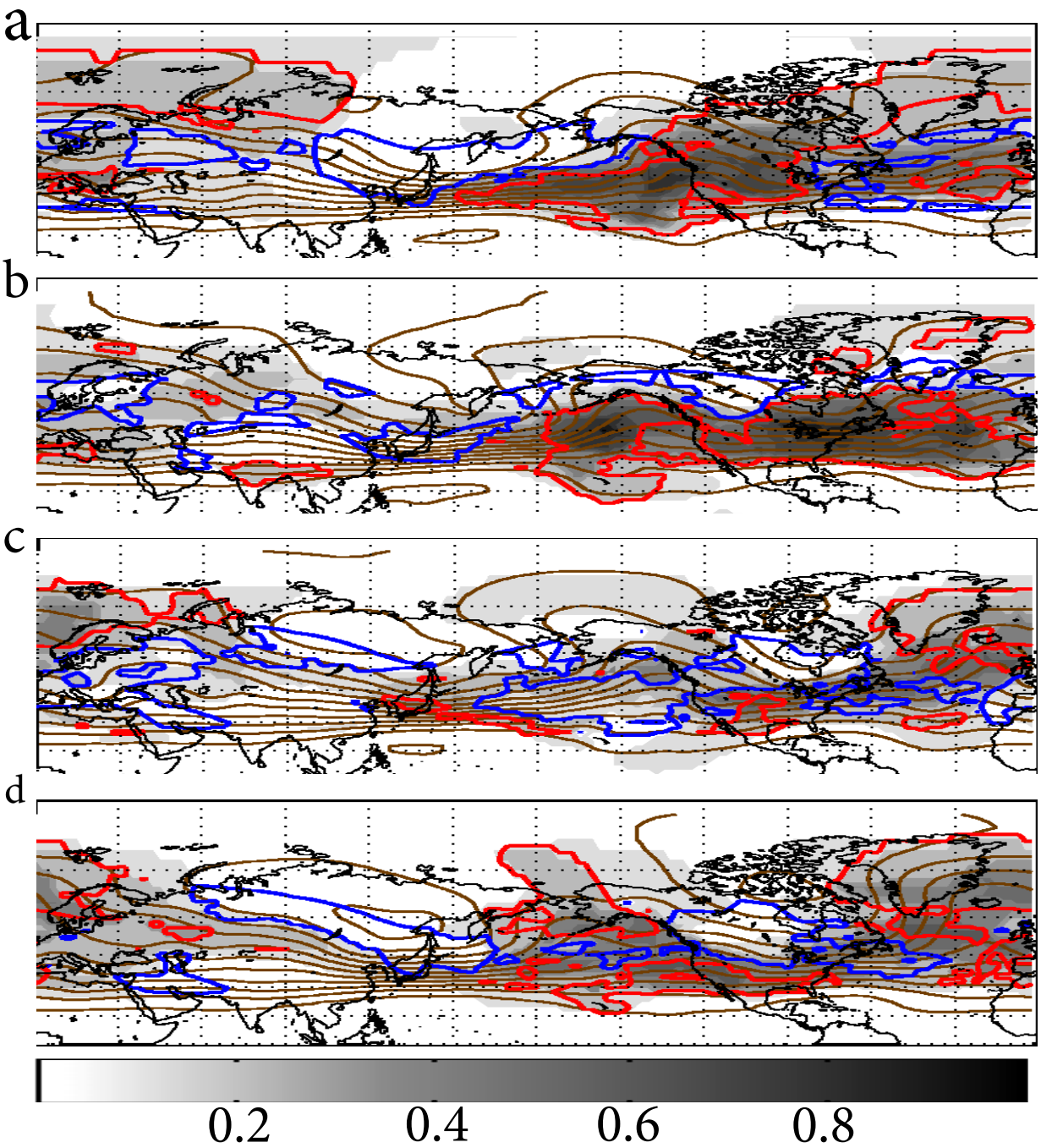

Fig. 4.15 - Representative 300 hPa geopotential height (contoured every 12 dam and obtained by adding the composite height anomaly to the DJF mean height), probability of WPA exceeding 14 m s-1 (shaded every 0.1), and regions where the differences between the probability of exceedence and the DJF mean probability is statistically significant ($p < 0.05$), with positive anomalies in red and negative anomalies in blue. The composite includes 59 cases where the 5-day-smoothed AO index began above 1.0, fell at least 3 and ended below -1, centered on the day where the AO dropped below zero. Five days prior to center date (a), 3 days prior (b), 1 day prior (c) and 2 days after (d) are shown.

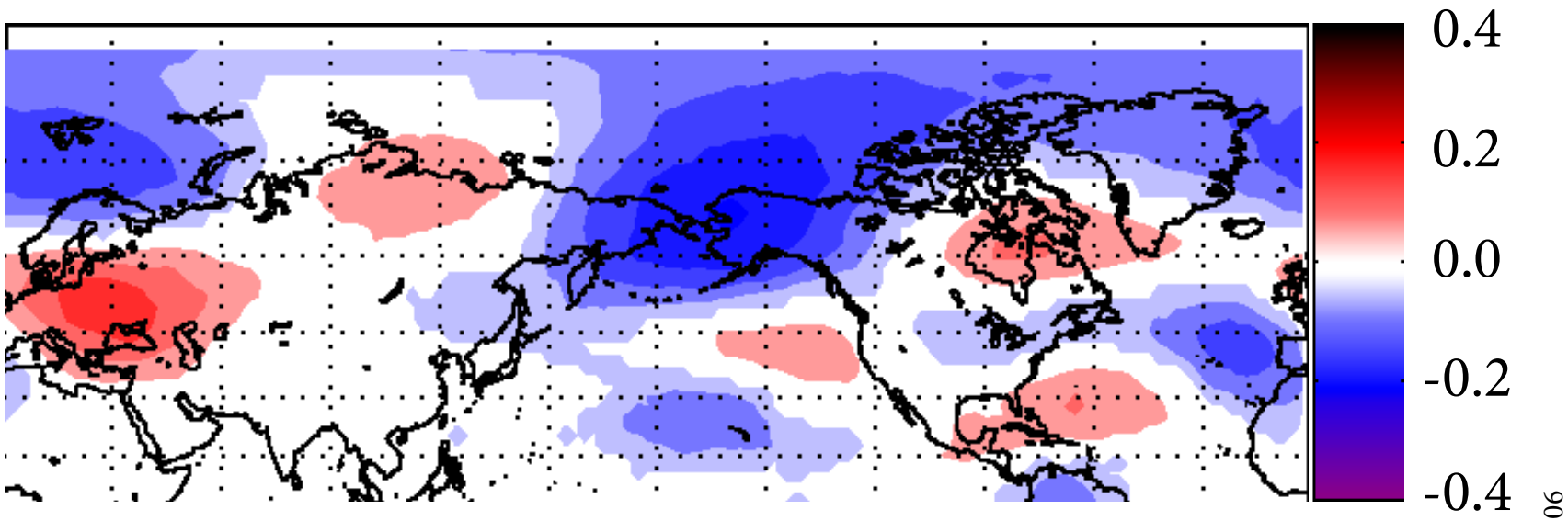

Fig. 4.16 - Single point correlation analysis as before in Fig. 4.13, except comparing WPA anomaly with the 5-day-smoothed daily PNA Index. All insignificant correlation values are masked as before - coefficients are contoured every 0.05.

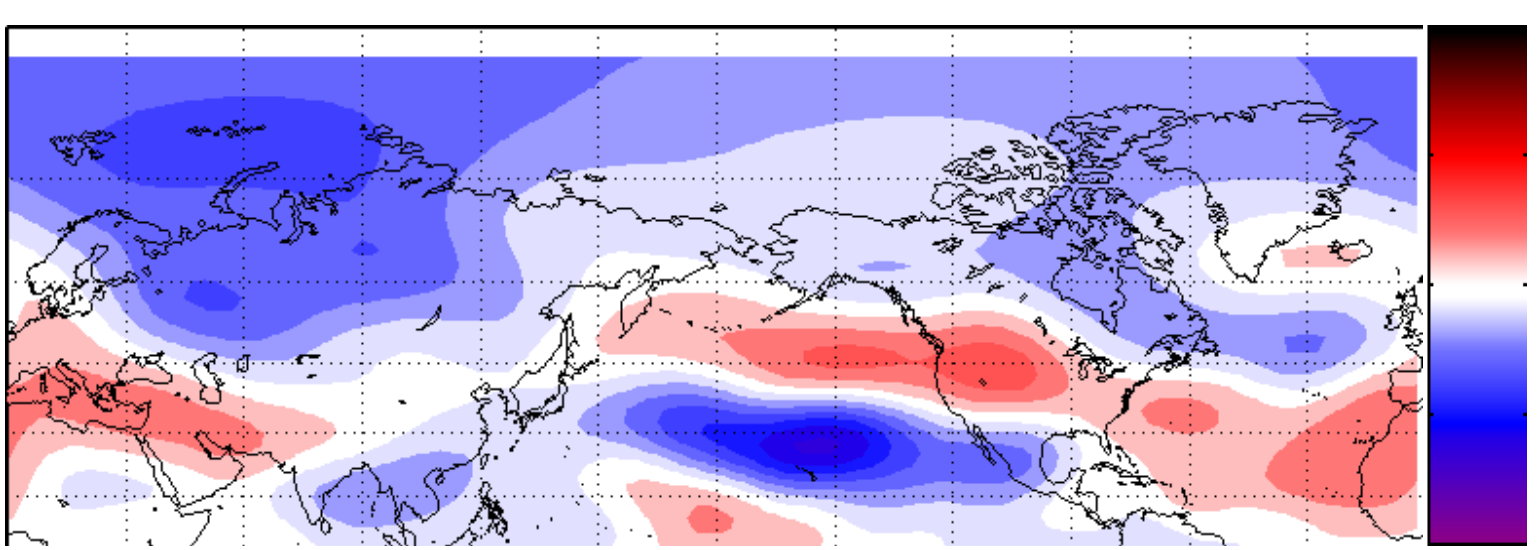

Fig. 4.17 - The rate of change in WPA Activity expressed through single point linear regressions relating DJF mean WPA Activity at each grid point and the year. Values represent the slope of the regression line (positive means WPA activity has increased from 1980 to 2010) and are contoured every 0.02 m s^{-1} $year^{-1}$.

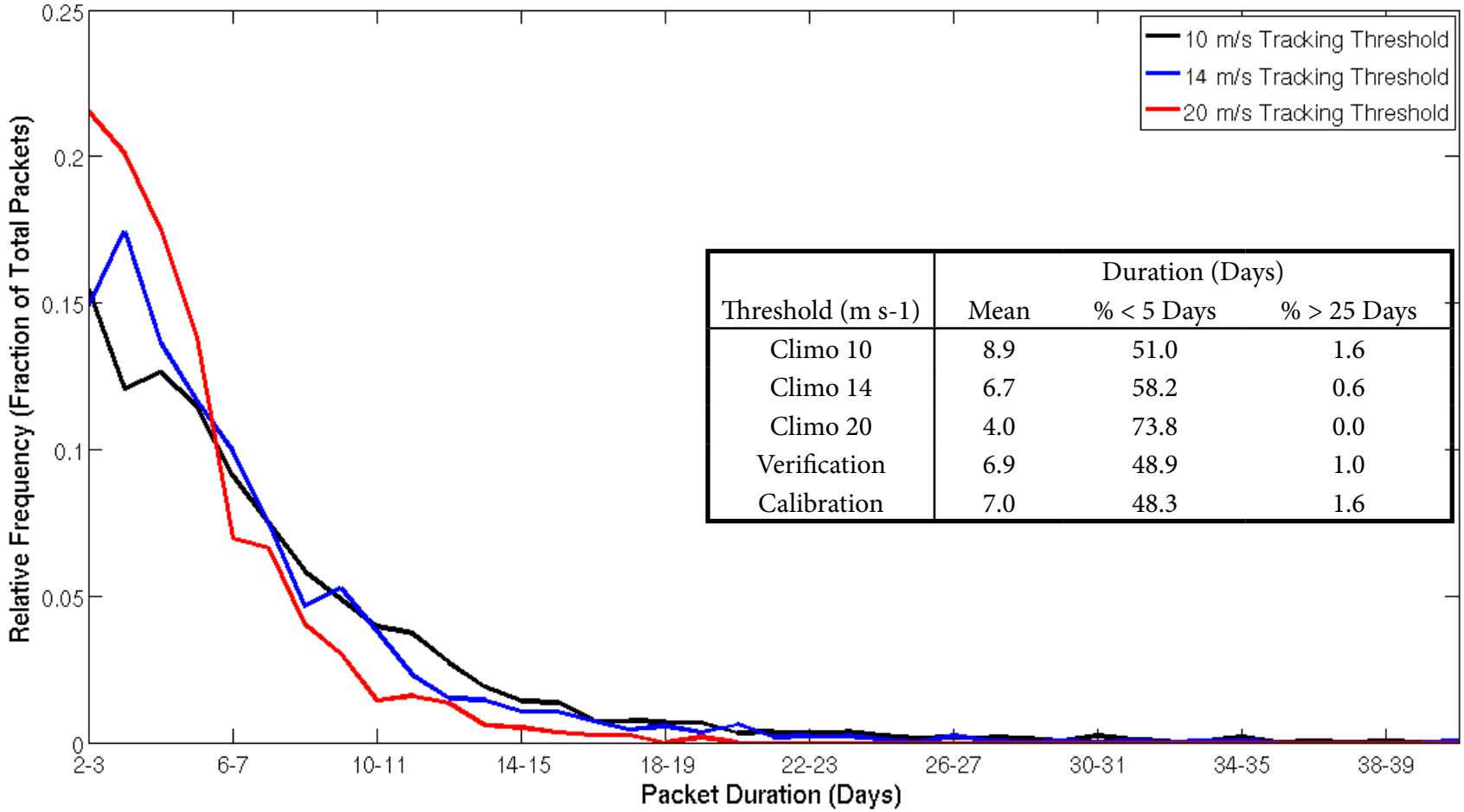

Threshold (m s-1)	Duration (Days) Mean	% < 5 Days	% > 25 Days
Climo 10	8.9	51.0	1.6
Climo 14	6.7	58.2	0.6
Climo 20	4.0	73.8	0.0
Verification	6.9	48.9	1.0
Calibration	7.0	48.3	1.6

Fig. 5.1 - Relative frequency distributions of RWPs found by Hybrid 2 tracking using three different minimum tracking thresholds along with summary statistics for each threshold in the inset panel. Climo 10, 14 and 20 refer to the distribution drawn from the entire climatology period (1979-2010) at various minimum tracking thresholds. Verification refers to the seasonal verification period defined in Chapter 3. Calibration refers to the period used in calibrating the tracking rules (JAN-MAR, 2009 and JAN 2010) - the latter two are not displayed in the line plot, as the samples are too small for useful plotting.

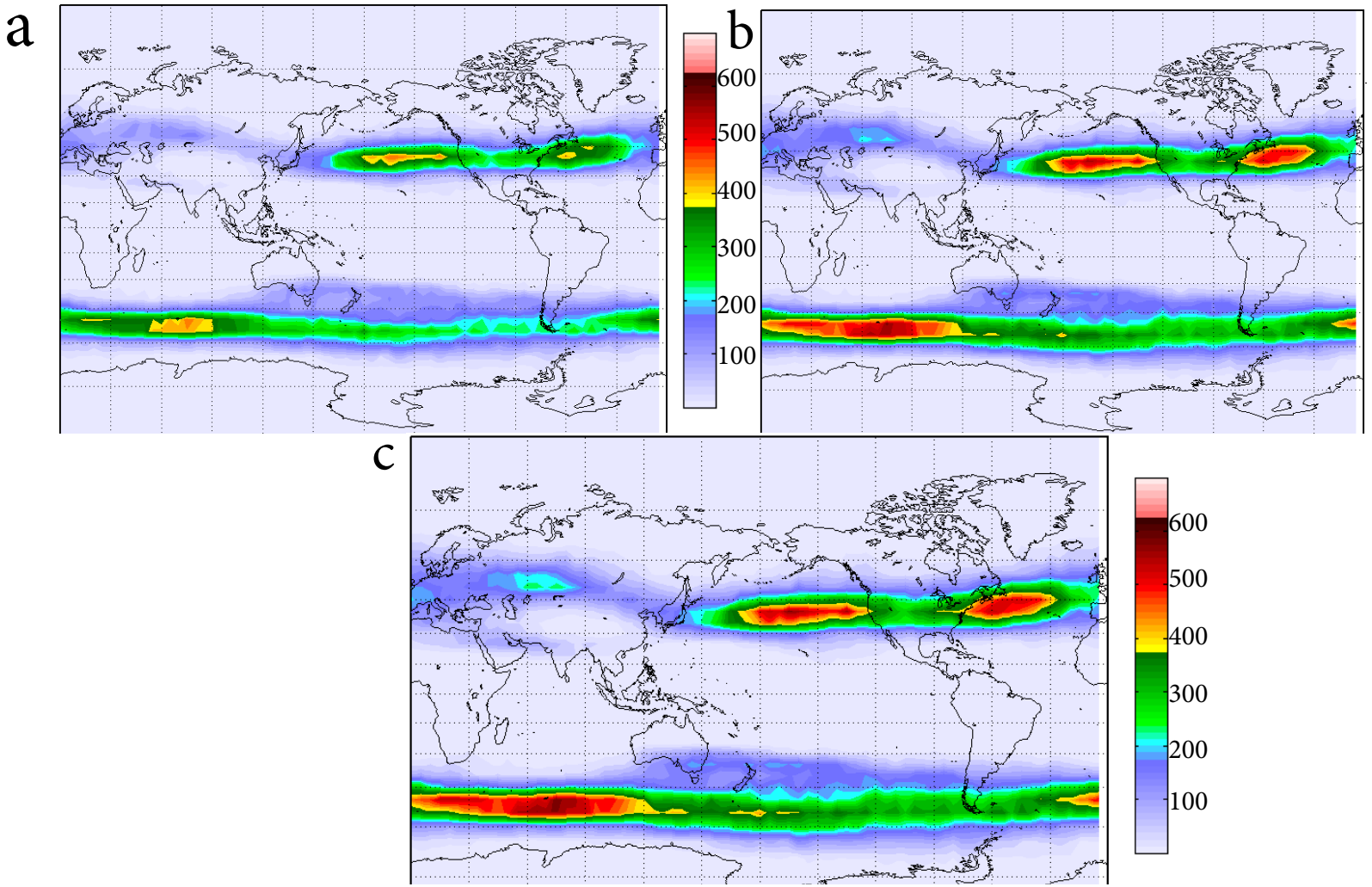

Fig. 5.2 - Number of track centroids within five degrees of a given grid point observed during the common satellite era for RWPs with varying thresholds for minimum lifetime intensity: (a) 25 m s^{-1}, (b) 20 m s^{-1} and (c) 14 m s^{-1}.

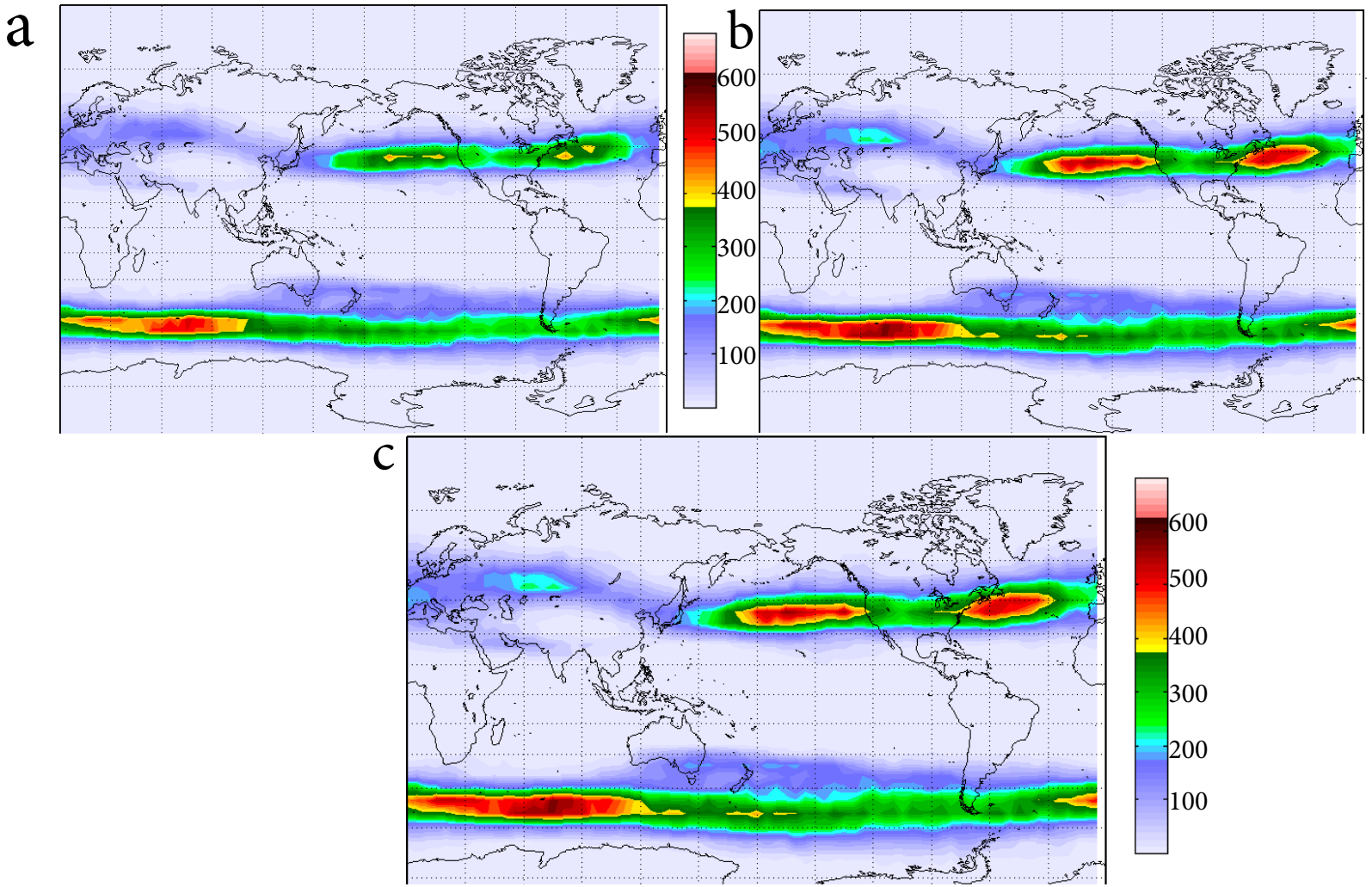

Fig. 5.3 - Number of track centroids within five degrees of a given grid point observed during the common satellite era for RWPs with varying thresholds for minimum propagation distance (longitude degrees easatward: (a) 80, (b) 40 and (c) 20.

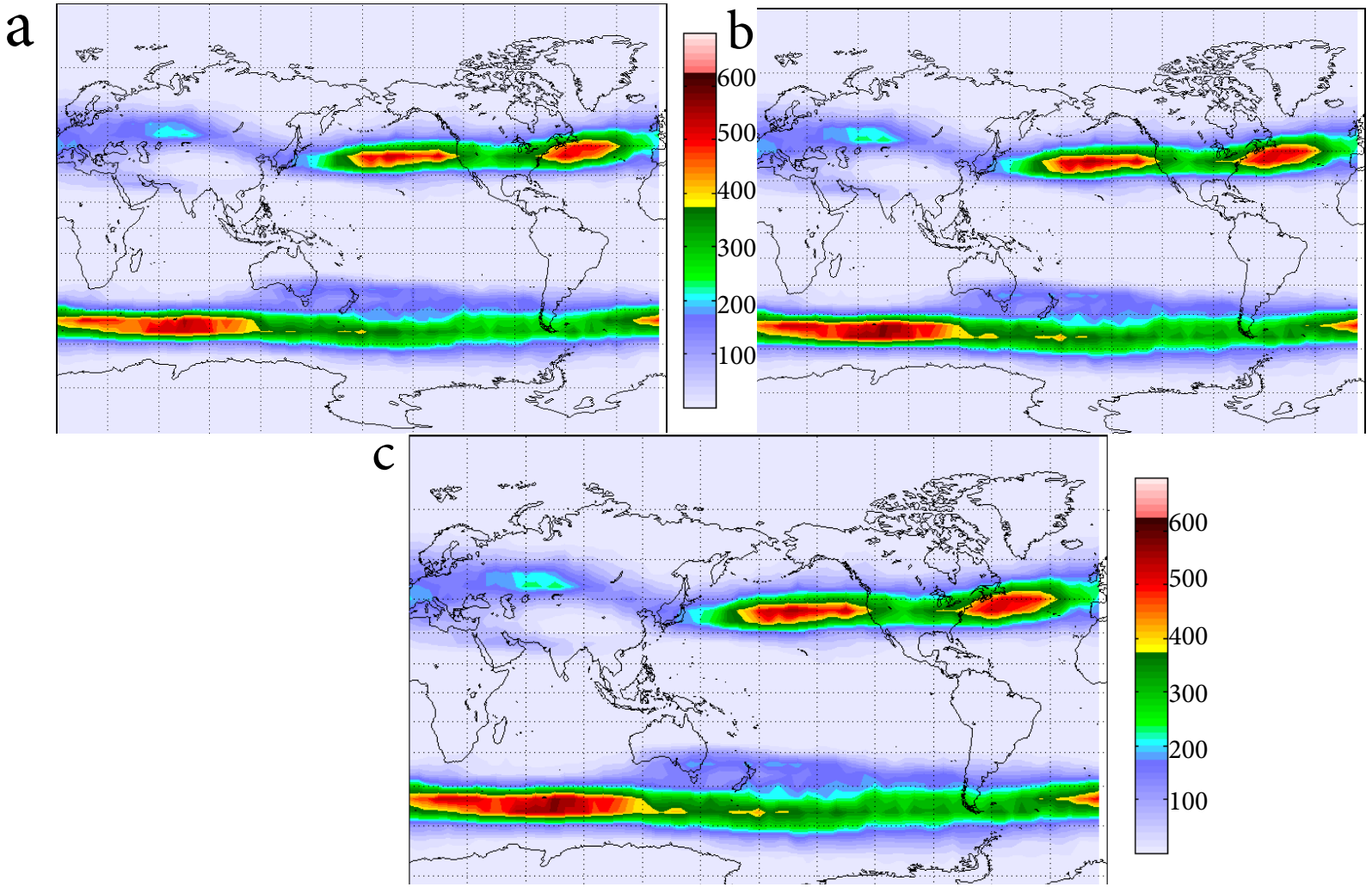

Fig. 5.4 - Number of track centroids within five degrees of a given grid point observed during the common satellite era for RWPs with varying thresholds for minimum duration: (a) 3 days, (b) 2 days and (c) 1 day.

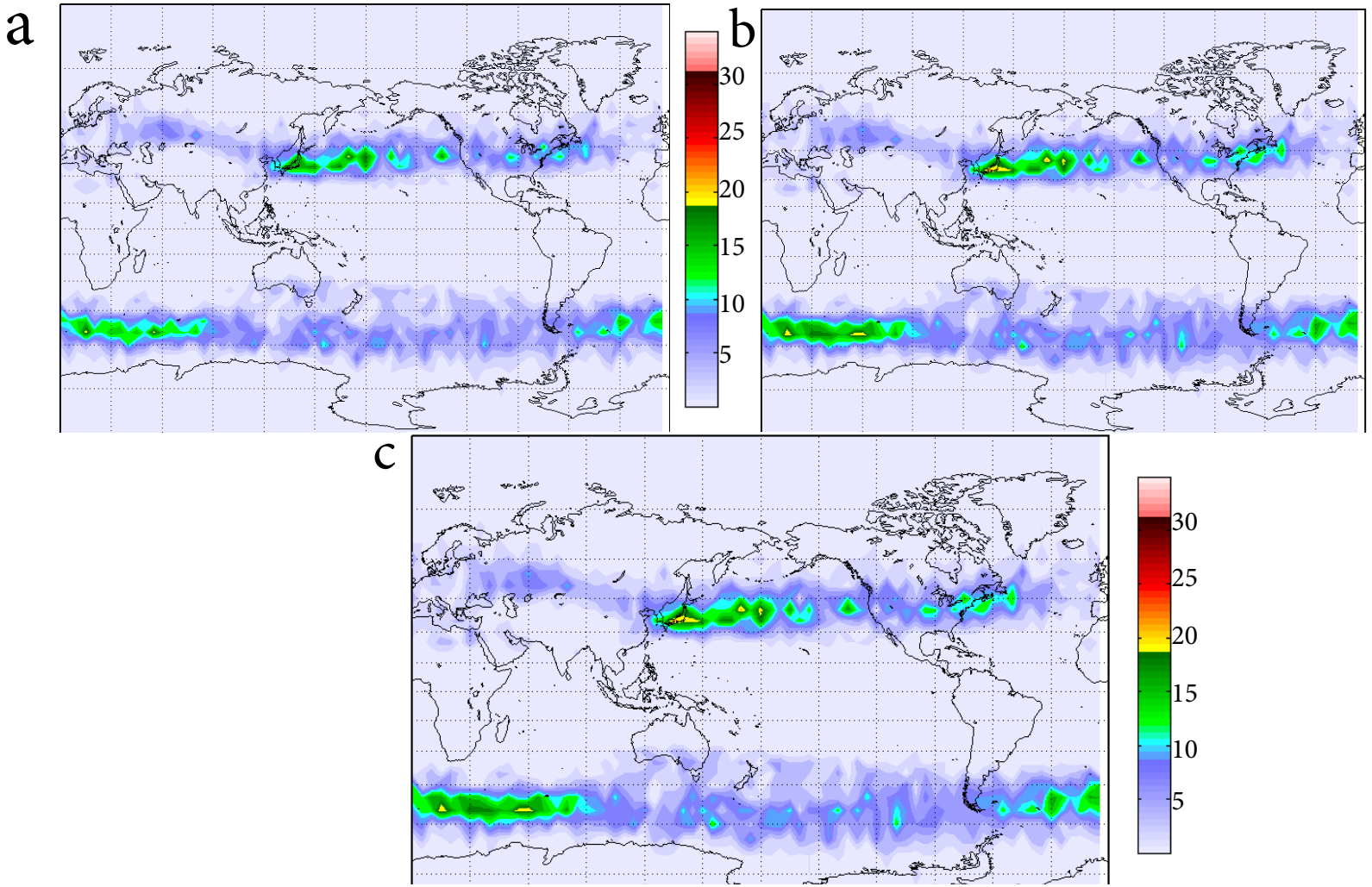

Fig. 5.5 - Number of track formation points within five degrees of a given grid point observed during the common satellite era for RWPs with varying thresholds for minimum duration: (a) 3 days, (b) 2 days and (c) 1 day.

Threshold WPA ($m\ s^{-1}$)	#Tracks	False Detections			Missed Detection		
		False	Missed Merge	False Split	Miss	False Merge	Missed Split
10	17	5	3	0	0	6	0
12	17	3	3	0	0	4	0
14	16	0	4	0	0	3	0
15	15	0	4	0	1	3	0
20	11	0	6	0	7	3	0
Hand	15	0	0	0	0	0	0

Table 5.1 - One-month (JAN, 2010) verification of RWPs tracked using various minimum tracking thresholds.

Filter Resolution	#Tracks	False Detections			Missed Detection		
		False	Missed Merge	False Split	Miss	False Merge	Missed Split
T15	43	0	8	3	1	11	3
T21	54	1	8	3	1	3	1
T28	57	1	10	3	1	3	0
T42	66	3	13	9	1	2	0
Hand	47	0	0	0	0	0	0

Table 5.2 - Three-month (JAN-MAR, 2009) verification of RWPs tracked using WPA filtered at various horizontal wavelengths.

Filter Width (hr)	Corr Coeff.
0	0.657
12	0.723
24	0.760
48	0.758

Table 5.3 - Regional correlation between WPA and WPI for all local WPA maxima (and grid points within 5 degrees in all directions) deemed significant by Hybrid 2 given varying temporal filter widths and T21 spatial filtering in the common satellite era.